

University of Kentucky

UKnowledge

Theses and Dissertations--Toxicology and
Cancer Biology

Toxicology and Cancer Biology


2022

EXTRACELLULAR VESICLES AND CANCER THERAPY: AN INSIGHT INTO THE ROLE OF OXIDATIVE STRESS

Jenni Ho

University of Kentucky, jenni.ho123@gmail.com

Author ORCID Identifier:

 <https://orcid.org/0000-0002-9690-7779>

Digital Object Identifier: <https://doi.org/10.13023/etd.2022.382>

[Right click to open a feedback form in a new tab to let us know how this document benefits you.](#)

Recommended Citation

Ho, Jenni, "EXTRACELLULAR VESICLES AND CANCER THERAPY: AN INSIGHT INTO THE ROLE OF OXIDATIVE STRESS" (2022). *Theses and Dissertations--Toxicology and Cancer Biology*. 44.
https://uknowledge.uky.edu/toxicology_etds/44

This Doctoral Dissertation is brought to you for free and open access by the Toxicology and Cancer Biology at UKnowledge. It has been accepted for inclusion in Theses and Dissertations--Toxicology and Cancer Biology by an authorized administrator of UKnowledge. For more information, please contact UKnowledge@lsv.uky.edu.

STUDENT AGREEMENT:

I represent that my thesis or dissertation and abstract are my original work. Proper attribution has been given to all outside sources. I understand that I am solely responsible for obtaining any needed copyright permissions. I have obtained needed written permission statement(s) from the owner(s) of each third-party copyrighted matter to be included in my work, allowing electronic distribution (if such use is not permitted by the fair use doctrine) which will be submitted to UKnowledge as Additional File.

I hereby grant to The University of Kentucky and its agents the irrevocable, non-exclusive, and royalty-free license to archive and make accessible my work in whole or in part in all forms of media, now or hereafter known. I agree that the document mentioned above may be made available immediately for worldwide access unless an embargo applies.

I retain all other ownership rights to the copyright of my work. I also retain the right to use in future works (such as articles or books) all or part of my work. I understand that I am free to register the copyright to my work.

REVIEW, APPROVAL AND ACCEPTANCE

The document mentioned above has been reviewed and accepted by the student's advisor, on behalf of the advisory committee, and by the Director of Graduate Studies (DGS), on behalf of the program; we verify that this is the final, approved version of the student's thesis including all changes required by the advisory committee. The undersigned agree to abide by the statements above.

Jenni Ho, Student

Dr. Daret K. St. Clair, Major Professor

Dr. Isabel Mellon, Director of Graduate Studies

EXTRACELLULAR VESICLES AND CANCER THERAPY: AN INSIGHT INTO
THE ROLE OF OXIDATIVE STRESS

DISSERTATION

A dissertation submitted in partial fulfillment of the
requirements for the degree of Doctor of Philosophy in the
College of Medicine
at the University of Kentucky

By
Jenni Ho
Lexington, Kentucky
Director: Dr. Daret K. St. Clair, Professor of Toxicology and Cancer Biology
Lexington, Kentucky
2022

Copyright © Jenni Ho 2022

ABSTRACT OF DISSERTATION

EXTRACELLULAR VESICLES AND CANCER THERAPY: AN INSIGHT INTO THE ROLE OF OXIDATIVE STRESS

As a result of improvements in cancer detection and treatment methods, a growing population of cancer survivors are living with side effects associated with their cancer therapy. Oxidative stress plays a significant role in the development of cancer and as a mechanism for cancer therapy to exert its therapeutic effects, resulting in off-target tissue damage. Radiation has been long established as a means to utilize the generation of reactive oxygen species to kill cancer cells, and 50% of chemotherapy agents currently used are associated with inducing oxidative stress. One major side effect observed in cancer survivors is a decline in neurocognition, where oxidative stress has been demonstrated to contribute to neuronal injury. Detection of oxidative stress and neuronal injury markers may provide opportunities for intervention to improve the quality of life of cancer survivors. Extracellular vesicles (EVs) are lipid-bound organelles that are excreted from cells and contain the molecular content of their cell of origin. Therefore, the molecular content within EVs may provide insight into biochemical alterations that occur following cancer treatment. Utilizing a mouse model given cranial radiation, we established that EVs are sensitive indicators of oxidative damage by measuring 4-hydroxy-2-nonenal (HNE) and astrocyte activation and glial fibrillary acidic protein (GFAP). These initial findings demonstrate the sensitivity of EVs compared to serum and brain tissue as an indicator of radiation-induced injury.

Pediatric acute lymphoblastic leukemia (ALL) patients are particularly susceptible to neuronal injury as a result of oxidative stress due to their median age of diagnosis between 2 to 5 years, a critical point during development. EVs isolated from these patients were shown to be more sensitive indicators of oxidative damage throughout consolidation treatment compared to patient sera and cerebrospinal fluid (CSF). A decrease in the neurogenesis marker, brain-derived neurotrophic factor (BDNF), was also observed throughout the treatment course, illustrating the sensitivity of EVs as markers of decreased neuronal stability. The relationship between oxidative stress, inflammation, and neuronal injury is well-established. Therefore, we determined whether the EVs generated from the leukemia cells contributed to inflammation, utilizing an *in vitro* system. We found that EVs produced from leukemia cells increased following treatment with the chemotherapy agent, methotrexate. Our findings reveal that EVs can be used as sensitive indicators of oxidative stress and neuronal injury.

KEYWORDS: extracellular vesicles, oxidative stress, leukemia, cancer therapy,
4-hydroxy-2-nonenal

Jenni Ho

11/1/2022

Date

EXTRACELLULAR VESICLES AND CANCER THERAPY: AN INSIGHT
INTO THE ROLE OF OXIDATIVE STRESS

By
Jenni Ho

Dr. Daret K. St. Clair

Director of Dissertation

Dr. Isabel Mellon

Director of Graduate Studies

11/1/2022

Date

DEDICATION

This dissertation is dedicated to my family.

ACKNOWLEDGMENTS

First and foremost, I would like to acknowledge and thank my biggest advocate and mentor for her continuous guidance throughout this adventure, Dr. Daret St. Clair. She continuously mentored me with compassion, kindness, a firm hand, and helped me build confidence as a scientist. I could not have asked for a better mentor with her guidance, tough love, and wisdom. In no way am I able to express my sincere gratitude to Dr. St. Clair. I must also mention two other mentors that helped me achieve this monumental goal: first, I would like to thank Dr. Luksana Chaiswing for her continued guidance at the bench, in the redox field, and as a scientist overall. Thank you Dr. Chaiswing for your patience throughout my training. I would also like to thank Dr. Suriyan Sukati, who was monumental in my first year in the lab. Without you taking me under your wing, I would probably not have survived the first year.

Additionally, I could not have selected a better dissertation committee to guide me through this process. Thank you Dr. D. Allan Butterfield for always being patient and kind when teaching me anything chemistry related; thank you Dr. John D'Orazio for your clinical insight and always being able to lighten up my committee meetings; and, finally, thank you Dr. Qiou Wei for being an incredible mentor and caring so much about your students. And thank you to Dr. Subbarao Bondada for being my outside examiner and for your guidance throughout graduate school. Other faculty and staff mentors that have contributed to my development I would like to acknowledge are: Dr. Isabel Mellon, Dr. Nathan Vanderford, Dr. Bill St. Clair, Dr. Edward Kasarskis, Dr. Kathleen O'Connor, Dr. Erin Oakley, Dr. Christine Brainson, Dr. Nathaniel Holcomb, and Dr. Pradoldej Sompol.

A special acknowledgment is needed for the St. Clair and Chaiswing labs: Teresa Noel, Fangfang Xu, Dr. Sanjit Dhar, Dr. Yanming Zhao, Caitlin Miller, Dr. Nicole Rummel, Nolan Marcum, and James Campbell. Without each of my lab members, this dissertation would not have come to fruition.

My dissertation work would not have been made possible by an army of individuals to help support me in this endeavor. I would like to acknowledge my fellow graduate students first for their support in surviving graduate school: Tanner Ducote, Dr. Stephanie Rock, Dr. James Drury, Dr. Fan Chen, Dr. Aria Byrd, Nicholas Howard, Sapta Ganguly, Alex Fenton, Mackenzie Ryan, and Kassie Naughton. My friends outside of graduate school have also helped tremendously: Courtland Stephens, Eric Mackin, Brandon King, Brooke Harden, Megan Budoi, Lee Hayes, Rodney Blackburn, and Will Kennedy.

Finally, and most importantly, I would like to acknowledge my loving family for their support throughout this journey. My parents have provided my sisters and I with unconditional love to allow us to achieve our goals. My big sisters, Judy and Angel, are my best friends in the world and their support throughout this journey has helped me achieve this milestone. I guess I'll acknowledge my brothers-in-law (Ted Simpson and Burk Meyrose) for supporting me, too, but I truly cannot thank my family enough for everything they have done for me. And thank you to the love of my life, Logan Murray, for your support, kindness, and love for the part of this journey you have been on.

TABLE OF CONTENTS

ACKNOWLEDGMENTS	iii
LIST OF TABLES	vii
LIST OF FIGURES	viii
CHAPTER 1. Introduction	1
<i>Extracellular Vesicles: Biogenesis and Characterization</i>	3
Biogenesis of EVs	6
Exosome Biogenesis	6
Microvesicle Biogenesis.....	8
EVs Content	9
EVs Characterization.....	11
EVs Isolation	17
<i>Oxidative Stress: Pro-oxidants and Antioxidants</i>	20
Oxidants and ROS	20
Antioxidants and Redox Couples	21
Redox Signaling	23
Oxidative Stress and Cancer Therapy.....	25
HNE and EVs	26
<i>Role and Function of EVs: Current Understanding and Future Directions</i>	28
EVs in Cancer	29
Translational uses of EVs.....	31
EVs and Cancer Therapy	32
<i>Research Objective</i>	37
CHAPTER 2. Extracellular vesicles released after cranial radiation: An insight into an early mechanism of brain injury	38
<i>Overview</i>	38
<i>Introduction</i>	38
<i>Materials and Methods</i>	41
Animals and Treatment	41
Blood Samples and Isolation of EVs	42
Nanoparticle Tracking Analysis	42
HNE adducted protein measurement	43
Protein Immunoblotting	43
Immunohistochemistry.....	44

Statistical Analysis.....	44
<i>Results</i>	45
Cranial radiation causes significant weight loss and increased levels of serum proteins.....	45
Radiation caused no significant differences in GFAP or HNE in brain tissue	46
Radiation- induced differences in astrocyte marker and oxidative stress are detectable in EVs	47
<i>Discussion</i>	51
CHAPTER 3. Extracellular vesicles released by acute lymphoblastic leukemia patients contain HNE-adducted proteins: implications of collateral damage.....	55
<i>Overview</i>	55
<i>Introduction</i>	56
<i>Materials and Methods</i>	59
Patients	59
Patient Sample Storage	62
Isolation of EVs from Patient Sera.....	62
Protein Concentration Measurement and Concentration of EVs	65
HNE-adducted Protein Immunoblotting	65
Nanoparticle Tracking Analysis	66
Electron Microscopy	67
Protein Immunoblotting	67
Quantification of Serum Pro-inflammatory Cytokines	68
Cell Culture and Viability	69
EV Isolation in vitro.....	69
Inflammatory Cytokines Released by Macrophage Cells	72
Statistics	73
<i>Results</i>	74
Therapy induced changes in HNE-adducted protein levels in serum but not in CSF	74
HNE-adducted proteins increased during the consolidation phase in EVs..	77
Decrease in neuronal growth factor observed in EV lysates	81
Decrease in pro-inflammatory cytokines in serum after therapy.....	86
ALL derived EVs contribute to pro-inflammatory cytokine production and their production is increased by MTX treatment	88
<i>Discussion</i>	92
CHAPTER 4. Conclusion and future directions	100

<i>Conclusion</i>	100
<i>Future Directions</i>	102
APPENDICES	106
<i>APPENDIX A: ACRONYMS</i>	106
REFERENCES	109
VITA	136

LIST OF TABLES

Table 1.1 EVs Characterization	12
Table 1.2 Methods of EV Isolation.....	18
Table 3.1 Patient Demographics	61
Table 3.2 Patient Bone Marrow Blast Percentage at collection time points.....	75
Table 3.3 Bone marrow cell surface markers for pre-B cell ALL patients at pre-treatment	82
Table 3.4 Chemotherapy and steroids used at different collection time points ..	90

LIST OF FIGURES

Figure 1.1 Biogenesis of Exosomes and Microvesicles.....	5
Figure 2.1 Different changes in mice weight and protein concentration were observed in the sham and IR group.....	46
Figure 2.2 IHC staining of brain tissue and brain tissue lysates revealed no observable changes.	47
Figure 2.3 Elevated levels of HNE and astrocyte activation were observed in the EVs obtained from the IR mice.	49
Figure 2.4 Size distribution of EVs, neuronal specific enolase (NSE), and brain-derived neurotrophic factor (BDNF) in the sham and IR groups.....	51
Figure 3.1 Schematic of collection time points.....	60
Figure 3.2 Characterization of EVs Isolated from patient sera based on MISEV2018.	65
Figure 3.3 Characterization of EVs isolated from ALL cells based on MISEV2018.	72
Figure 3.4 Characterization of patient sera and CSF.....	76
Figure 3.5 Characterization of EVs isolated from ALL patients.....	80
Figure 3.6 Immunoblotting of protein markers in EV lysates.	84
Figure 3.7 Protein immunoblotting in patient CSF.	85
Figure 3.8 Quantification of pro-inflammatory cytokines in patient sera.	88
Figure 3.9 ALL cell-derived EVs contribute to pro-inflammatory cytokine production and their production is increased by MTX treatment.	91
Figure 3.10 Proposed effect of systemic chemotherapy on neurocognitive decline and the ability of EVs to be a sensitive indicator of oxidative stress and decreased neuronal stability.....	99

CHAPTER 1. INTRODUCTION

Extracellular vesicles (EVs) are membrane-enclosed particles that contain molecular content that is excreted from most cells and can modulate downstream targets following uptake [1, 2]. Isolated molecular content within EVs may provide insight into the interior state of a cell [1]. The lipid membrane of EVs protects the molecular content from enzymatic degradation making these organelles promising potential diagnostic and drug delivery tools [3, 4]. The role of EVs in normal and pathophysiological cell interactions is being extensively researched [5-9]. For example, while EVs have been identified as playing a role in normal cell-to-cell communication, when homeostasis is altered in a system (such as, an increase in oxidative stress), EVs content may change and alter molecular patterns following interactions with downstream targets [2, 8, 10]. The role of EVs in normal and pathophysiological processes warrants continued research to determine the potential utilization of EVs in translational research, since EVs can be isolated from body fluids, providing biochemical insights into the patients. However, the role of EVs and the molecular content of EVs following cancer therapy have not been fully elucidated, in particular, those EVs with increased levels of oxidative damage following cancer therapy.

Advancements in diagnostic methods, screening technology, and cancer treatments have led to a steady decline in the cancer death rate since the 1990s [11]. Specifically, a 2018 review of pediatric oncology patients showed that the death rates for both children (ages 0 to 14) and adolescents (15 to 19) had declined by more than half since 1975 (from 4.9 to 2.0 in children and from 5.9 to 2.9 in

adolescents) [11]. Ironically, as cancer therapy becomes more effective, more patients are surviving cancer and living longer, but they are often living with unintended consequences caused by therapy. A prominent consequence observed in pediatric cancer survivors is cancer therapy-induced cognitive impairment [12]. While the underlying pathogenesis of cognitive impairment is complex, a growing body of evidence implicates oxidative damage, which results from an imbalance in the reduction-oxidation (redox) regulatory system where the amount of oxidants exceeds the capacity of the antioxidant system to remove the excessive amount of reactive oxygen species (ROS), an important mechanism contributing to damage in the brain microenvironment [13]. In particular, the role of 4-hydroxy-2-nonenal (HNE, a highly reactive end-product of lipid peroxidation) in neurodegenerative disorders is well-established and HNE has been shown to be elevated in a number of different diseases [14-18].

The consequences of cancer therapy on pediatric and adolescent patients, who are still developing neurocognitive capabilities, and who have the potential to live long and productive lives, is critically important to solve [19, 20]. It has been demonstrated that oxidative stress may be a contributing factor to the off-target tissue effects in patients receiving cancer therapy, since at least 50% of current chemotherapies are associated with increased ROS production, and radiation therapy utilizes free radicals to exert its therapeutic effects [21, 22]. In addition to the direct impact of oxidative stress in contributing to off-target tissue side effects (particularly, to the brain [23, 24]), pro-inflammatory cytokines such as TNF- α have

also been demonstrated to contribute to the negative consequences of oxidative stress by increasing ROS production and mitochondrial dysfunction [25-27].

Current methods to detect alterations in the brain are not sensitive enough to detect these changes early enough to effectively treat or mitigate cancer therapy-induced cognitive impairment, making earlier detection of cancer therapy-induced cognitive impairment vital [28]. Our group is interested in investigating the role of oxidative stress in EVs genesis and the potential use of EVs as an indicator of oxidative damage following cancer therapy, which may contribute to the decline in cognitive impairment observed in cancer survivors.

The overall goal of this project is to investigate the utilization of EVs as an early indicator of oxidative stress and the downstream implications following EV generation when utilizing different forms of cancer therapies. In this introduction, we briefly summarize the current understanding of the biogenesis, classification, and methodologies used to study EVs; the importance of oxidative stress and how it may contribute to EVs generation; and, finally, how EVs content relates to oxidative stress and cancer therapy. In particular, we focus on the utilization of oxidatively modified EVs as biomarkers of cancer and tissue injury in children with acute lymphoblastic leukemia.

Extracellular Vesicles: Biogenesis and Characterization

EVs are membrane-enclosed particles that contain molecular components specific to their cell of origin and circulate freely throughout the body [29]. Originally believed to be a mechanism for the cell to dispose of unwanted molecular products that could not be degraded by other methods, EVs are now known to be conduits

of cell-to-cell communication. Nucleic acids (e.g., mRNA and miRNA) are often among their contents, and they have the ability to alter the phenotype of their target cell following internalization [30]. The classification of EVs encompasses a highly heterogeneous group of extracellular particles. The two major groups of EVs are based primarily on their size but also on their biogenesis, contents, and the physiological roles that they play. Even though it remains a challenge to separate the two distinct groups during application [31], it is important to highlight the two main groups that form the generic term “extracellular vesicles.”

Exosomes constitute the first category of EVs. They typically range from 30-150 nm in diameter and are derived from the endosomal membrane budding inward, forming intraluminal vesicles (ILVs) during multivesicular endosome (MVE) maturation [1]. These liposomal particles are then secreted from the cell upon the fusion of MVE with the cell surface lipid bilayer. Due to their MVE origin (also known as multivesicular bodies, MVBs), they contain markers that are associated with the endosomal pathway [2]. Exosomes are secreted by various cell types in the body and may play a role in cell-to-cell communication and elimination of undesirable products within the cell, and are part of the normal and pathophysiological processes in the body [2].

Microvesicles are the second category of EVs. These molecules are larger in diameter (100 to 1000 nm) than exosomes and have a different route of biogenesis. Microvesicles are formed by budding of the plasma membrane and may possess markers such as integrins and P-selectin [1, 2]. The outward budding of the plasma membrane due to apoptosis that creates an apoptotic body has been

long known; however, the study of microvesicles budding from healthy cells is a more recent area of interest. The current understanding of microvesicle biogenesis includes flippases, floppases, scramblases, and calpain rearranging the composition of the phospholipid bilayer, allowing for physical bending of the membrane, and also allowing for microvesicle formation to occur more efficiently [1]. **Figure 1.1** provides a schematic of the differences in biogenesis between the two different types of EVs.

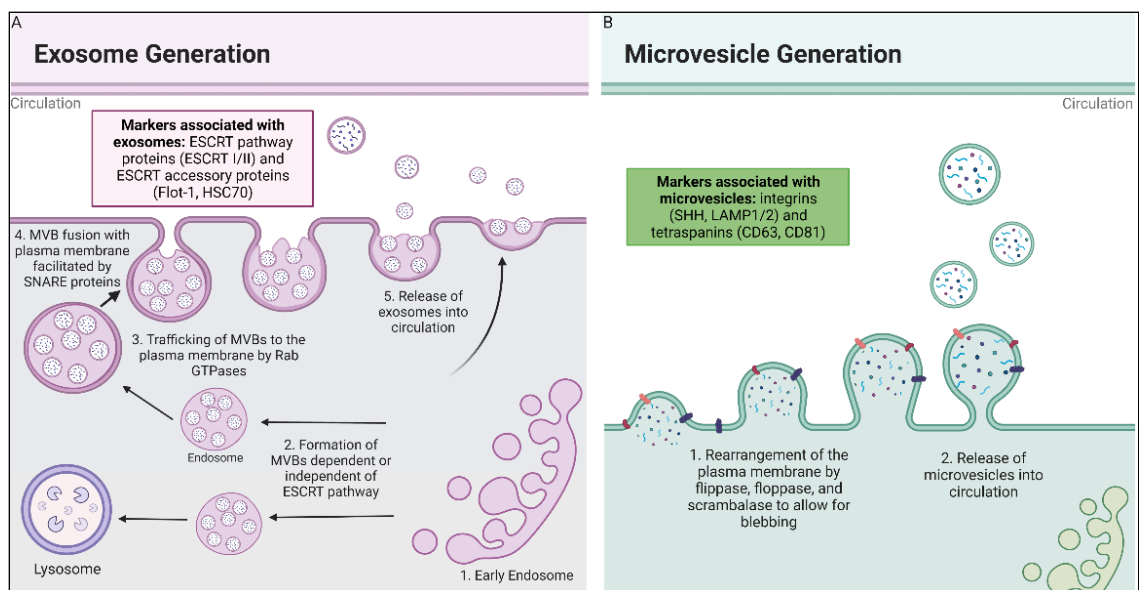


Figure 1.1 Biogenesis of Exosomes and Microvesicles

(A) Exosomes are derived from fusion of multivesicular endosomal bodies with the plasma membrane, which releases exosomes into extracellular space. Early endosomes are formed by the inward budding of either the plasma membrane or the Golgi Apparatus, where they then mature to late endosomes and become MVBs. The MVBs are then trafficked to the cell membrane, where they are fused with the plasma membrane by SNARE

proteins [29, 32, 33]. **(B)** Microvesicles are formed by the rearrangement of the plasma membrane facilitated by flippase, floppase, scrambalase, and calpain, leading to the budding of the microvesicles from the cell membrane [34].

Biogenesis of EVs

Exosome Biogenesis

The biogenesis of exosomes and microvesicles occurs by two very distinct pathways. Exosomes are derived from ILVs present in MVBs that are formed during the transition of early endosomes to late endosomes. These ILVs are released when MVBs fuse with the plasma membrane and release the ILVs as exosomes into the extracellular space. Because of their origin as ILVs, exosomes have molecular markers related to the endosomal pathway [2]. ILVs form into MVBs by two distinct pathways: one that is dependent on the endosomal sorting complex required for transport (ESCRT), and one that is independent of the ESCRT.

The ESCRT-dependent pathway consists of four complexes (ESCRT-0, ESCRT-I, ESCRT-II, and ESCRT-III) and some associated proteins that sort molecular content into ILVs. ESCRT-0 and its accessory proteins recruit content in an ubiquitin-dependent manner, which begins the formation of ILVs by recruitment of the coat protein, clathrin [35]. ESCRT-I and ESCRT-II cause bud formation, with ESCRT-III driving vesicle scission. Associated proteins (primarily VPS4, an ATPase) dissociate and recycle ESCRT machinery from ILVs [36]. Previous studies that inhibited components of the ESCRT machinery showed that

MVBs still formed in mammalian cells, resulting in further exploration of a secondary ILVs formation pathway independent of the ESCRT machinery [37].

In comparison to the relatively well-characterized ESCRT-dependent pathway, how exosomes form independent of the ESCRT pathway is only speculation. Attempts have been made to identify the proteins or lipid molecules that promote inward budding of the MVB membrane and produce ILVs. One such protein is ceramide, which was shown to promote the inward curvature of the MVBs membranes that form ILVs in oligodendrocytes [36]. In the same cells, it was shown that drug-induced or genetic mutation-induced cholesterol accumulation in MVBs resulted in an increase in exosome formation in a flotillin-2 dependent manner [38]. While these are just two possible alternative mechanisms of exosome biogenesis, Kowal *et al.* outlined other possibilities in their review [36]. It is clear that the formation and release of ILVs in MVBs is a multifaceted process that is dependent on many different factors, which makes it challenging to simply categorize their formation into just ESCRT-dependent and -independent pathways.

Following the formation of MVBs by either pathway, the next step for release of the exosomes into circulation is intracellular trafficking of MVBs to the plasma membrane [29], which is facilitated by cytoskeleton filaments but also is regulated by different proteins [29, 39]. The most well-established proteins associated with regulating the trafficking of these intracellular organelles are Rab GTPases, which facilitate vesicle budding, uncoating, motility, and fusion [40]. The final step in release of exosomes into circulation is fusion of the MVBs with the plasma

membrane, which is driven by SNARE (soluble NSF attachment protein receptor) proteins [29, 32, 33].

In summary, exosome biogenesis is derived from the endosomal pathway, leading to exosomes differing from microvesicles by having more molecular markers characteristic of the endosomal pathway that produced them. Following their formation MVBs are then trafficked to the plasma membrane by cytoskeleton filaments and proteins, where, facilitated by SNARE proteins, they fuse with the cell's plasma membrane and the exosomes are released into circulation. Whether the ILVs within a single MVB are all from one pathway or a combination of both ESCRT-dependent and ESCRT-independent pathways remains to be addressed by further research.

Microvesicle Biogenesis

While exosomes are derived from ILVs, microvesicles are a result of direct budding of the plasma membrane of the cell; their biogenesis is not as well understood as the biogenesis of exosomes [29]. The first step in the process of microvesicle biogenesis is rearrangement of various plasma membrane components, including lipids and proteins, and changes in calcium levels, which allow for calcium-dependent enzymatic machinery such as flippases, floppases, scramblases, and calpain to alter the composition of the bilayer [6]. Flippases and floppases are aminophospholipid translocases whose main role is to transport phosphatidylserine and phosphatidylethanolamine from one side of the lipid bilayer to the other [1]. Flippases catalyze the movement of these different phospholipid species from the outer leaflet to the cytosolic leaflet, and floppases catalyze the

movement in the opposite direction [41]. Both of these enzymes are ATP-dependent and can only transport in one direction. In contrast, scramblases are ATP-independent and can transfer phospholipids bidirectionally. Calpain is a calcium-activated protease which cleaves actin-capping proteins, causing the disruption of the cytoskeleton protein network that leads to membrane budding [34]. The result of these enzymes working together is that the composition of the phospholipid bilayer is rearranged and the actin cytoskeleton is restructured, allowing for the formation of microvesicles budding off the membrane. While the enzymes that help promote formation of microvesicles have been studied, the underlying mechanism and key regulators in formation of microvesicles is not as well-understood as the biogenesis of exosomes.

EVs Content

Due to different routes of biogenesis, some molecular content of exosomes and microvesicles may differ. However, these two different forms of EVs also share similarities in molecular content. Overall, both forms contain proteins, lipids, and nucleic acids characteristic of their cell of origin, but they do have distinct profiles based on their biogenesis.

The composition of the lipid membrane of EVs shares many similarities with their cell of origin. Exosomes typically contain sphingomyelin and gangliosides; however, they have lower levels of phosphatidylcholine and diacylglycerol compared to their cell of origin [42]. Indicative of their route of biogenesis in comparison to exosomes, the lipid composition of microvesicles shows more similarities with the cellular membrane from which the microvesicles are derived.

They do, however, have increased polyunsaturated glycerophosphoserine and phosphatidylserine, as these lipids are more prominent in lipid rafts and are not evenly distributed in the lipid membrane of the cell [43]. Despite the two different biogenesis routes for exosomes and microvesicles, overall the phospholipid components of exosomes and microvesicles remain relatively constant [34].

In contrast to the similar phospholipid composition of EVs, the proteins in these liposomal particles are more heterogeneous. For example, exosomes contain proteins that are associated with the ESCRT pathway (such as TSG101 and ALIX), while microvesicles are associated with integrins and selectins [2]. However, microvesicles and exosomes do have some similarity in their protein content due to their formation. Both categories of EVs contain different kinds of tetraspanins (CD63, CD81, CD9), the antigen presenting proteins involved in signal transduction (e.g., EGFR), and other transmembrane proteins, such as LAMP1 and TfR [44]. Along with the proteins associated with their biogenesis, EVs contain proteins specific to their parental cell. For example, EVs released from antigen presenting cells contain membranes enriched in MHC-I, MHC-II, and co-stimulatory molecules, while those released from tumor cells contain pro-apoptotic molecules, such as TNF-related apoptosis-inducing ligand (TRAIL) and FasL in microvesicles derived from colorectal cancer cells [34, 45].

EVs are also enriched with small RNAs such as mRNA, microRNA (miRNA), rRNA, and non-coding RNA (ncRNA), which are typically fragmented, but not with DNA in a small number of cases, especially by tumor cell derived EVs [44, 46]. Similar to proteins, the nucleic acid content of EVs reflects the types and levels of

nucleic acid in the cytoplasm of the parental cell and can provide insight into the physiological state of the cell of origin; however, some studies have illustrated that the RNA content of EVs does differ somewhat from that of the parental cell [5, 44, 47]. In their findings, Pigati *et al.* demonstrated that EVs released by malignant mammary cells but not normal epithelial cells contained elevated levels of miR-451 (shown to downregulate macrophage migration inhibitory factor, MIF, and multi-drug resistance, MDR1, in cancer cells) [47]. This finding demonstrates how different cell types may selectively export nucleic acids via EVs, releasing nucleic acid that may help promote cancer growth whereas their normal cell counterparts do not release these microRNAs.

EVs Characterization

The International Society of Extracellular Vesicles (ISEV) published the Minimal Information for Studies of Extracellular Vesicles (MISEV) guidelines in 2014, and updated them in 2018 [31]. Based on the different components of EVs, They *et al.*, proposed the standard measurements and quantifications needed to characterize EVs to promote rigor and reproducibility. They discussed the challenge of isolating one class of EVs due to the limitations in isolation methods and techniques that make it extremely difficult to ensure that a population of EVs is exclusively exosomes or microvesicles. However, the differences in biogenesis and origin of these two categories enable measurement of certain characteristics of EVs that may provide some insight into which category of EVs may be more prominent in a sample. **Table 1.1** shows the MISEV2018 characteristics that

determine the purity and efficacy of EVs isolation and the suggestions of the society for any publications that report studies of EVs.

Table 1.1 EVs Characterization

Parameter	Purpose	Suggested Methods	Additional Notes
1. Quantification of EVs	To best quantify the amount of EVs present in a sample. Starting volume that EVs are being isolated from also needs to be taken into account [31].	1. Protein concentration (e.g., BCA, Bradford, total protein on SDS-PAGE) 2. EVs particle number quantification (e.g., nanoparticle tracking analysis, standard or high-resolution flow cytometry)	Either total protein as measured by BCA or particle number is most commonly used. Quantification of total lipids, specific molecules, or total RNA may also be used
2. General characteristics of EVs by protein composition	To quantify the purity of EVs isolation with a minimum of 3 positive markers (at least 1 transmembrane or lipid-bound protein and at least 1 cytosolic protein). Additionally, a negative or contamination marker must be used for a minimum total of at least 4 protein markers [31].	1. Western blotting 2. Flow cytometry 3. Capillary based automated western blot Jess [48] 4. Reverse phase protein array (RPPA) [49] 5. Mass Spectrometry [50]	Two other categories of protein markers are suggested in MISEV2018 but are not required [31]. 1. Proteins localized in/on intracellular compartments of eukaryotic cells to identify specificity of small EVs subtype(s) (e.g. LMNA and CYC1) 2. Secreted or luminal proteins that can bind to receptors on the EVs surface for mode of association of EVs (e.g. EGF, VEGFA, and collagen)
3. Characterization of single vesicles	Provide some parameters regarding the individual EVs present in the bulk population of EVs that	1. Electron microscopy (SEM, TEM, cryo-EM), SPM, Atomic Force Microscopy (AFM) [51],	The authors of MISEV2018 provide many potential methods that can be used

	are being used for study. Two methods must be used. The first should provide a high-resolution image of the EVs and the second should calculate biophysical parameters of single EVs that can be used to quantify a large number of EVs [31].	super-resolution microscopy 2. Nanoparticle tracking analysis, high-resolution flow cytometry, fluorescence correlation spectroscopy	for the characterization of single vesicles but emphasize the significance of proper documentation of the experimental conditions, such as documentation of the source of the EVs, the starting volume of the source, the conditions of isolation, etc.
4. Characterization of topology of EVs-associated components	To determine the location of some proteins between the lumen and the surface of EVs [31].	1. Mild digestions, permeabilizations, or antibody studies followed by SDS-PAGE, RT-PCR, etc. 2. Flow cytometry and fluorescence microscopy with antibodies 3. EM with immunolabeling	Topology may be a result of unknown mechanisms localizing cytosolic components to the surface and may be important for function

BCA, bicinchoninic acid; EM, electron microscopy; EVs, extracellular vesicles; MISEV, minimal information needed to study extracellular vesicles; SDS-PAGE, sodium dodecyl sulfate polyacrylamide gel electrophoresis; RT-PCR, reverse transcriptase polymerase chain reaction; SEM, scanning electron microscopy; SPM, scanning-probe microscopy; TEM, transmission electron microscopy

The purpose of this Table is to summarize the parameters outlined by MISEV2018.

For optimal characterization of EVs, please refer to the original article by Thery C et al. for detailed information about MISEV2018 guidelines [31]. The first column is the four different parameters that must be assessed when studying EVs; the second column gives the reasoning and purpose of assessing this parameter; the third column provides methods suggested by MISEV2018; and the fourth column cites any additional notes highlighted in the publication [31].

When studying EVs, it is first necessary to quantify the amount of EVs isolated. MISEV2018 emphasizes that such methods as quantifying lipid content, DNA content, or specific markers of EVs unavoidably lead to contamination [28]. Therefore, a more accurate way of quantifying the number of EVs is by the protein concentration (such as with a BCA or Bradford assay) and the particle number (e.g., nanoparticle tracking analysis). Our group uses the BCA method to quantify EVs protein concentration to complement findings from our nanoparticle tracking analysis method that uses Zeta View by Particle Metrix. Moreover, protein concentration normalized by the particle number may also provide insight into how much of the protein detected is part of the population of isolated EVs and is not contaminated starting material.

The second step in the study of EVs is to investigate the different protein markers associated with EVs, and a method such as western blotting can be used to quantify protein expression in an isolated sample. Measuring these markers in a given population of isolated EVs can be challenging, as the quantity of isolated EVs can be limiting. Improvements in western blot techniques increase sensitivity to these markers from a small sample size, and have been achieved by using Jess by Protein Simple [52]. Utilizing this system has allowed for effective quantification of proteins of interest, even when EVs were isolated from a limited amount of mice sera, highlighting the effectiveness of the system compared to a traditional western blot [48]. Exosomes and microvesicles have different positive markers that may indicate which population is being analyzed (summarized in **Table 1**). Markers indicating exosomes include cytosolic proteins, while markers of microvesicles

include transmembrane or lipid-bound proteins. The use of at least three positive markers of EVs is recommended and, furthermore, at least one should be a cytosolic protein and one a transmembrane protein. Finally, the use of a negative or contamination protein marker is also recommended in order to indicate how much contamination is present in the isolated sample. In summary, at least three positive markers and one negative (contamination) marker are required for studying the protein composition of EVs. In addition, MISEV2018 recommends two other categories of markers that are not required but would provide optimal conditions for functional studies of EVs. The first category encompasses proteins localized in or on intracellular compartments to further demonstrate the population is predominantly exosomes and derived from MVBs; the second is secreted or luminal proteins on the EVs surface for mode of association of EVs [31].

The first two steps outlined above (quantification of EVs by measuring EVs protein concentration and measurement of purification by quantifying EVs markers) assess the purity of the sample by looking at the entire population of isolated EVs. The third step aims to provide details about individual EVs that are present in this bulk population. It is suggested that at least two different but complementary methods can be utilized to characterize individual vesicles. The first method is utilization of a technique such as scanning electron microscopy, transmission electron microscopy, or cryo-electron microscopy to provide a high-resolution image of individual vesicles. Additionally, a technique called atomic force microscopy (AFM) has recently shown promise to visualize the topography of EVs, highlighting its use in analyzing single EV molecules [51]. Utilization of one

of these methods allows for analysis of the morphology of EVs that were isolated. The second method uses a complementary assay that measures individual biophysical properties of the EVs. For example, nanoparticle tracking analysis utilizes the light scattering properties and Brownian motion of the EVs to measure the size distribution and particle number in a given liquid suspension; these properties are measured in each individual vesicle in order to determine information about the whole population of isolated EVs.

The final information required for the study of EVs, as suggested by MISEV2018, is characterization of the topology of EVs-associated components. This serves to provide further evidence of the functionality of EVs and the proteins encompassed within them. For example, to establish the location of the proteins in the EVs, Cvjetkovic *et al.* used EVs isolated from HMC-1 mast cells through differential ultracentrifugation, followed by one of the following treatments: 1) no treatment of the isolated EVs; 2) EVs treated with proteinase K (degrading proteins on the surface of EVs); 3) EVs treated with trypsin/Lys-C (digestion of surface proteins) followed by a biotin tag [53]. Using MS/MS analysis, they found that the proteomic profiles of the treatment groups differed. This finding gave them some insight into which proteins overlapped on the surface of the EVs compared to inside the EVs; it also demonstrated that the location of proteins in the EVs vary, which may be responsible for potential downstream signaling [53]. The protocol followed by Cvjetkovic *et al.* is one example of how the topology or location of the protein of interest may be vital in understanding the mechanism of EVs. They *et al.* provide other examples of how to measure this topology by using different

enzymes and detergents to acquire samples with different surface and internal levels of degradation. For further details on this type of methodology, please refer to MISEV2018 [31].

EVs Isolation

A number of different isolation methods are currently employed to study EVs, and the method used varies depending on: 1) type and quantity of the EVs fluids that were isolated; 2) resource limitations; and 3) study endpoints. Here, we briefly summarize some of the methods utilized for EVs isolation.

The most common method of EVs isolation currently used internationally is ultracentrifugation, with approximately 81% of researchers utilizing this method due to its low cost, purity, and ability to handle a large volume of starting material [54]. Carnino and colleagues demonstrated that while there are a number of benefits, there are still limitations, such as access to ultracentrifugation equipment, tedious step-by-step protocols, and successful extraction of EVs being dependent on the rotor size of the ultracentrifuge and resulting g force [55]. Based on an ISEV survey, other common methods used are density gradient centrifugation (20% of researchers), filtration (18%), and size exclusion chromatography (15%) [55]. **Table 1.2** summarizes the advantages and disadvantages of these methods, as well as ultracentrifugation and some commercially available kits that utilize polyethylene glycol (PEG) precipitation that are used to decrease the solubility of EVs so they can be isolated by precipitation [54-56].

A number of different commercial kits are available through manufacturers, such as System Biosciences, ThermoFisher, HansaBioMed, Exiqon, and Qiagen,

to name a few. While the table is not all-inclusive, it summarizes notable advantages and disadvantages of the most common types of isolation methods used by researchers. It is important to note that a majority of the researchers who responded to the questionnaire (all members of ISEV) utilized a combination of isolation techniques (59%) [54]. As previously mentioned, when selecting a method of EVs isolation, a number of different parameters should be taken into account. For example, isolation of EVs from human serum may limit the volume of the starting sample, whereas this is not typically a limiting factor when isolating EVs from cell culture media. Additionally, depending on the downstream applications, a higher and more pure yield of EVs may be required for additional experiments. Nevertheless, it is important to note the variety of different methods available to researchers for EVs isolation, and customized optimization of these different techniques should be employed to identify the best approach for the researcher's purpose [54-56].

Table 1.2 Methods of EV Isolation

Method	Advantages	Disadvantages
Ultracentrifugation	<ul style="list-style-type: none"> • Low cost • Able to process high volume of sample • No additional chemicals needed 	<ul style="list-style-type: none"> • Need access to ultracentrifugation equipment • Tedious and time-consuming protocols <ul style="list-style-type: none"> • Efficacy of isolation is dependent on rotor* • Potential damage to EVs integrity

Density gradient centrifugation	<ul style="list-style-type: none"> • Purity of isolation • No additional chemicals needed 	<ul style="list-style-type: none"> • Need access to ultracentrifugation equipment • Difficult to perform with small volume of initial material • Loss of sample during isolation
Filtration	<ul style="list-style-type: none"> • Straightforward protocol • Can isolate from numerous samples at once • No limitation on starting sample volume 	<ul style="list-style-type: none"> • Potential loss of sample <ul style="list-style-type: none"> • Sample contamination • Larger sample size may result in lower yield
Size exclusion chromatography	<ul style="list-style-type: none"> • Purity of isolation • Preservation of vesicle integrity • Prevention of EVs aggregates • Able to isolate EVs based on size to differentiate between categories • Short time for isolation 	<ul style="list-style-type: none"> • Only able to process small sample volumes • Tedious protocols <ul style="list-style-type: none"> • Need for specialized equipment

* Cvjetkovic *et al.* observed differences in EVs isolation purity when utilizing the same protocol for different rotor types, indicating that it is necessary to optimize protocols and calculate the purity and reproducibility of the isolated EVs [57].

Advantages and disadvantages of some methods currently used to isolate EVs are listed. This table reflects and aims to summarize the findings of Gardiner et al., Carnino et al., and Brennan et al. [54-56]. For original detailed information, please refer to their papers.

In summary, EVs have emerged as a research area of interest because their molecular content identifies their cell of origin and they have potential downstream consequences. The next section of this review will emphasize how

the generation and modification of EVs may provide insights into cellular damage, leading to the potential monitoring of disease development, treatment outcome, and tissue damage in a clinical setting.

Oxidative Stress: Pro-oxidants and Antioxidants

Oxidative stress results from increased ROS or reactive nitrogen species (RNS), where the ROS or RNS pro-oxidant conditions cannot be mitigated due to inefficient antioxidant systems or dysregulation of the redox pathways that control the balance between pro-oxidants and antioxidants. The resulting oxidative stress can cause oxidative damage, which has been demonstrated to increase with age and has been linked with numerous neurodegenerative diseases [16, 17]. Oxidative stress has also been linked with the increased risk of developing cancer, which is due, in part, to genetic mutations that favor development of cancer and which contributes to a pro-tumorigenic microenvironment [58-60]. Therefore, the careful regulation of redox balance is critical for normal physiological function.

Oxidants and ROS

Oxidants are molecules that are capable of oxidizing or taking electrons from other atoms or molecules, causing a change in the molecule charge. Many oxidants are generated through normal physiological pathways in the body and are primarily produced in the mitochondria. For example, through the buildup of the electron gradient to generate ATP during oxidative phosphorylation, the electron transport chain produces superoxide anion radical ($O_2^{\bullet-}$) primarily at complex I (mainly in the matrix) and at complex III (mainly in the matrix and intermembrane space) of the mitochondria [61].

Free radicals are molecules that contain at least one unpaired electron. Examples of free radicals are the hydroxyl radical (OH^\bullet) and $\text{O}_2^{\bullet-}$. ROS are molecules derived from molecular oxygen (O_2) but have more reactivity than O_2 due to the atomic orbital these electrons occupy. Whether ROS are considered free radicals depends on whether the ROS has an unpaired electron (i.e., hydrogen peroxide, H_2O_2 , does not have an unpaired electron and is therefore a ROS but not a free radical). Hund's rule states that every electron orbital must be occupied by a single electron before any one orbital is doubly occupied and unpaired electrons contribute to the high reactivity of free radicals and ROS [13]. An increase in either type of molecule beyond its antioxidant capacity can cause damage to macromolecules or reactions with certain chemical groups that activate or inactivate protein functions [62-64].

Antioxidants and Redox Couples

Due to the negative consequences of high levels of ROS, the body possesses numerous antioxidant mechanisms to combat oxidants. Here, we summarize some key antioxidant enzymes that are critical for redox regulation and mention some non-enzymatic antioxidants and the six major redox couples present in cells of the human body. The major group of enzymes that detoxify superoxide radicals in the cell is a family of three enzymes known as superoxide dismutase (SODs), which catalyze the conversion of $\text{O}_2^{\bullet-}$ to H_2O_2 and O_2 . Copper zinc SOD (SOD1) is a homodimer that has Cu^{2+} and Zn^{2+} at the catalytic site and is located in the cytoplasm, the intermembrane space of the mitochondria, in the nucleus, and in lysosomes [65]. Manganese SOD (SOD2) is a homotetrameric enzyme containing

Mn²⁺ and is located within the mitochondrial matrix. Extracellular SOD (SOD3) is a Cu²⁺ and Zn²⁺-containing homotetramer residing on the cell surface [66]. The dismutation of the superoxide radical into H₂O₂ is particularly important due to the downstream effects of hydrogen peroxide. H₂O₂ is oxidized by ferrous iron to produce ferric iron, a hydroxyl radical, and a hydroxide ion ($\text{Fe}^{2+} + \text{H}_2\text{O}_2 \rightarrow \text{Fe}^{3+} + \text{OH}^\bullet + \text{OH}^-$). The ferric iron can itself be reduced by O₂^{•-} to produce ferrous iron and O₂ ($\text{Fe}^{3+} + \text{O}_2^{\bullet-} \rightarrow \text{Fe}^{2+} + \text{O}_2$). This pair of reactions results in the following net reaction (known as the Fenton reaction): $\text{H}_2\text{O}_2 + \text{O}_2^{\bullet-} \rightarrow \text{OH}^\bullet + \text{OH}^- + \text{O}_2$ [67]. The Fenton reaction is a seminal contribution to the field of free radical biology and it has been accepted as the primary mechanism of cellular oxidative stress in organisms. Due to the high production of ROS from the mitochondria, the localization of MnSOD in the mitochondrial matrix establishes the importance of MnSOD as the most vital SOD enzyme, and our lab has worked for over two decades to investigate the relationship between MnSOD and its role in cancer [68, 69].

Following the dismutation of superoxide to O₂^{•-} to H₂O₂ and O₂, two H₂O₂ molecules are then broken down into two molecules of water and O₂ ($2\text{H}_2\text{O}_2 \rightarrow 2\text{H}_2\text{O} + \text{O}_2$) by catalase. Catalase is another vital antioxidant enzyme that is present in almost all aerobic organisms that mitigate oxidative damage. Catalase dysfunction or inhibition has been implicated in aging, another indication of the effects of oxidative damage in human disease [70]. Additionally, H₂O₂ can be reduced to two water molecules catalyzed by glutathione peroxidase (GPx), where glutathione (GSH) is used as a cofactor and is oxidized to glutathione disulfide

(GSSG) ($\text{H}_2\text{O}_2 + 2\text{GSH} \rightarrow 2\text{H}_2\text{O} + \text{GSSG}$) [71]. The oxidized glutathione (GSSG) is then converted back to its reduced form, catalyzed by glutathione reductase, with FAD as a cofactor.

In addition to the SOD enzymes, catalase, and GPx, the body also utilizes non-enzymatic antioxidants such as vitamin C, vitamin E, carotenoids, and lipoic acid to assist in the redox regulation of a system [72]. Moreover, the cell contains six major redox couples that ensure the availability of electrons within the cell: 1) NADH/NAD; 2) NADPH/NADP; 3) cysteine/cystine; 4) GSH/GSSG; 5) peroxiredoxin (Prx)/sulfoxiredoxin (Srx); and 6) thioredoxin (Trx)/thioredoxin disulfide (TrxSS). These six major redox couples are in different subcellular and extracellular compartments where they minimize some of the potential for damage caused by free radicals. Prevention of oxidative stress and damage to the cell depends on the balance among these different molecules being tightly regulated to promptly remove ROS produced by the cell.

Redox Signaling

Despite the negative consequences of a surplus of ROS, many ROS serve additional positive roles in normal physiological functions [73, 74]. For example, at lower levels, H_2O_2 plays an important role in a variety of cellular functions, such as cell proliferation, differentiation, migration, and apoptosis [75, 76]. However, because homolytic fission of H_2O_2 produces two OH^\bullet [77], the level of H_2O_2 , as well as the by-products of H_2O_2 , must be tightly regulated.

While antioxidants balance the levels of ROS, an abundance of ROS can result in DNA damage when double bonds are added to DNA bases or if a hydrogen

atom is abstracted from the DNA [78]. Additionally, elevated levels of ROS have been shown to play a role in tumor development and progression, primarily by acting as a second messenger in signaling pathways that promote cell proliferation and survival by oxidatively modifying regulators of these pathways (e.g., MAPK/ERK, PI3K/AKT, and NF- κ B activation pathways) [79]. For example, in the presence of high levels of ROS, the MAPK/ERK pathway has increased activity of Erk1/2 because of continuous ubiquitination and loss of endogenous mitogen-activated protein kinase phosphatase 3 (MKP3), which negatively regulate Erk1/2 activity [80].

Cancer cells have also been demonstrated to have a higher antioxidant capacity compared to normal cells, which overcomes apoptotic signals induced by oxidative stress [81, 82]. As a result, monitoring the balance of redox state within a cell may provide significant insight into cancer progression or severity of disease. Overall, the contribution of ROS to cancer progression and development is understood to be facilitated by the induction of DNA mutations, genetic instability, epigenetic changes, and cell proliferation; additionally, stabilization of cells withstands the elevated amount of oxidative stress and allows for cancer survival under stress conditions [83]. While there is a significant amount of literature elucidating the significant role of oxidative stress in cancer biology, to identify potential targets of intervention, much remains to be understood about which players and mechanisms are more susceptible to oxidative damage.

Oxidative Stress and Cancer Therapy

The effect of oxidative stress in cancer therapy is especially critical due to the utilization of radiation therapy as a common cancer treatment modality. Ionizing radiation (IR) effectively causes cancer cell death by directly ionizing macromolecules or generating ROS through the homolytic fission of water into the hydrogen radical (H^\bullet) and the hydroxyl radical (OH^\bullet), where OH^\bullet is then a potent oxidant and can damage molecules, for instance, by reacting to guanosine sugar in DNA and causing DNA breakage [22].

In addition to radiation therapy, at least 50% of chemotherapies currently used are associated with the generation of ROS [21]. Examples of chemotherapy agents that generate ROS are anthracyclines (e.g., doxorubicin and daunorubicin) and alkylating agents (e.g., cyclophosphamide, carboplatin, and cisplatin) [84, 85]. While the utilization of oxidative stress aims to destroy cancer cells, off-target normal tissue injury may occur as a result of the free radicals generated by these treatment modalities. For example, the generation of $\text{O}_2^{\bullet-}$ by doxorubicin, which removes one electron from the NADH dehydrogenase at complex I and donates it to O_2 , can result in increased OH^\bullet because the SOD enzymes catalyze the dismutation of $\text{O}_2^{\bullet-}$ to H_2O_2 [86]. As a result, this can initiate an oxidation chain reaction, especially on membrane lipid bilayers, causing LPO that compromises the integrity of the lipid membranes, but also products such as the toxic aldehyde HNE that can lead to further target-specific damage [87]. Generation and accumulation of these toxic aldehyde by-products can have a myriad of downstream effects and may ultimately contribute to oxidative stress-mediated

normal tissue injury as a result of cancer treatment, since the accumulation of these by-products (particularly, HNE) has been implicated in neurodegenerative diseases such as Alzheimer's [14, 17].

HNE and EVs

It is well-established that HNE is derived from the oxidation of omega-6 polyunsaturated fatty acids, such as lipids containing linoleic acid and arachidonic acid, which are commonly found in the cell membrane. An increase in HNE and its downstream effects following HNE adduction have been implicated in disease pathologies [88-92]. The high reactivity of this aldehyde molecule is predominantly through two different reactions: it has the ability to covalently adduct to histidine, cysteine, or lysine residues of proteins via a Michael addition due to the double bond between the C2 and C3 carbons; and it can form Schiff bases with the N-termini of peptide chains and the ϵ -amino groups of lysine residues of proteins [14, 93].

Despite being a by-product of LPO, these reactions between HNE and protein residues demonstrate the impact of increased oxidative stress causing protein misfolding and ultimately modifying protein activity. Additionally, HNE accumulation has long been established as inhibiting proteasome function, which results in modifying protein turnover, due to it preventing proper degradation of these protein aggregates [94]. Particularly, HNE has been linked with Alzheimer's and other neurodegenerative diseases associated with protein aggregation formation [95-98]. Other examples of diseases involving HNE are atherosclerosis and heart disease [99, 100]. A previous study by our group demonstrated that doxorubicin treatment affected HNE-adducted proteins by altering energy

metabolism, which ultimately lead to the cardiac tissue injury that is seen as a major obstacle when doxorubicin is used as a chemotherapy agent [101]. Moreover, another study by our group demonstrated how an increase in HNE-adducted proteins was found in EVs isolated from mice treated with doxorubicin compared to the control mice [102]. These two studies suggest that not only is HNE a contributor to oxidative stress-mediated tissue injury but that monitoring HNE-adducted proteins levels may provide insight into off-target tissue injury that results from cancer treatment. Overall, high levels of HNE can have significant impact on disease development and they may also be an indicator of potential downstream negative impact because of increased oxidative stress.

As previously mentioned, one of the consequences of increased HNE is the effect on proteasome function, which could lead to an increase in the number of damaged proteins that accumulate within the cell due to the dysregulation of the cell's removal processes [98]. When this happens, another method for the cell to dispose of oxidatively damaged molecules is by exportation through EVs. One of the previous studies by our group demonstrated that treatment with the oxidative stress-inducing chemotherapy agent doxorubicin resulted in increased EVs generation [102]. This correlation between increased oxidative stress and increased EVs generation suggests that EVs may be a method by which cells dispose of oxidatively modified proteins in the presence of proteasome damage induced by increased oxidative damage. However, the consequences of oxidative stress on EVs generation and formation are not fully understood. Studies to elucidate the impact of oxidative stress on EVs biogenesis are underway in our lab

and the findings from these studies will lead to novel redox-based therapeutic targets to alleviate disease burden [103].

Role and Function of EVs: Current Understanding and Future Directions

The fundamental role of EVs in both normal and pathophysiological conditions has been demonstrated, and more research is underway to explore the potential use of EVs in the clinical setting. EVs play a variety of roles in maintaining normal physiological functions within the body. Their content allows for delivery of effectors (e.g., transcription factors, nucleic acids, oncogenes) to recipient cells or for the proteins or lipids they contain to activate surface receptors [104]. Many of the earlier studies elucidating the role of EVs in both normal and pathological physiologies emphasized the use of EVs to transport nucleic acids to target cells, which results in alterations in gene expression. Valadi *et al.* demonstrated the various kinds of nucleic acids (i.e., mRNA, miRNA) found in exosomes released from both human and murine mast cells, and elucidated how delivery of these nucleic acids altered the protein expression in target cells after they were harvested [30]. The role of EVs in the immune system has also piqued interest in recent years; their ability to present antigens and trigger different immune responses are of interest to immunologists, who are investigating their potential use in the clinic [9]. Additionally, miRNAs within exosomes have been demonstrated to modulate inflammation responses, revealing their contribution to compensatory mechanisms that maintain homeostasis [105]. EVs have also been shown to be released from a variety of stem cell populations, where they help maintain plasticity and are able to promote proliferation and vascularization in

damaged tissues [106]. Moreover, EVs have also been shown to take part in the coagulation cascade, neuronal communication in the brain, and cell phenotype modulation [8, 104].

EVs in Cancer

Along with their function in normal physiological processes, EVs have also been shown to be mediators in a variety of disease pathologies. Numerous studies have demonstrated the role EVs play in cancer, mostly how they promote tumorigenesis by altering the microenvironment to be more favorable to metastatic growth [6, 107]. EVs secreted directly from tumor cells have also been shown to promote cell proliferation, stimulate angiogenesis, promote matrix remodeling, and suppress or modify the immune system to a pro-tumorigenic phenotype [5-7, 107, 108]. Along with the tumor cells releasing EVs, macrophages associated with tumors have been shown to promote tumor invasiveness by delivering oncogenic miRNAs [109]. These findings demonstrate the different pathways and methods by which EVs can be utilized by a tumor to promote its survival. Additionally, EVs have been implicated in other roles, such as activating immune cells in inflammatory diseases and facilitating neurodegenerative diseases by delivering toxic aggregates [110, 111].

It is well- established that a number of transcription factors are sensitive to redox alterations (e.g., Nuclear factor kappa B, NF- κ B, and Nuclear factor erythroid 2-related factor 2, Nrf2); therefore, monitoring the levels of oxidative stress in cancer cells may provide information about the characteristics of the cancer [103]. In particular, a number of therapy-resistant cancers have been shown to have

increased levels of ROS but also an up-regulation in a number of antioxidant enzymes that can avoid oxidative stress-induced apoptosis [81, 112]. This dysregulation of redox proteins may facilitate some of the therapeutic resistance seen in aggressive cancers, and, ultimately, may provide insight into an optimal therapeutic approach to overcome this resistance. While a benefit of monitoring oxidative stress levels utilizing EVs would provide an accurate, real-time quantification of the oxidative damage induced by both the cancer and cancer therapies, a limitation is the inability to identify the origin of the EVs. EVs can be isolated from a number of different bodily fluids, with the most common being blood. However, the EVs isolated from patient serum or plasma may have been released from any tissue present within the patient. While identification of tissue-specific markers may allow for some identification of the tissue of origin, the efficacy of detection along with acquiring enough EVs from one specific tissue would be significantly challenging [31]. Additionally, some markers of oxidative stress may be difficult to measure because the kinetics of some of the reactions allow for only a short time frame for detection. As a result, oxidative stress markers must be carefully selected to ensure they are able to reflect the redox status of the system. Nevertheless, despite some of these challenges, the potential utilization of EVs and the oxidative modifications within EVs, such as the HNE-adducted EVs, may provide vital insights into the redox status of the patient as a result of the cancer and cancer treatment, thus emphasizing the importance of continuous studies advancing the use of EVs as a diagnostic tool.

Translational uses of EVs

Current studies are hoping to elucidate and optimize drug delivery utilizing EVs as a means to directly target certain tissue types or increase therapeutic efficacy. A study by Ohno *et al.* demonstrated that miRNAs delivered in EVs decreased breast cancer development in a mouse model [113]. Another study by Yao *et al.* utilized a similar application, where EVs derived from anti-inflammatory M2 macrophages were able to inhibit cell migration and invasion in a glioma cell line by delivery of miRNA targeting the PI3K/AKT/mTOR signaling pathway [114]. While these are just two examples of engineering EVs to be utilized for therapeutic purposes, many research groups are conducting research in hopes of identifying clinical applications of engineered EVs as a drug delivery tool [4, 115, 116].

Since the content of EVs is dependent on their cell of origin, characterization of EVs may allow for insights into the state of their cell of origin, such as in monitoring disease progression [117]. Balaj *et al.* demonstrated that EVs generated from cancer cells *in vitro* possessed nucleic acid content that reflected the genetic landscape of the tumor, while they also contained genetic information that may be used for horizontal gene transfer and as a potential biomarker [118]. In addition to *in vitro* studies, it has been demonstrated that EVs isolated from the blood of pancreatic cancer patients can provide insight into the genetic mutations in a patient's tumor, allowing for precision therapeutic options [119].

Proteomic profiling of EVs has also shown diagnostic potential: Liu *et al.* demonstrated how a small volume of serum from cancer patients and from healthy individuals (n=102) allowed for accurate detection of cancer (99% accuracy) and

was further able to specify the cancer type (68% accuracy) [120]. Previous findings in our lab utilized EVs to detect myocardial damage induced by the chemotherapy drug doxorubicin in mice by detecting glycogen phosphorylase (PYGB) in EVs, where an increase in PYGB in EVs correlated with a decrease in its expression in cardiac tissue compared to control mice [102]. Interestingly, this study demonstrated that EVs were a more sensitive indicator of cardiomyocyte damage following doxorubicin treatment compared to the current method, which considers troponin levels. This study highlights the limitation of using doxorubicin in the clinic; namely, its deleterious effects on cardiac tissue, and suggests that EVs may be useful as an early indicator of these effects, potentially allowing for mitigation of these consequences in patients receiving doxorubicin. These studies illustrate the potential diagnostic use of EVs to monitor off-target tissue damage.

EVs and Cancer Therapy

While nucleic acid, protein, and lipid markers enable use of EVs as a diagnostic tool in the clinic, it is critical that modifications to these molecular components not be overlooked, as they may provide understanding about other damage that may be occurring in the model from which they were isolated. For example, an increased amount of oxidative stress markers (e.g., HNE-adducted proteins) may indicate that oxidative damage is occurring in the system. Particularly, as some forms of cancer therapy contributes to increased oxidative stress, oxidatively modified EVs can be an excellent tool to assess the redox status and the potential side effects associated with cancer therapy.

Our group recently studied EVs derived from murine models that received a single 10-Gray dose of cranial radiation, a dose that mimics human whole brain radiation and causes neurocognitive alterations in mice [121, 122]. Our study illustrated that there were no HNE adduction changes in the brain tissue of the mice (using IHC staining) or glial fibrillary acidic protein (GFAP, a marker of reactive astrocytes; IHC staining and homogenized brain tissue lysate were used for measurement), but when the mice were euthanized 48 hours after cranial radiation, EVs isolated from the mice had statistically significant elevated levels of HNE-adducted proteins and GFAP compared to the EVs isolated from the control mice. This study shows: 1) the advantages of utilizing HNE adducts in EVs as a marker of oxidative stress that alter redox homeostasis in the system; and 2) the potential use of EVs as an early indicator of astrocyte reactivity as a result of damage to the brain microenvironment induced by cranial irradiation [48].

As previously mentioned, our group has demonstrated how an increase in HNE adduction mediated cardiac damage following doxorubicin treatment and that an increase in HNE adducts was present in EVs isolated from mice treated with doxorubicin compared to the control mice [101, 102]. These findings suggest that: 1) an increase in HNE as a result of increased oxidative stress is a mediator of normal tissue injury during cancer therapy; and 2) quantification of oxidative modifications (e.g., HNE adducts) in EVs has clinical potential as a diagnostic tool to monitor downstream implications of increased oxidative stress and disease progression. Additionally, one of the most common off-target tissue injuries seen

is damage to the brain induced by cancer treatment. Therefore, monitoring damage to the brain microenvironment is critical, especially in pediatric cancer.

Acute lymphoblastic leukemia (ALL) is the most commonly diagnosed form of pediatric cancer, with a median age of diagnosis of between 2 and 5 years of age [11]. Overall, the survival rate of pediatric ALL is high (~90%); however, numerous published studies report significant neurobehavioral and neurocognitive differences between these survivors and healthy age-matched counterparts [19, 20, 28]. Despite a majority of pediatric ALL patients no longer receiving cranial radiation as a proactive treatment to decrease the potential of CNS invasion of the leukemia, the percentage of pediatric ALL survivors that report neurocognitive decline (~33%) emphasizes the necessity for early detection of these off-target tissue effects to allow for intervention [123-126].

The current treatment regimen for pediatric ALL patients encompasses multiple phases of therapy (induction, consolidation, and maintenance), and several different chemotherapy agents are given to these patients during this time [127, 128]. Induction is the first phase of the ALL treatment, with the goal for the patient to be in remission, with a current success rate of 95% [127]. The results from the clinical trial, AALL0932, recommend cytarabine, methotrexate, pegaspargase, vincristine, and dexamethasone during the induction phase [129]. Some protocols may also include the addition of an anthracycline, such as daunorubicin or doxorubicin [128]. Cytarabine has previously been demonstrated to induce apoptosis by increasing mitochondrial ROS production, where the addition of N-acetyl cysteine (NAC) reversed the increase in apoptosis that was previously seen

when cells were treated with cytarabine [130]. Daunorubicin has also been shown to contribute to mitochondrial dysfunction, ultimately leading to increased ROS production that induces DNA damage and cell death [85]. Additionally, dependent on the protocol the consolidation and maintenance phases may introduce more chemotherapy agents, such as mercaptopurine. Altogether, it is clear these patients receive a diverse combination of drugs to kill the leukemia cells. Moreover, following the AALL0932 guidelines, cytarabine and methotrexate are given to patients via an intrathecal injection, leading to direct exposure of the central nervous system (CNS) to these chemotherapy drugs. The mechanism of action of a number of these chemotherapy drugs, combined with the direct exposure to the CNS by cytarabine and methotrexate, may contribute to the decline in neurocognition observed in these patients [131-133].

The significance of increased ROS production as a product of cancer therapies (e.g., radiation and different chemotherapy agents) may ultimately contribute to the decline in neurocognition that is seen in pediatric ALL survivors. Oxidative stress has been well-established to have a number of downstream consequences to the brain that can ultimately contribute to neuronal decline, such as: 1) inducing apoptosis; 2) proteasome malfunction; 3) mitochondrial dysfunction; 4) protein misfolding; and 5) glial cell activation [23]. In addition to proteasome malfunction, oxidative stress has been demonstrated to lead to lysosome dysfunction as a result of oxidation of the lysosome membranes [134]. Proper lysosomal and autophagy functions have been shown to be critical for proper myelination of neurons by oligodendrocytes and lead to neurodegenerative disease *in vivo* [135, 136]. As

previously mentioned in the *HNE and EVs* section of this introduction, the increase in oxidative stress may ultimately lead to the accumulation of HNE within the cell. Our group, therefore, hypothesizes that the accumulation of misfolded proteins by HNE-adductions, in combination with proteasome and lysosome dysfunction, leads to the excretion of misfolded proteins in EVs, where isolation of EVs may provide the opportunity to: 1) quantify oxidative stress markers (i.e., HNE-adducted proteins) that would provide insights into the redox dysregulation occurring throughout a patient's treatment; and 2) increase sensitivity to detect proteins associated with off-target tissue damage (e.g., GFAP indicating astrocyte activation as a result of increased ROS and potential neuronal injury).

Previous studies assessing this hypothesis have thus far demonstrated: 1) the ability of EVs to be a more sensitive indicator of oxidative stress and myocardial death following treatment with the chemotherapy agent doxorubicin *in vivo* than the current method of measuring troponin levels [102]; and 2) EVs are a more sensitive indicator of astrocyte activation and oxidative stress than the brain tissue and serum of mice euthanized 48 hours following cranial radiation [48]. Thus, our group has hypothesized the putative ability of EVs to be used as a sensitive indicator of oxidative stress and off-target tissue damage following treatment with both chemotherapy [66] and radiation [48] utilizing *in vivo* models. Further studies of EVs derived from pediatric ALL patients are needed to validate the translational use of EVs to detect alterations and may identify earlier targets of intervention to mitigate the by-product of off-target tissue damage in cancer patients.

Research Objective

The aims of this study were to investigate whether EVs could be used as sensitive indicator of off-target tissue damage (specifically, in the brain) and oxidative stress as a result of cancer therapy.

In chapter two, we demonstrate that EVs isolated from mice following cranial radiation are more sensitive markers of astrocyte reactivity and oxidative stress compared to brain tissue and serum.

In chapter three, we report the characteristics of EVs isolated from the sera of pediatric ALL patients throughout the first two months of their treatment course. Our study investigated whether the EVs were more sensitive markers of oxidative stress and off-target tissue damage compared to serum and CSF, and of the downstream effects of cancer therapy-induced pro-inflammatory cytokine stimulation.

The results from this study provide a novel insight into using EVs as early indicators of off-target tissue damage and oxidative stress. Moreover, understanding the downstream consequences of EVs that contain elevated levels of oxidative damage allows for potential identification of new targets for intervention to alleviate some of the negative consequences of cancer therapy.

CHAPTER 2. EXTRACELLULAR VESICLES RELEASED AFTER CRANIAL RADIATION: AN INSIGHT INTO AN EARLY MECHANISM OF BRAIN INJURY

Overview

Cranial radiation is important for treating both primary brain tumors and brain metastases. A potential delayed side effect of cranial radiation is neurocognitive function decline. Early detection of CNS injury might lead to therapies to prevent further neuronal damage. Extracellular vesicles (EVs) have emerged as a potential diagnostic tool because of their unique membranous characteristics and cargos. We investigated whether EVs can be an early indicator of CNS injury by giving C57BJ/6 mice 10 Gy cranial IR. EVs were isolated from sera to quantify: 1) number of EVs using nanoparticle tracking analysis (NTA); 2) Glial fibrillary acidic protein (GFAP), an astrocyte marker; and 3) protein-bound 4-hydroxy-2-nonenal (HNE) adducts, an oxidative damage marker. Brain tissues were prepared for immunohistochemistry staining and protein immunoblotting. The results demonstrate: 1) increased GFAP levels ($p < 0.05$) in EVs, but not brain tissue, in the IR group; and 2) increased HNE-bound protein adduction levels ($p < 0.05$). The results support using EVs as an early indicator of cancer therapy-induced neuronal injury.

Introduction

Radiation therapy (RT) is a well-established and commonly used treatment for cancer patients because it effectively causes cancer cell death by targeting specific areas and minimizes undesired side effects in non-target tissues [22]. However, despite treatment advances, damage to normal cells can cause serious, negative

consequences; particularly, patients receiving cranial radiation can result in cognitive impairment (CI) as damage to healthy neurons is caused by cranial radiation, which negatively impacts patient quality-of-life. Therapy-induced CI causes alterations in learning, memory, behavior, and mood [12]. Neuronal damage is detected by neuroimaging techniques and neuropsychological evaluations [28, 126]. Neuroimaging techniques, such as computed tomography, positron emission tomography, magnetic resonance imaging, and functional MRIs, detect structural and functional integrity of the brain, do not detect cellular level damage. Once neurobehavioral consequences resulting from cancer therapy have been detected, the efficacy of interventions declines [28]. As cognition remains altered long after the cessation of RT, the development of early indicators of neuronal damage would provide intervention capability.

The unique characteristics of extracellular vesicles (EVs) make them useful clinical tools: they are circulating, membrane-bound organelles released by nearly every cell in the body and contain molecular cargo that are protected from enzymatic degradation by a lipid bilayer [1, 104]. While the roles of EVs in normal and pathophysiological diseases have been extensively studied, the clinical use of EVs has only recently been appreciated [1-3, 137]. We have demonstrated their potential as an earlier detector of cardiomyocyte damage following doxorubicin (DOX) treatment than the current standard method of measuring troponin levels [4, 102].

Ionizing radiation (IR) generates ROS, leading to increased oxidative damage [22]. Under normal physiological conditions, reduction-oxidation (redox) regulation

is tightly controlled by coordinating endogenous antioxidant systems [16]. The hydroxyl radical ($\bullet\text{OH}$) can attack polyunsaturated fatty acids and initiate lipid peroxidation, making it an especially damaging free radical that IR generates [14]. 4-hydroxy-2-nonenal (HNE) is a highly reactive product of lipid peroxidation and can covalently adduct to histidine, cysteine, or lysine residues of proteins through a Michael addition reaction or can form Schiff bases with the N-termini of peptide chains and the ϵ -amino groups of lysine residues of proteins [14, 93]. HNE adduction can cause protein misfolding and modify protein activity [138].

Studies have demonstrated damage to the brain microenvironment caused by 10 Gy cranial radiation [121, 122]. Tomé et al., reported spatial memory deficits in mice receiving whole brain radiation. Decreased neuronal cell proliferation and neurogenesis were observed in mice euthanized 48 h after receiving radiation, where these observations were further augmented in mice euthanized 8 days after radiation, establishing that consequences from cranial radiation are more difficult to detect immediately following the radiation compared to later [122]. We used the same animal model to determine the potential use of EVs as an early indicator of neuronal injury induced by cranial radiation. We analyzed oxidative stress and neuronal cell markers within EVs and compared them to brain tissue, identifying HNE-adducted proteins and glial fibrillary acidic proteins (GFAP) as EVs' cargos that increased early following cranial radiation. This study provides insights into biochemical markers of astrocyte activation and oxidative damage following cranial radiation and reveals the potential use of EVs as an early indicator of brain injury.

Materials and Methods

Animals and Treatment

Male C57BL/6J mice 10-12 weeks old and 25-28 grams body weight were housed at the University of Kentucky (UK), following the American Veterinary Medical Association Guidelines for the Care and Use of Laboratory Animals; UK's Institutional Animal Care and Use Committee approved their use. Ketamine at 100 mg/ml (Henry Schein, Inc.) with Xylazine at 20mg/ml (Akorn, Inc.) diluted in saline were used as anesthesia prior to cranial radiation treatment. Irradiated mice received one dose of 10 Gray cranial radiation using the X-ray irradiator, X-RAD 225XL, Precision X-ray (PXI), Inc. (225 kVp peak voltage, 0.3 mm Cu filtration, and 0.92 mm Cu beam quality). The irradiator was calibrated with in-air method following American Association of Physicist in Medicine TG-61 protocol [139] with an ADCL calibrated A1SL ion chamber (Standard Imaging Inc.) [140]. Radiation field was set at 1.41 by 1.2 cm with field light guidance to cover the mice brain. Source to skin distance of mice on panel was 40 cm. The 10 Gy dose was prescribed at 5 mm depth. A Monte Carlo simulation assessed the effect of attenuation and backscatter from the mice and panel. Irradiation varies from 390-398 sec as the dose rate fluctuates, but dose delivered stays constant (<0.1%). Control mice were also anesthetized. Mice were returned to the UK Animal Care Facility following radiation and body weight was measured at 24 h and 48 h. A total of 22 sham mice and 23 IR mice were treated. Blood samples were collected via left ventricle puncture and mice brains were isolated and separated via sagittal dissection.

Blood Samples and Isolation of EVs

Isolated blood was allowed to clot at room temperature for 30 min and then was centrifuged at 1,300 g for 15 min to separate the serum, which was then separated into aliquots and stored at -80°C. EVs were isolated from serum using SmartSEC™ HT EV Isolation System for Serum & Plasma (System Biosciences), which isolates EVs into two different fractions (fractions 1 and 2) using size exclusion chromatography. From the total number of mice used during radiation, a total of 15 sham mice and 16 IR mice were selected for EV isolation. Fraction 2 was used for protein immunoblotting with Jess Protein Simple technology (San Jose, CA, USA) and nanoparticle tracking analysis (NTA); fraction 1 was used for HNE protein adduction measurement. BCA assay from ThermoFisher measured protein concentration.

Nanoparticle Tracking Analysis

EVs particle size distribution was determined by NanoSight NS300 (Malvern Panalytical, UK). Fraction 2 of SmartSEC HT isolated EVs were diluted with PBS to achieve particle range of 20-100 particles per frame on an instrument. Specimens were analyzed at 25°C at camera level 15 and detection threshold level at 4. Five 60-second videos were recorded for each specimen. Each video was analyzed with NTA 3.2 software (Malvern, UK) and data were recorded and analyzed.

HNE adducted protein measurement

4-hydroxy-2-nonenal protein adductions in mouse serum and EVs isolated from the serum were measured using standardized immunoblots from the Redox Metabolism Shared Resource Facility of the UK Markey Cancer Center. The facility utilizes the previously documented slot-blot method to quantify the number of HNE protein adducts [141]. EVs from fraction 1 were lysed with radioimmunoprecipitation assay buffer and protein concentration was measured by BCA assay kit (ThermoFisher). Bands from HNE immunoblotting were documented with Adobe Photoshop and quantified using Scion Image. Band intensities for HNE protein adducts were normalized utilizing sample standards across multiple blots to compare detected intensities. Samples from 14 mice in each group were used for serum and EV HNE- adducted proteins.

Protein Immunoblotting

EVs or homogenized brain tissue samples were lysed with RIPA buffer and separated by capillary electrophoresis using Jess by Protein Simple © technology (San Jose, CA, USA). The primary GFAP antibody was purchased from Aviva Systems (OAEB01041, 1:20 dilution). The anti-goat secondary antibody used was supplied by Protein Simple. Compass Software analyzed the data. Protein normalization plates were used for EVs samples, and total area under the curve for each peak detected by the responding protein antibody was normalized by the total protein area.

Immunohistochemistry

Half of the brain was fixed in 4% paraformaldehyde in PBS for 48 h and then in 30% sucrose for staining by the Biospecimen Procurement and Translational Pathology Shared Resource Facility of the Markey Cancer Center. Immunohistochemistry (IHC) staining for GFAP was performed using the Ventana Discovery Ultra Autostainer. The antigen retrieval was set at “cc1 standard” and incubated with the primary antibody (1:2000, Abcam, ab7260) at 37°C for 1 h prior to detection by Ventana OmniMap HRP and Ventana DAB, according to manufacturer’s recommendations. Ventana Discovery Ultra Autostainer also performed HNE IHC staining, at a “cc2 mild” setting and a horse serum blocking step. The primary antibody for HNE (1:100, Abcam, ab46545) was incubated at room temperature for 1 h prior to detection by Ventana OmniMap HRP and Ventana DAB, according to manufacturer’s recommendations. Following IHC staining, slides were uploaded onto Aperio eSlide Manager and then quantified with HALO software (version 3.2) by Indica Labs. The area quantification algorithm v2.1.7 was used to detect positive staining of the markers indicated; quantity of positive staining in the sham and IR groups was assessed. 5 representative mice from both sham and IR groups were utilized for IHC staining.

Statistical Analysis

Descriptive statistics, including means and standard deviation, that were calculated for each group are represented in bar graphs. Pairwise comparisons of sham vs. IR were performed using two-sample t-test for several quantitative endpoints, including EVs protein levels, EVs particle size, AUC of several proteins,

HNE, IHC levels. Body weight measurements were repeatedly summarized and compared using linear mixed models to account for repeated measurements of mice. A nonlinear mixed model was employed to determine the association of vesicle count migration as a function of vesicle diameter, treatment group (IR vs. sham) and interaction between these two factors. The vesicle count was modeled as a negative binomial distribution allowing for random effects of intercept across mouse blood samples and separate covariance specifications for each treatment group. Validity of assumptions and equality of variance of parametric tests and models were tested; data were log transformed as necessary. Statistical analyses were performed using SAS version 9.4.

Results

Cranial radiation causes significant weight loss and increased levels of serum proteins

To monitor general radiation effects, we determined body weight, serum protein concentration, and serum HNE levels of male C57BJ/6 mice, which were given 10 Gy cranial radiation, the dose reported to cause cognitive impairment in mice and replicates effects seen in human patients who receive whole brain radiation treatment [121, 122]. Decrease in body weight of mice after radiation was statistically significant ($p < 0.05$) (**Fig. 2.1A**). Increase in serum protein concentration in the IR group was statistically significant compared to sham group ($p < 0.05$, **Fig. 2.1B**). No differences were observed in the amount of HNE-adducted proteins in the serum of the IR mice compared to the sham group ($p = 0.95$, **Fig. 2.1C**).

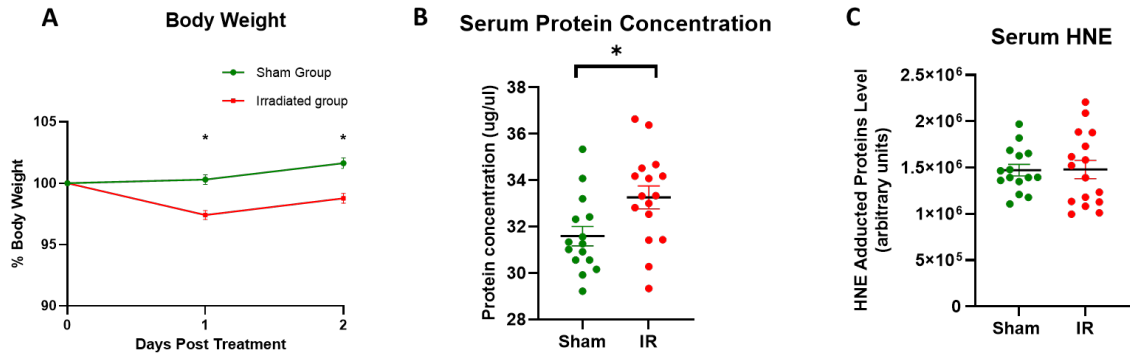


Figure 2.1 Different changes in mice weight and protein concentration were observed in the sham and IR group.

(A) Significant change was observed in the mice that received the cranial radiation compared to the sham group ($p < 0.05$). (B) Serum protein levels were elevated in the IR group (red dots) compared to the sham group (green dots) as measured by the BCA assay. (C) The levels of HNE adducted proteins were measured and the differences were not significant in the two groups.

Radiation caused no significant differences in GFAP or HNE in brain tissue

Mice brains were removed and separated sagittally. The brain half that was to be homogenized was first separated into the hippocampus and cortex for quantification of GFAP. The two groups showed no significant difference in the amount of GFAP in brain tissue lysate (**Fig. 2.2A**). Each tissue slice of the hippocampus, which plays a role in new memory formation, was used for quantification, which considered brain tissue heterogeneity. The two groups

showed no significant statistical difference in IHC staining of HNE (**Fig. 2.2B**). IHC measurement of GFAP in brain tissue was not significantly different (**Fig. 2.2C**).

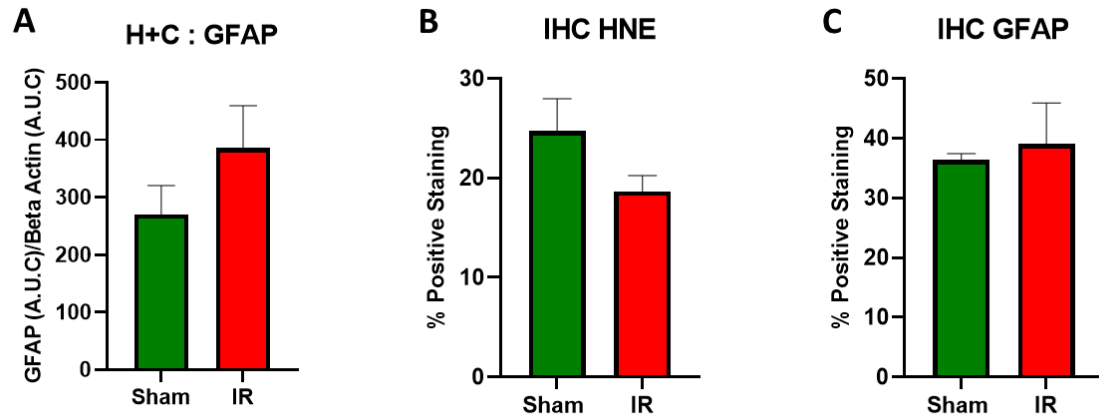


Figure 2.2 IHC staining of brain tissue and brain tissue lysates revealed no observable changes.

Probing for GFAP in the brain tissue lysate (**A**) also revealed no significant differences. Additionally, quantification of IHC staining of HNE (**B**) and GFAP (**C**) in the brain tissue resulted in no significant differences.

Radiation- induced differences in astrocyte marker and oxidative stress are detectable in EVs

EVs isolated from mouse sera were evaluated for protein concentration differences (**Fig. 2.3A**) and for the number of EVs particles released by the two groups, utilizing nanoparticle tracking analysis (NTA) (**Fig. 2.3B**); the two groups showed no significant differences in EVs protein concentration or in the number of EVs particles observed. However, when the comparison of vesicle counts between the IR versus sham groups was adjusted for vesicle size, there was a significant

difference between the two groups ($p < 0.05$); specifically, the difference between groups is evident and dependent according to vesicle size (**Fig. 2.4A**) which is corroborated by seeing a significant interaction term ($p < 0.01$) between group and vesicle size in the analysis model. To evaluate the amount of oxidatively modified proteins in the EVs, the EVs were lysed and measured for HNE adductions by HNE immunoblotting. Unlike both mice brain tissue and serum, HNE adducted proteins showed a statistically significant increase in the EVs isolated from the radiation-treated mice compared to the control (**Fig. 2.3C**, $p < 0.05$). A significant increase was consistently detected in the amount of GFAP in EVs from the IR mice compared to the sham group (**Fig. 2.3D**, $p < 0.01$).

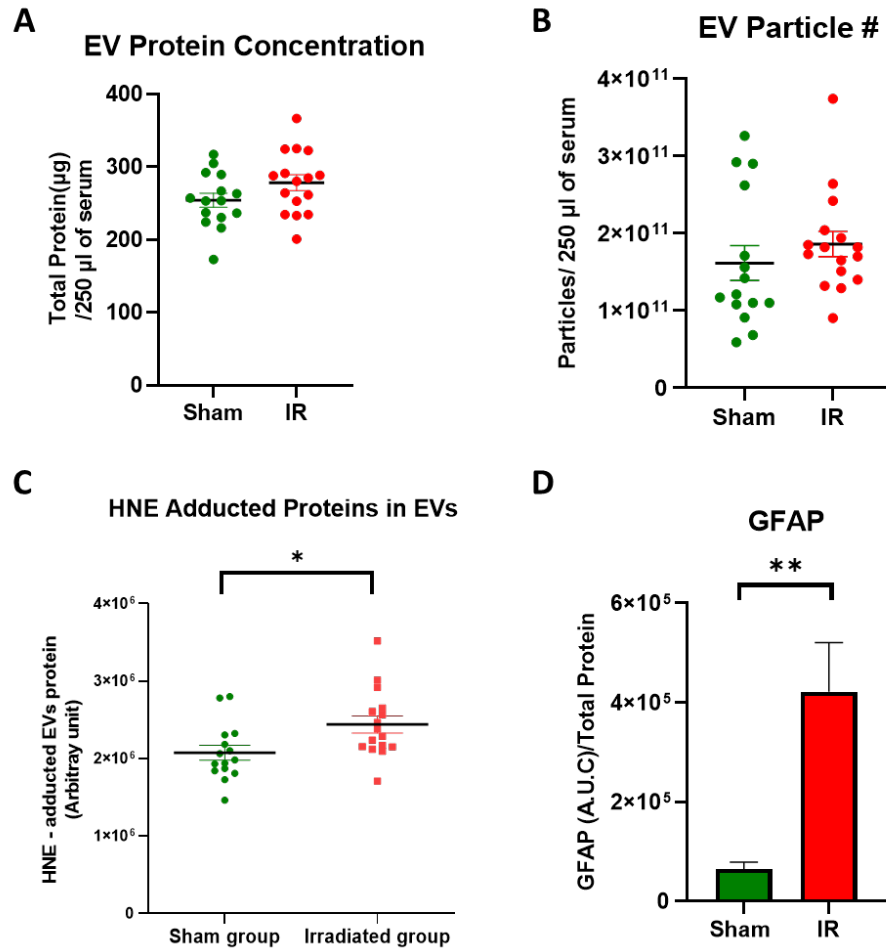
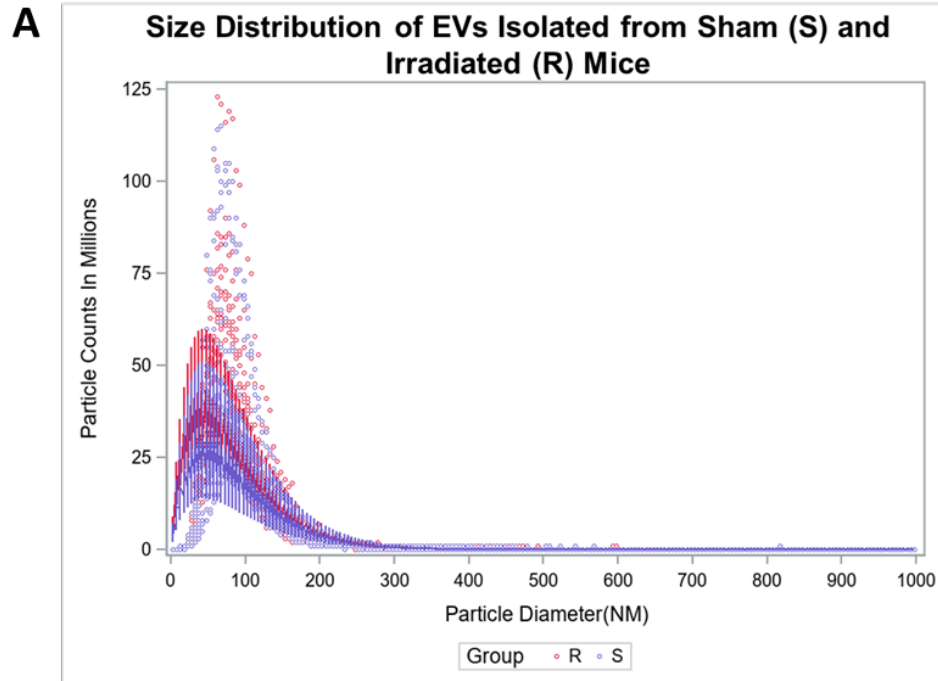
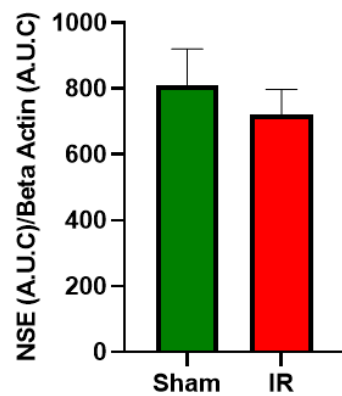


Figure 2.3 Elevated levels of HNE and astrocyte activation were observed in the EVs obtained from the IR mice.

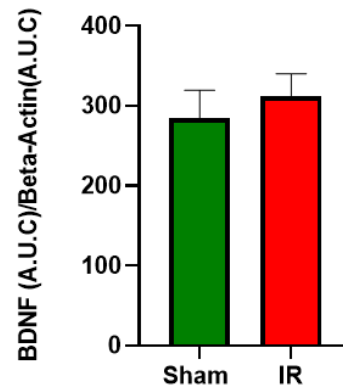
The protein concentration (**A**) and the number of EVs particles (**B**) appeared to be elevated in the IR mice compared to the sham group, though neither reached statistical significance ($p=0.059$ and $p=0.282$, respectively). However, EVs lysates isolated from the IR mice had an increase in HNE adducted proteins (**C**, $p<0.05$) and GFAP (**D**, $p<0.05$) compared to the sham group.



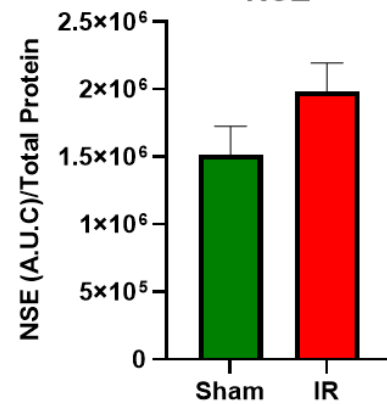
B **H + C : NSE**



C **H + C : BDNF**



D **EV Lysate: NSE**



E **EV Lysate: BDNF**

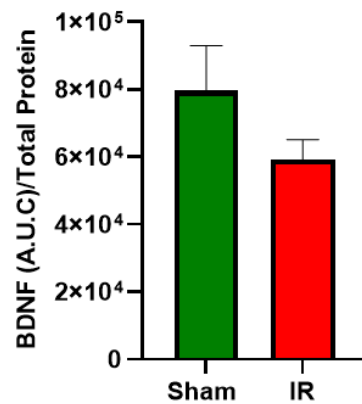


Figure 2.4 Size distribution of EVs, neuronal specific enolase (NSE), and brain-derived neurotrophic factor (BDNF) in the sham and IR groups.

(A) There is a difference in vesicle counts between IR vs. sham ($p < 0.05$) which is dependent on vesicle size. Specifically, there is a significant interaction ($p < 0.01$) between group and vesicle size in the analysis model. Observed data (in dots) and fitted data (lines) from the model indicate separation of vesicle counts between groups according to vesicle size. **(B)** Neuronal- specific enolase (NSE, a marker of neuronal damage) and **(C)** Brain- derived neurotrophic factor (BDNF, indicator of neuronal genesis) were probed in homogenized brain tissue; no statistically significant differences were observed. **(D)** NSE and **(E)** BDNF were also not significant when measured in the EVs lysates in the two groups.

Discussion

Cancer therapy-induced cognitive impairment is a serious side effect seen in cancer survivors. Neuroimaging and neuropsychological evaluations, the standard methods currently used to detect brain alterations associated with neurocognition decline, are limited and do not detect neuronal damage early enough for intervention to occur that would mitigate consequences [28, 126]. In this study, we assessed whether markers of brain injury could be detected earlier in serum EVs than in brain tissue, utilizing radiation exposure as a model. Our results demonstrate that within 48 h following radiation treatment, radiation-induced brain injury, indicated by elevated levels of HNE-adducted proteins and radiation-

induced an increase in GFAP, are detectable in EVs. Other potential markers of neuronal damage (NSE) and neuronal genesis (BDNF) were quantified in both homogenized brain tissue and EV lysates, but resulted in no statistical significance between the two groups (**Fig. 2.4B-E**). This work suggests EVs are an early indicator of alterations to the brain microenvironment following cranial radiation. The results are consistent with our previous studies showing the levels of HNE-adducted proteins in mitochondrial lysates of animals treated with doxorubicin are increased nearly two-fold [102]. Importantly, this method provided earlier detection than the standard method of measuring cardiac troponin levels does [12]. Therefore, our findings support a potential role of EVs as an early indicator of damage to the brain following toxic insults to the brain.

While we did not detect significant changes in biochemical markers in brain lysates or immunohistochemical analysis of brain tissues, we observed a trend of increase in GFAP (**Fig. 2.2**). These observations are also consistent with previous studies that demonstrate how changes in neuronal generation and microglia activation were minor at 48 h after radiation treatment [122]. One potential mechanism leading to this observed difference between the increase in GFAP measured in the EVs and GFAP in the brain tissue could be a compensatory mechanism to dispose of oxidatively modified proteins due to the cranial radiation. It has been shown that EVs are being used to remove oxidatively modified proteins from the brain [142]. Thus, it is possible that the observed increase in GFAP in EVs but not in the brain tissue between the two groups is due, in part, to increased removal of oxidatively modified proteins by EVs.

The presence of HNE-adducted proteins in EV lysates also implicates a mechanism of tissue injury because HNE is a highly reactive end product of lipid peroxidation. The consequences of oxidative stress, and notably HNE, on the progression of neurodegenerative disorders have been extensively reviewed [15-18]. The role of oxidative stress, indicated by the level of HNE, on declining neurocognition substantiates that EVs containing HNE-adducted proteins are valuable indicators of tissue damage.

GFAP, a marker of reactive astrocytes, which is activated by injury to the brain and has been shown to be increased in a variety of CNS disorders and neurodegenerative diseases, such as Alzheimer's disease [143, 144], was also significantly increased. Finding GFAP increased in EVs but not in brain tissue further corroborates the benefit of using EVs as an early and more sensitive indicator than tissue histology of potential progression of neurodegeneration. The increase of GFAP and HNE observed in the EVs, but not detectable in either mice brain tissue or serum, may be a result of the EVs protecting their molecular content from proteolytic degradation prior to EVs release or while in circulation. Because HNE is highly reactive, exposure to other cellular components in circulation may provide more challenges to quantifying HNE-adducted proteins in serum compared to EVs, where HNE-adducted proteins remain stable.

We and others have previously demonstrated the role of oxidative stress and inflammation in neurodegenerative diseases and cancer therapy- induced cognitive impairment [145]. Possibly, the observed increase in HNE-adducted proteins in EVs could potentially contribute to inflammation. Inflammatory

cytokines such as TNF- α have been shown to induce reactive astrocytes, which could cause the increased expression of GFAP observed in this study [21, 25, 146-149]. However, extensive cause/effect relationship studies will be needed to support this proposed link.

In summary, the present study demonstrates the benefit of using EVs as an early marker of brain damage following treatment with a dose of cranial radiation that has been documented to cause long-term neuroanatomical alterations. Our results highlight the significance of changes in the markers of oxidative stress and glial cell activation observed in EVs prior to structural changes in brain tissue. Importantly, these tests can be performed using small amounts of available mice serum, suggesting the study is applicable to situations where only small amounts of blood are available. A limitation of the study is GFAP is not only present in brain cells but is also expressed in other tissues, particularly, cancer tissues. However, since the animals used did not have any cancer, this limitation does not detract from the observation that EV cargos are an early indicator of alterations to the brain microenvironment and are potential indicators of cancer therapy-induced cognitive impairment.

CHAPTER 3. EXTRACELLULAR VESICLES RELEASED BY ACUTE LYMPHOBLASTIC LEUKEMIA PATIENTS CONTAIN HNE-ADDUCTED PROTEINS: IMPLICATIONS OF COLLATERAL DAMAGE

Overview

Off-target neuronal injury is a serious side-effect observed in cancer survivors. It has previously been shown that pediatric acute lymphoblastic leukemia (ALL) survivors have a decline in neurocognition compared to healthy age-matched counterparts. Elevated oxidative stress has been documented to be a mediator in off-target tissue damage in cancer survivors. Early detection of oxidative stress markers may prevent off-target tissue damage. Extracellular vesicles (EVs) have surfaced as a potential diagnostic tool due to their lipid membrane and molecular cargo they contain. We investigated the potential for EVs to be a sensitive indicator of oxidative stress and off-target tissue damage by isolating EVs from pediatric ALL patients throughout their first 2 months of treatment. EVs were measured throughout the collection points for: 1) number of EV particles generated using nanoparticle tracking analysis (NTA); 2) markers of neurons (NeuN), astrocyte activation (GFAP), neuronal stability (BDNF), 3) markers of pre-B cell ALL (CD19 and CD22); and 4) 4-hydroxy-2-nonenal (HNE) adducted proteins. HNE protein adductions were measured in the patient sera and CSF. Pro-inflammatory cytokine levels were also measured in patient sera because of their contribution to oxidative stress and neuronal injury. Our results: 1) demonstrate EVs are a sensitive indicator of oxidative damage; 2) suggest EVs as a marker of a decline in neuronal stability; and 3) show the presence of leukemia has a greater contribution to pro-inflammatory cytokine production than the cancer

treatment. The results support the utilization of EVs as a sensitive marker of oxidative stress.

Introduction

In 2022, there are projected to be 15,000 new cases of pediatric and adolescent cancer in the United States [11]. While the mortality rate for cancer patients has been in decline because of advances in cancer therapies and detection methods, some cancer therapies may result in off-target tissue damage, including damage to the central nervous system (CNS), due in part to increased oxidative stress. For example, radiation generates reactive oxygen species (ROS) to kill cancer cells [22], and 50% of chemotherapeutic agents currently being used have been associated with increased ROS generation [21]. In particular, pediatric cancer patients are highly susceptible to off-target neuronal damage due to their active development and the various chemotherapy agents they receive during their cancer treatment [128].

Acute lymphoblastic leukemia (ALL) is the most commonly diagnosed pediatric malignancy, with a median age of diagnosis between 2 and 5 years of age. Because of its high survival rate (~90% at 5 years), pediatric ALL patients often experience off-target tissue damage post-treatment, which can affect quality of life following the cessation of cancer therapy [11, 150]. Long-term studies demonstrate a decline in neurocognitive function in approximately one third of survivors of pediatric ALL compared to healthy age-matched counterparts [28, 124, 151]. It is thus critical to identify early markers of neurocognitive decline to mitigate this off-target tissue injury [124].

Pediatric ALL patients receive a number of different chemotherapy agents over their approximately two-year treatment regimen [129]. Previously, patients received cranial radiation to mitigate the potential of CNS metastases [152]; currently, following the clinical study AALL0932, methotrexate (MTX, an anti-folate) and cytarabine (an antimetabolite) are given to the patients via intrathecal (IT) injection rather than cranial radiation [129]. Additional chemotherapy agents given to these patients intravenously or orally include pegaspargase, vincristine, cyclophosphamide, mercaptopurine, danorubicin, and one or more steroids [129]. Despite this change in treatment protocol from cranial radiation to solely chemotherapy agents for a majority of pediatric ALL patients, the decrease in neurocognitive function in pediatric ALL survivors compared to healthy age-matched counterparts remains [28], perhaps due to oxidative damage caused by ROS generation.

ROS in the brain induces glial cell activation, accumulation of misfolded proteins, mitochondrial dysfunction, and lysosome and protease dysfunction [23, 134]. Additionally, the generation of ROS, specifically the hydroxyl radical ($\bullet\text{OH}$), can lead to lipid peroxidation (LPO). When LPO of omega-6 polyunsaturated fatty acids occurs, 4-hydroxy-2-nonenal (HNE) is formed [14]. HNE is an electrophilic aldehyde that reacts with the cysteine, lysine, and histidine amino acids on proteins via a Michael addition, making HNE the most reactive product of LPO [14]. HNE is elevated in several different disease pathologies and has been implicated in neurodegenerative diseases associated with protein aggregates, such as Alzheimer disease [17, 18]. We hypothesize that the overproduction of ROS leads

to intracellular accumulation of misfolded proteins via the inhibition of the cell's canonical methods of removing unwanted molecular products. Therefore, the cell needs another way to discard this molecular debris.

Extracellular vesicles (EVs) are lipid-bound organelles that are secreted from nearly every cell in the body and can modulate downstream events following uptake by other cells [1, 2]. The lipid membrane of EVs protects their molecular content from enzymatic degradation once in circulation, allowing it to be assessed for indications of dysregulation within a system, and this feature of EVs has been exploited for the purpose of drug delivery [3, 4, 29]. Research highlighting the role these organelles play in both normal and pathophysiology is abundant [5-9]. For example, miRNAs isolated from EVs can modulate the immune response [105], and EVs have been shown to promote a pro-tumorigenic environment by promoting epithelial- to- mesenchymal transition [6]. These studies highlight the role of EVs in normal and pathophysiology and the necessity to further explore their clinical potential.

Previously, our group characterized EVs as early indicators of cardiomyocyte damage *in vivo* following treatment with the ROS-generating chemotherapy agent doxorubicin [102]. As shown in chapter 2, we also recently demonstrated that EVs are a more sensitive indicator of oxidative stress than astrocyte activation in brain tissue isolated from mice treated with a single dose of 10 Gy cranial radiation [48]. Together, these findings demonstrate that EVs are an early indicator of off-target tissue damage following doxorubicin and radiation therapy and highlight the downstream effects of elevated levels of oxidative stress.

Based on these important findings, we aimed to determine if EVs would contain markers of neuronal injury associated with the observed alteration in neurocognition in pediatric ALL survivors [124, 151].

In this study, we investigated the HNE adduct levels of selected neuronal proteins utilizing EVs derived from pediatric ALL patients during the first two months of their cancer treatment, based on the idea that the presence of HNE adducted proteins is the result of chemotherapy-induced oxidative stress. We found that EVs are a more sensitive indicator of changes in HNE adduction compared to both the serum and the cerebrospinal fluid (CSF). We also observed a decrease in the neurogenesis marker, brain derived neurotrophic factor (BDNF), in the EVs throughout the treatment of the patients. Moreover, we demonstrated the effect of EVs derived from leukemia cells on the generation of pro-inflammatory cytokines. Our findings suggest the potential for the use of EVs as an indicator of oxidative damage and neurogenesis decline in ALL survivors.

Materials and Methods

Patients

The University of Kentucky's Medical Institutional Review Board reviewed and approved this clinical study prior to engagement or enrollment of the participants (IRB #46811). Pediatric ALL patients treated at the Dance Blue Kentucky Children's Hospital Hematology/Oncology Clinic were recruited to participate in the study between January 26, 2019, and March 14, 2022. All study participants and/or their legal guardians provided written informed consent to participate in the study. During the patient's routine blood draws, an additional 3

mL of blood was drawn for this study. Additionally, any discarded CSF available after the child's routine care and treatment for cancer was collected. The blood and CSF were collected at five different time points during the patient's treatment: day 1 and day 29 of their induction therapy, and days 1, 8, and 15 during their consolidation therapy (shown schematically below in **Figure 3.1**). On day 1, CSF and serum were collected prior to the administration of chemotherapy agents. A total of 21 patients were recruited for the study; 17 had both blood and CSF collected for all five collection time points. Patient age, sex, race, ethnicity, ALL subtype, and known genetic defects are listed in **Table 3.1**.

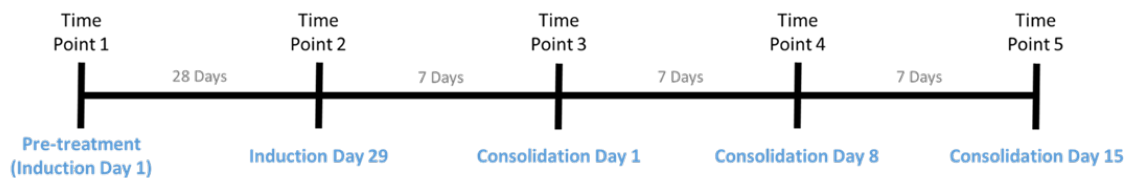


Figure 3.1 Schematic of collection time points

The above figure documents the three phases of treatment where patient samples were collected: Pre-treatment, Induction, and Consolidation. At time point 1 blood was collected on their first day of treatment, prior to the introduction of any chemotherapy agents, at time point 2, blood was collected at the end of their induction therapy, and at time points 3, 4, and 5 blood samples were collected during their consolidation phase.

Table 3.1 Patient Demographics

PT NO.	AGE (YEARS) AT PRE- TREATMENT	SEX (MALE/ FEMALE)	RACE	ETHNICITY	ALL SUBTYPE	KNOWN GENETIC DEFECTS
1	6	M	White	Non-Hispanic	Pre-B Cell	ocular albinism
2	4	M	White	Non-Hispanic	Pre-B Cell	N/A
3	9	M	White	Non-Hispanic	Pre-B Cell	N/A
5	6	M	White	Non-Hispanic	Pre-B Cell	N/A
6	2	M	White	Non-Hispanic	Pre-B Cell	N/A
7	6	F	White	Non-Hispanic	T-Cell	N/A
8	7	F	White	Non-Hispanic	Pre-B Cell	N/A
9	13	F	White	Non-Hispanic	Pre-B Cell	N/A
10	3	F	Bi-racial	Non-Hispanic	Pre-B Cell	N/A
11	3	F	White	Non-Hispanic	Pre-B Cell	protein s deficiency
12	4	M	White	Non-Hispanic	T-Cell	N/A
13	4	M	White	Non-Hispanic	Pre-B Cell	N/A
14	7	F	White	Non-Hispanic	Pre-B Cell	N/A
15	7	M	White	Non-Hispanic	Pre-B Cell	N/A
17	4	M	White	Non-Hispanic	Pre-B Cell	N/A
18	1	M	White	Non-Hispanic	Pre-B Cell	N/A
19	3	F	Bi-racial	Non-Hispanic	Pre-B Cell	N/A
20	3	M	White	Non-Hispanic	Pre-B Cell	N/A
21	2	M	White	Non-Hispanic	Pre-B Cell	N/A
22	18	M	Black	Non-Hispanic	Pre-B Cell	N/A
23	1	M	White	Non-Hispanic	Pre-B Cell	N/A

Patient Sample Storage

The blood was collected in BD Vacutainer Serum 4.0 mL tubes (catalog #: 367812). Within 15 minutes of blood collection in the clinic, the blood was allowed to clot at room temperature for 30 minutes. Next, the tube was centrifuged at 4 °C for 10 minutes x 1700g for separation of the serum and red blood cells. Serum was placed in a cryogenic vial. If large amounts of serum remained, the remaining serum and part of the red blood cell pellet were allocated into a 1.5 mL Eppendorf tube and centrifuged again at 4 °C for 10 minutes x 1700g, prior to transferring into cryogenic vials. Samples were then stored in a -80 °C freezer.

The CSF was centrifuged at 4 °C for 10 minutes x 2000 g immediately following collection from the clinic to remove debris. After centrifugation, the CSF was allocated into cryogenic vials and stored at -80 °C.

Isolation of EVs from Patient Sera

EVs were collected from patient sera utilizing the SmartSEC™ HT EV Isolation System for Serum & Plasma from System Biosciences (catalog #: SSEC096A-1). The serum was thawed on ice and then centrifuged at 4 °C for 5 minutes at 2500 rpm to collect serum at the bottom of the vial. The supernatant was then transferred into a 1.5 mL Eppendorf tube and further centrifuged at 4 °C for 15 minutes x 3000g to pellet debris. The supernatant was transferred again to a new 1.5 mL Eppendorf tube and centrifuged at 4 °C for 15 minutes x 12000g to pellet debris. The supernatant collected after this time was used for the EV isolation. The EVs were isolated following the manufacturer's protocol. Briefly, 330 µL of serum were placed in the columns in the SmartSEC™ HT EV Isolation plate

for isolation of EVs and incubated at room temperature for 30 minutes. The plate was then centrifuged to collect the first fraction of EVs. Next, 330 μ L of buffer provided by the manufacturer were allotted into each column and collected through centrifugation. This collected EV fraction was used for downstream applications. In compliance with recommendations for the “Minimal information for the studies of extracellular vesicles” published by Thery *et al.* in 2018 (MISEV2018), we probed for three markers of EVs (**Figure 3.2a-c**) and a contamination marker (**Figure 3.2d**) using protein immunoblotting [31]. Transmission electron microscopy (TEM) was also performed to assess EV morphology (**Figure 3.2e**).

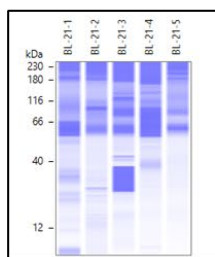
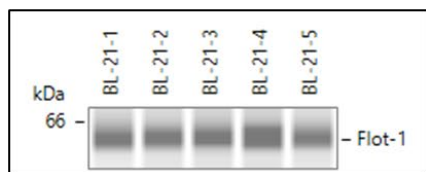
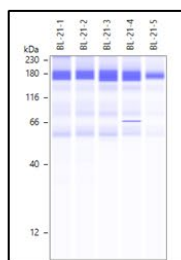
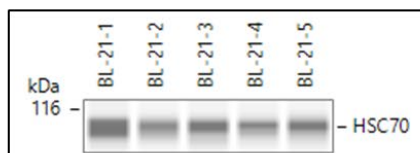
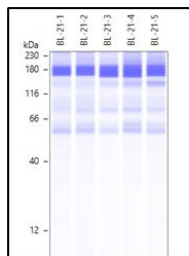
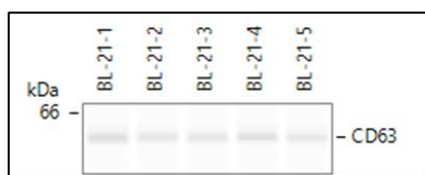
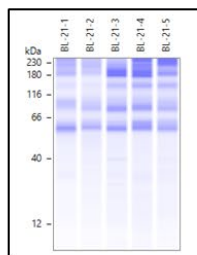
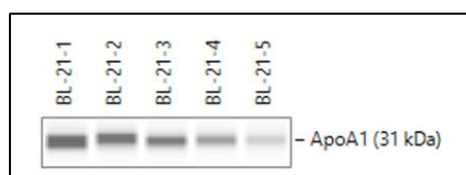
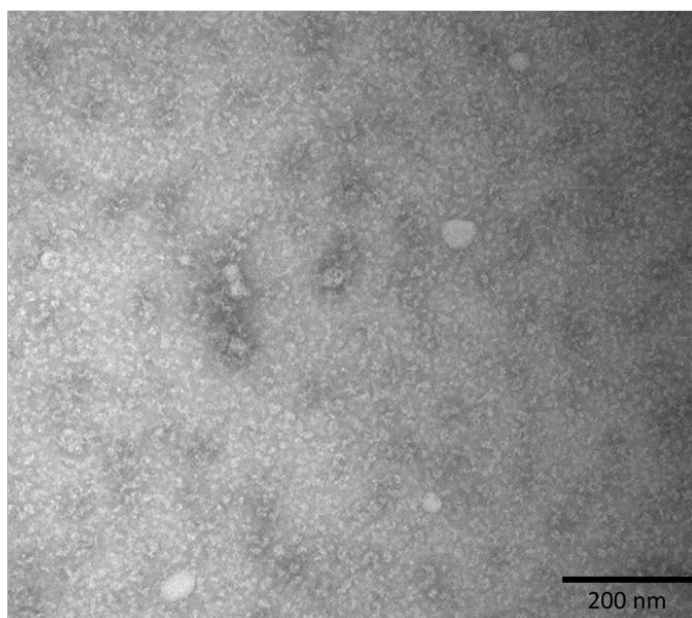
A**B****C****D****E**

Figure 3.2 Characterization of EVs Isolated from patient sera based on MISEV2018.

Based on MISEV2018 recommendations, protein immunoblotting was used to measure three markers associated with EVs in EVs isolated from patient sera: Flot-1 **(A)**, HSC70 **(B)**, and CD63 **(C)**. A serum contamination marker (ApoA1) was also measured in the EVs **(D)**. Morphology was assessed using TEM **(E)**.

Protein Concentration Measurement and Concentration of EVs

Protein concentrations for the patient- and cell culture-derived EVs, EV lysates, CSF, and serum derived from patients were quantified by the bicinchoninic acid (BCA) method using a kit from ThermoFisher Scientific (catalog #: 23228). The manufacturer's protocol was followed.

For EVs, if a higher protein concentration ($>1 \mu\text{g}/\mu\text{L}$) was needed for downstream applications such as protein immunoblotting, EVs were placed in a centrifugal filter (Amicon Ultra-15, catalog #: UFC900324) from Millipore Sigma (St. Louis, MO). EVs were then centrifuged at 4°C at $14000g$ for 10-60 minutes, depending on the starting protein concentration (e.g., samples with a starting protein concentration of $0.9\text{-}1.2 \mu\text{g}/\mu\text{L}$ were centrifuged for 10 minutes, $0.7\text{-}0.89 \mu\text{g}/\mu\text{L}$ for 20 minutes, and so on). No EVs were centrifuged for more than 60 minutes to maintain the integrity of the EVs.

HNE-adducted Protein Immunoblotting

Concentrated EVs were first lysed by adding 5x RIPA buffer (Alfa Aesar, catalog #: J62524) supplemented with EDTA and protease inhibitor cocktail

(ThermoFisher Scientific, catalog #: 78430). After measuring the protein concentration of the EV lysates using the BCA method (ThermoFisher), the samples were provided to the Redox Metabolism Shared Resource Facility at the University of Kentucky's Markey Cancer Center. The facility utilizes the standardized slot-blot immunoblotting method as previously described [141]. A total of 250 ng of protein were used for quantification. Images of the bands from the immunoblotting were saved in Adobe Photoshop and quantified using Scion Image. Band intensities for HNE-adducted protein were normalized across the plates by having common samples on multiple plates, calculating the ratio from those samples, and normalizing the new plate by the ratio. All five (or all available) time points were quantified for each patient on the same plate for comparison and analysis.

Nanoparticle Tracking Analysis

Size distribution and particle number were measured by nanoparticle tracking analysis (NTA) using a ZetaView® Basic NTA instrument (Particle Metrix, Germany). EVs were diluted in phosphate-buffered saline (PBS) to obtain an optimal 20-200 particles in each frame. Eleven videos were recorded for each specimen for 0.5 seconds at room temperature. The conditions for NTA analysis were as follows: sensitivity = 70, shutter speed = 65, frame rate = 30, 1 cycle, minimum brightness = 20, maximum area = 1000, minimum area = 15, trace length = 30. The videos were analyzed using ZetaView software version 8.05.12.

Electron Microscopy

TEM and immunogold labeling were performed by Kristy Meyer in the lab of Dr. Weixiong Zhong at the University of Wisconsin-Madison. EVs were fixed by combining the sample 1:1 in 2% glutaraldehyde in 0.1 M sodium phosphate pH 7.4 (10 μ L sample + 10 μ L 0.1 M sodium phosphate pH 7.4, 1:2 dilution) for 30 minutes at room temperature. After 30 minutes, if further dilution was needed, a solution of 1:1 in 0.1 M sodium phosphate pH 7.4 for the 1:4 dilution (6 μ L of each) was used. A total of 5 μ L of fixed EVs were then placed on parafilm. A copper grid was placed on the drop for 10 minutes. Excess liquid was removed by blotting, washing twice for 5 minutes in 100 μ L sterile water, then blotted again to remove water. The final product was stained in 30 μ L 1.5% uranyl acetate in water for 45 seconds to 1 minute, blotted, and then used to perform the assay. For the immunogold labeling for HNE-adducted proteins, the antibody from Abcam (catalog #: ab48506) was diluted at 1:25. EVs were fixed as described above and then probed with the antibody to HNE-adducted proteins. EVs were diluted either 1:2 or used without dilution to acquire a similar number of EV particles in each frame. Grids were photographed with a Hitachi H-600 electron microscope.

Protein Immunoblotting

Lysed EVs and CSF were separated using capillary electrophoresis with Jess by Protein Simple © technology (San Jose, CA). The manufacturer's protocol for Jess with Protein Normalization was followed for all protein immunoblotting. The primary antibodies and their dilution used were: flotillin-1 (Flot-1) (1:20) from Bioss (catalog: BS-7798R), HSC70 (1:20) from Santa Cruz (catalog: sc-7298),

CD63 (1:10) from Santa Cruz (catalog: sc-5275), ApoA1 (1:50) from Cell Signaling (catalog: 3350), CD22 (1:50) from Protein Tech (catalog: 66103-1-Ig), CD19 (1:10) from Abcam (catalog: ab227019), GFAP (1:20) from Aviva Systems (catalog: OAEB01041), BDNF (1:50) from Abcam (catalog: ab10505), PYGB (1:50) from Novus (catalog: NBP1-32799) and NeuN from Novus (catalog: NBP1-92716). All secondary antibodies used were provided by Protein Simple. Compass Software was used to analyze the data and quantify the area under the curve with the baseline set at threshold of 1, window of 15, and stiffness of 5; the peak find was set at a threshold of 10, width of 15, and dropped lines calculation was used. The area under the curve for each protein of interest was normalized with protein normalization to account for variance in loading.

Quantification of Serum Pro-inflammatory Cytokines

Serum samples that were previously aliquoted into the cryovials and stored at -80 °C were placed on ice to thaw. Approximately 70 µL of serum was allotted into a 1.5 mL Eppendorf tube and provided to the Biomarker Analysis Lab at the University of Kentucky's Center for Clinical and Translational Science for execution of the assay. Serum levels of IL-1 β , IL-6, IL-8, and TNF- α were determined by electrochemiluminescence immunoassay (Meso Scale Diagnostic V-PLEX Human Pro-inflammatory Panel II (4-Plex), catalog #: K15053D-1). The assay was performed according to the manufacturer's instructions. Briefly, serum samples were centrifuged to pellet debris and diluted 2-fold in assay buffer. Samples and standards were added to the wells of high binding carbon electrode-bearing MULTI-SPOT microplates and incubated at room temperature for 2 hours with

constant shaking at 800 rpm. After washing, plates were incubated with a mixture of secondary antibodies for 2 hours with shaking. A final wash was performed, followed by the addition of MSD Read Buffer. Data were captured by a MESO QuickPlex SQ120 and results were extracted using Meso Scale Discovery analysis software.

Cell Culture and Viability

Human pre-B cell ALL cell lines, Reh (ATCC, CRL-8286) and SEM (DSMZ, ACC 546), and the human monocyte cell line U937 (ATCC, CRL-1593.2) were maintained in RPMI media, supplemented with 10% fetal bovine serum (FBS), 1% penicillin/streptomycin, 1 mM pyruvate, 25 mM HEPES, and 2 mM glutamine. Routine mycoplasma testing was performed in all cell lines. Cells were incubated at 37 °C in 5% CO₂. Countess 3 FL Automated Cell Counter from ThermoFisher Scientific was used to count live and dead cells following treatment.

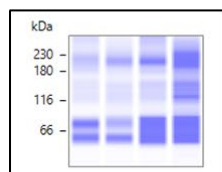
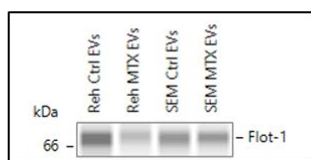
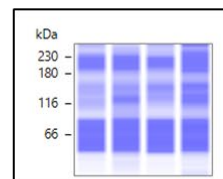
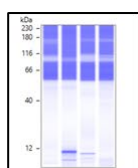
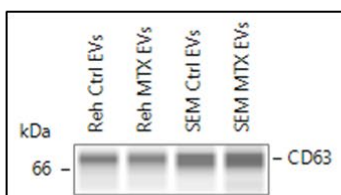
EV Isolation in vitro

Reh and SEM cells were treated with MTX at 1 µM to recapitulate the dose of MTX found in the CSF of pediatric ALL patients, as previously documented [153]. Reh and SEM cells (with a starting cell number of 5×10^7 to 7×10^7 on a 15 cm dish) treated with 1 µM of MTX were diluted directly in complete media and incubated for 24 hours. Cells were then collected in a 50 mL conical tube and centrifuged at 4 °C at 1400 rpm for 10 minutes. The media was removed, and cells were resuspended in 5 mL of PBS for rinsing. The cells were then centrifuged at 4 °C at 300g for 5 minutes, and PBS removed. The rinsing step was repeated twice. Next, the cells were resuspended in RPMI media supplemented with the

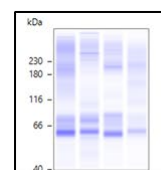
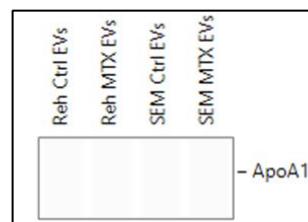
components mentioned in section 2.10, but with 10% exosome-free FBS (System Biosciences, catalog #: EXO-FBS-50A-1) and incubated for 24 hours.

After the incubation time, the cells and media were collected in a 50 mL conical tube and centrifuged at 4 °C at 300g for 5 minutes. Media was collected and placed in a separate tube. Cells were resuspended in 10 mL of PBS and counted using the Countess 3 FL Cell Counter from Invitrogen (Waltham, MA). The media collected was filtered through a 0.8 µm filter to remove large debris. The media was then placed in a centrifugal filter (catalog #: UFC900324) purchased from Millipore Sigma (St. Louis, MO) and centrifuged at 4 °C at 4000 rpm for 45 minutes. The final concentrated media (reduced to 2 to 5 mL from 35-38 mL of media) was used for EV isolation using the ExoQuick Ultra Tissue Culture kit (catalog: EQUltra-20TC-1) from System Biosciences (Palo Alto, CA) following the manufacturer's protocol.

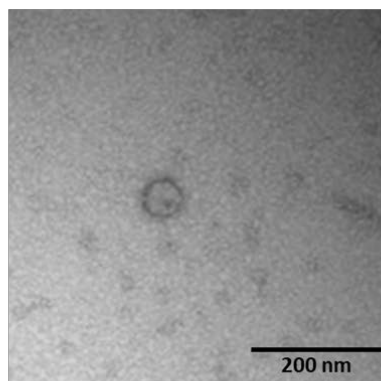
Positive markers of EVs (**Figure 3.3a-c**), contamination marker ApoA1 (**Figure 3.3d**), and TEM for the isolated EVs (**Figure 3.3e-h**) were measured in compliance with MISEV2018 guidelines to ensure proper EV isolation [31].

A**B****C**

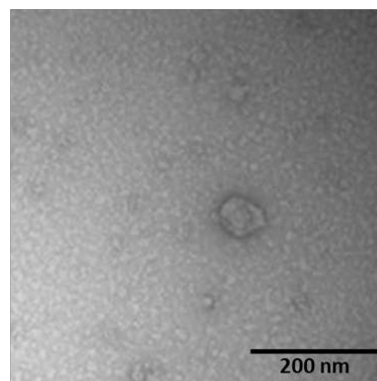
Reh Ctrl EVs (1:2 dilution)

D

Reh MTX EVs (1:2 dilution)

E

SEM Ctrl EVs (1:2 dilution)

F

SEM MTX EVs (1:2 dilution)

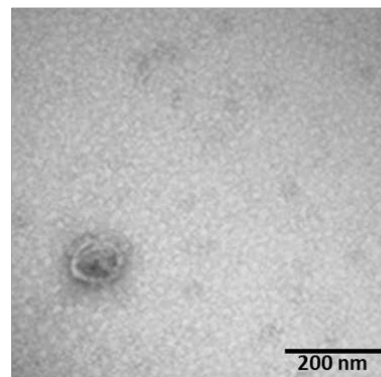
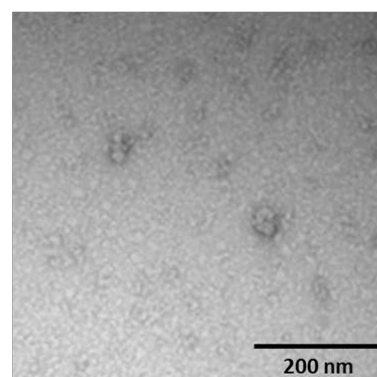
G**H**

Figure 3.3 Characterization of EVs isolated from ALL cells based on MISEV2018.

Markers associated with EVs were measured in EVs isolated from Reh and SEM cells: Flot-1 **(A)**, HSC70 **(B)**, and CD63 **(C)**. ApoA1 as a contamination marker was also measured **(D)**. Finally, TEM was performed on all four treatment groups to assess EV morphology: Reh control EVs **(E)**, Reh MTX EVs **(F)**, SEM control EVs **(G)**, and SEM MTX EVs **(H)**.

Inflammatory Cytokines Released by Macrophage Cells

A total of 3×10^6 U937 cells were plated in T75 flasks on RPMI supplemented with phorbol 12-myristate 13-acetate (PMA) at 50 ng/mL. Cells were incubated for 48 hours to allow for differentiation. Non-differentiated cells were removed by rinsing the flask with PBS. Differentiated cells were trypsinized and sub-cultured onto a 12-well plate at 5×10^5 cells per well and allowed to adhere overnight in complete media.

Media was removed, the cells were rinsed twice with PBS, and 500 μ L of FBS-free media was placed in each well. EVs isolated from the Reh and SEM cell lines were added to their respective wells at a concentration of 10 μ g of protein per well. The cells were incubated for 24 hours, and then the medium was removed from each treatment group and used for quantification of TNF- α and IL-1 β . Both the TNF- α (catalog #: 430204) and IL-1 β (catalog #: 437004) ELISA kits were purchased from Biolegend (San Diego, CA), and detection was performed

following the manufacturer's protocol. Results were analyzed using a SpectraMax Plus 384 microplate reader (Molecular Devices, San Jose, CA) with the reading at 570 nm normalized from the results at 450 nm.

Statistics

Descriptive statistics including means and standard error of the mean are calculated and presented graphically at each time point of follow up for quantitative measurements of EV and protein concentrations, HNE-adducted protein levels, cytokines, EV size distribution and particle number from NTA. Comparisons across time points were performed using linear mixed models to account for repeated measurements over time per patient; pairwise comparisons between time points were tested from the linear model. Normality assumptions on outcomes were assessed and data were log transformed if model assumptions were not met.

A nonlinear mixed model was employed to determine the association of EV particle counts as a function of EV size, time point of measurement, and the interaction between these two variables. The EV particle count was modelled as a Poisson distribution with an adjustment for overdispersion and allowing for a random effect of patient curves. The covariance modelled incorporated all the treatment groups. Specific pairwise comparisons between time points were performed for several EV sizes.

Results

Therapy induced changes in HNE-adducted protein levels in serum but not in CSF

Oxidative stress is linked to all aspects of cancer, from cancer development to cancer treatments. To gain insight into the oxidative state of ALL patients from the tumor-bearing state to the initial remission stage, as assessed by the absence of bone marrow blast cells (**Table 3.2**), we determined the level of HNE-adducted proteins in the serum and CSF. First, we measured the total protein in the serum and CSF of all children at all five time points (see **Figure 3.1**). No statistically significant difference in the protein concentration of the serum (**Figure 3.4a**) or the CSF (**Figure 3.4b**) collected from the patients was observed. Next, we measured the HNE-adducted protein levels in the serum (**Figure 3.4c**) to monitor oxidative stress. We observed a statistically significant decrease in the amount of HNE-adducted proteins from pre-treatment to induction day 29 ($p < 0.05$). HNE-adducted proteins measured during the consolidation phase statistically increased since induction day 29 ($p < 0.05$), and statistically decreased since pre-treatment ($p < 0.05$). Since CSF is used in the clinic to monitor potential CNS metastases, we also measured the level of HNE-adducted proteins in the CSF. Quantification of the signal from the immunoblotting of the CSF (**Figure 3.4d**) showed very low levels of HNE-adducted proteins in the CSF, and there was no statistically significant change throughout the treatment.

Table 3.2 Patient Bone Marrow Blast Percentage at collection time points

PT NO.	Pre-Treatment	Induction Day 29	Consolidation Day 1	Consolidation Day 8	Consolidation Day 15
1	64%	0%	0%	0%	0%
2	95%	0%	0%	0%	0%
3	80%	0%	0%	0%	0%
5	90%	2%	0%	0%	0%
6	90%	1%	0%	0%	0%
7	90%	0%	0%	0%	0%
8	90%	2%	0%	0%	0%
9	70%	1%	0%	0%	0%
10	87%	2%	0%	0%	0%
11	38%	0%	0%	0%	0%
12	90%	1%	0%	0%	0%
13	86%	0%	0%	0%	0%
14	97%	0%	0%	0%	0%
15	65%	0%	0%	0%	0%
17	87%	0%	0%	0%	0%
18	95%	1%	0%	0%	0%
19	90%	6%	0%	0%	0%
20	88%	0%	0%	0%	0%
21	77%	2%	0%	0%	0%
22	88%	0%	0%	0%	0%
23	94%	0%	0%	0%	0%

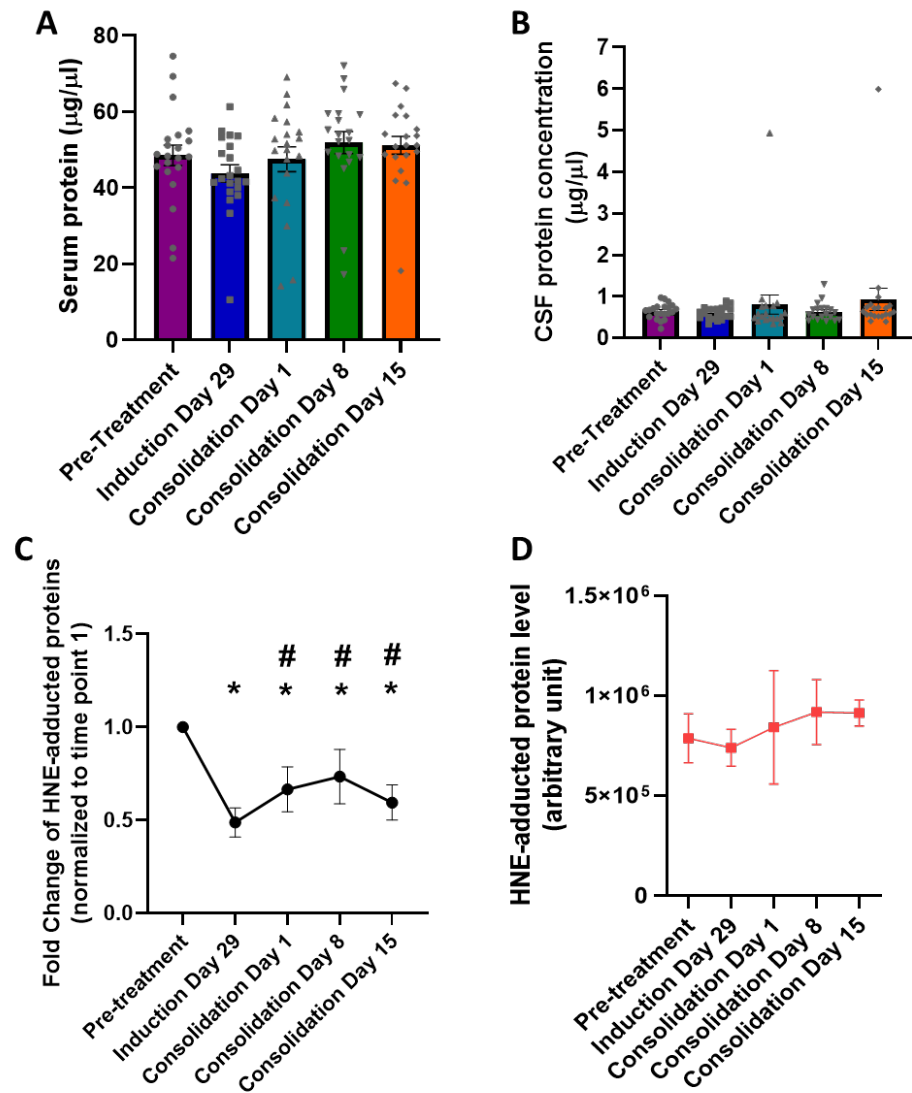


Figure 3.4 Characterization of patient sera and CSF

(A) Average serum protein concentration ($\mu\text{g}/\mu\text{L}$) for each time point. Each individual point represents a measurement from an individual patient. **(B)** Average CSF protein concentration ($\mu\text{g}/\mu\text{L}$) for each collection time point. **(C)** Relative changes in HNE-adducted proteins in serum. Each patient's individual fold change of HNE-adducted proteins in the serum was averaged

to determine overall fold change in the serum. Induction day 29 and consolidation days 1, 8, and 15 all statistically decreased compared to pre-treatment ($p < 0.05$). An increase from induction day 29 to consolidation days 1, 8, and 15 was also observed ($p < 0.05$). **(D)** HNE-adducted proteins in CSF. Average values provided for quantification of HNE-adducted proteins in the CSF from are shown. *denotes $p < 0.05$ when compared to pre-treatment and # denotes $p < 0.05$ when compared to induction day 29.

HNE-adducted proteins increased during the consolidation phase in EVs

Previously, our group has demonstrated that EVs are highly sensitive indicators of off-target tissue injury and oxidative stress [48, 102]. Therefore, we aimed to determine whether the EVs isolated from the patients in this study would contain proteins indicative of oxidative stress. A significant decrease in leukemia cells was observed from pre-treatment to induction day 29 (**Table 3.2**). Therefore, we analyzed EV protein concentration on induction day 29 and at each consolidation time point. A change observed between these time points would be a consequence of the exposure to chemotherapy agents and not an effect of the leukemia. A statistically significant decrease was seen from pre-treatment to induction day 29 ($p < 0.05$) (**Figure 3.5a**). A statistically significant increase at all 3 consolidation time points was observed compared to induction day 29 ($p < 0.05$), and from pre-treatment to consolidation days 8 and 15 ($p < 0.05$) (**Figure 3.5a**).

The highest number of EV particles generated (as measured with NTA) was observed at induction day 29 (**Figure 3.5b**), which was significantly increased

compared to pre-treatment, consolidation day 8, and consolidation day 15. However, no difference in the median size of EVs was observed throughout the treatment course (**Figure 3.5c**). A size distribution curve was also generated to visualize the relationship between particle size and EV number (**Figure 3.5d**). Finally, HNE-adducted proteins were measured in the EV lysate. Interestingly, while there was a decrease in HNE-adducted proteins from pre-treatment to induction day 29, in contrast to the HNE-adducted proteins in the serum, we saw an increase in HNE-adducted proteins in the EVs during the consolidation phase compared to both pre-treatment and induction day 29 (**Figure 3.5e**).

Furthermore, to validate that HNE-adducted proteins are located in the EVs, we performed immunogold staining of HNE-adducted proteins in isolated intact EVs. As observed in **Figure 3.5f**, HNE-adducted protein was detected on the membrane of the EVs, and some HNE-adducted proteins, which were associated with the EV on the outside near the membrane of the EV (**Figure 3.5g**).

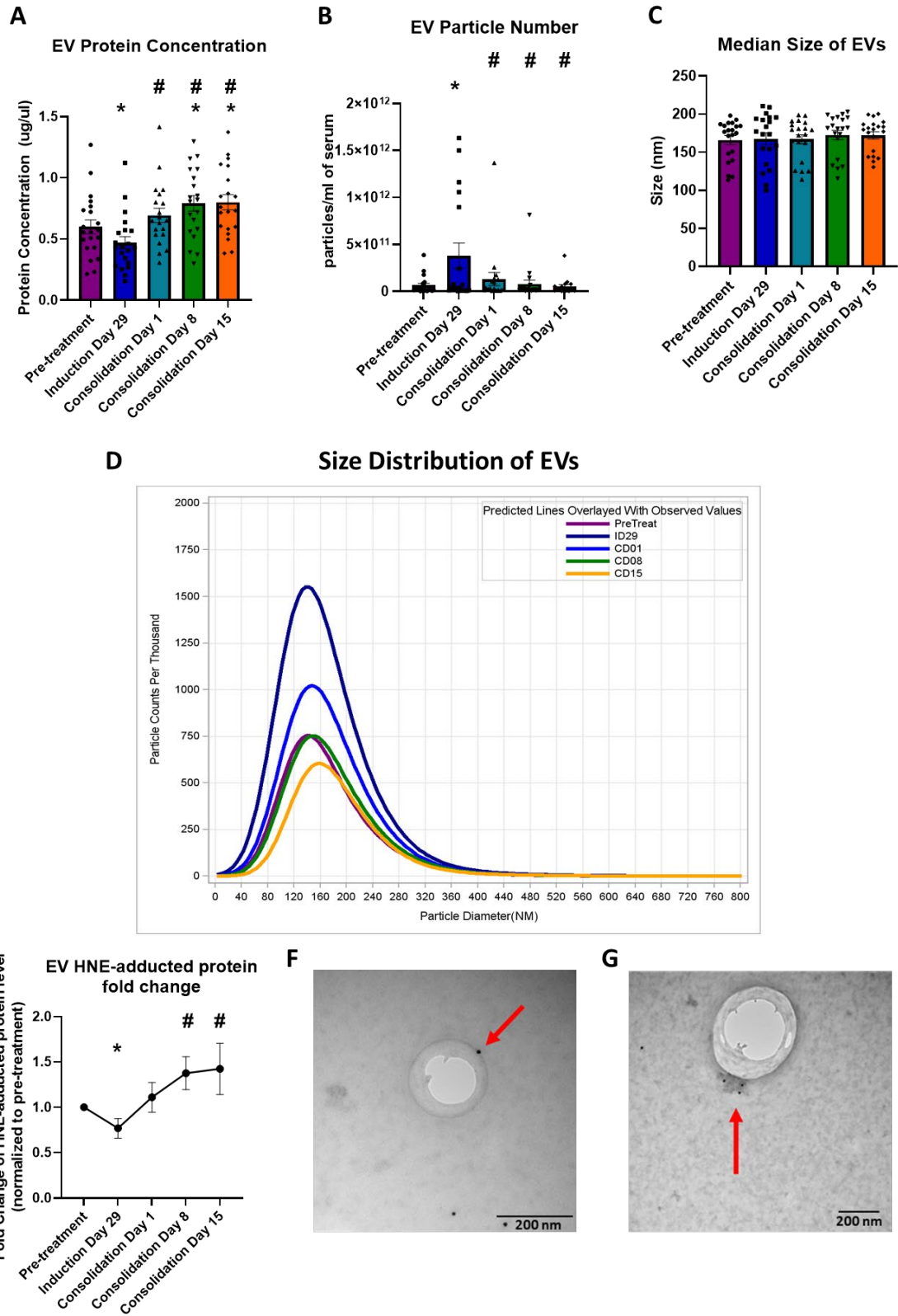


Figure 3.5 Characterization of EVs isolated from ALL patients.

(A) Average EV protein concentration ($\mu\text{g}/\mu\text{L}$) for each time point, with each individual value represented. A decrease from pre-treatment to induction day 29 was observed ($p<0.05$), while an increase compared to pre-treatment was observed at consolidation days 8 and 15 ($p<0.05$). A statistically significant increase in EV protein concentration was observed during all three time points during the consolidation phase when compared to induction day 29 ($p<0.05$). **(B)** The number of EV particles generated was measured using NTA. The number of EVs generated at induction day 29 was statistically increased compared to pre-treatment and compared to all time points in consolidation phase ($p<0.05$). **(C)** Median diameter of the EV particles was measured by NTA. No difference in size was observed throughout the various sample collection time points. **(D)** The size distribution comparing the number of particles (y-axis) to the size of the EVs in nanometers (x-axis) to visualize the relationship between particle size and EV number. **(E)** Each patient's individual fold change for HNE-adducted proteins measured in the EVs was averaged to analyze the overall fold change of HNE adductions throughout the course of treatment. A significant decrease was seen from pre-treatment to induction day 29 ($p<0.05$). Additionally, an increase was observed between induction day 29 and consolidation days 8 and 15 ($p<0.05$). **(F)** TEM showing immunogold labeling of HNE-adducted protein on the EV membrane (red arrow) and **(G)**

HNE-adducted proteins associated with a protein cluster at the outer membrane of the EVs.

Decrease in neuronal growth factor observed in EV lysates

Because EVs contain molecular components unique to their cell of origin, the composition of the protein within the EVs has the potential to serve as a source of novel insights about ALL before and after cancer therapy. Since we observed an increase in HNE-adducted proteins in the EVs during consolidation therapy and a decrease in HNE-adducted proteins in the serum, we wanted to further investigate changes in EV content associated with cancer and potential off-target tissue damage caused by cancer therapy.

First, we measured the amount of CD22 (**Figure 3.6a**) and CD19 (**Figure 3.6b**), two bone marrow cell surface markers used by the clinical team in the pre-B cell ALL patients (19 of 21 patients, **Table 3.3**) as a positive control of the EV content. CD19 is an established marker of pre-B cell leukemia and CD22 has been associated with ALL recurrence and refractory leukemia [154, 155]. No statistically significant difference was observed in CD19 (**Figure 3.6b**), but a significant increase was observed between pre-treatment to consolidation day 15 ($p < 0.05$) in CD22 (**Figure 3.6a**).

Table 3.3 Bone marrow cell surface markers for pre-B cell ALL patients at pre-treatment

Marker	Percentage of Patients with marker at pre-treatment
CD19	100%
CD10	84%
CD34	53%
CD38	53%
CD45	42%
CD22	37%
CD13	16%
HLA-DR	16%
CD56	5%
CD79A	5%
CD9	5%
CD20	5%

After confirmation of selected markers utilized by the clinical team as a positive control for our EV protein immunoblotting, we probed for different markers associated with alterations in the brain microenvironment. Astrocytes are a type of glial cell in the brain that increase in reactivity due to toxic insults, as we and others have previously found an increase in glial fibrillary acidic protein (GFAP) in EVs [48, 143, 144]. When we compared the level of GFAP in the EV samples, a significant decrease was observed at consolidation days 1 and 8 compared to both pretreatment and induction day 29 ($p < 0.05$) (**Figure 3.6c**). A similar trend was observed in the GFAP expression measured in the CSF, though no statistically significant difference was observed (**Figure 3.7a**). Next, we analyzed the neuronal

nuclear protein (NeuN), a universal marker of neurons [156]. In the EVs, NeuN decreased throughout the treatment course for these patients, though no statistical significance occurred (**Figure 3.6d**). Brain-derived neurotrophic factor (BDNF), a well-established neuronal growth factor, was shown to be statistically decreased at all four later time points compared to pre-treatment ($p < 0.05$) (**Fig. 3.6e**). We also measured NeuN in the CSF, but no significant difference was observed throughout the treatment of these patients (**Fig. 3.7b**); however, BDNF was not detectable in the CSF (data not shown).

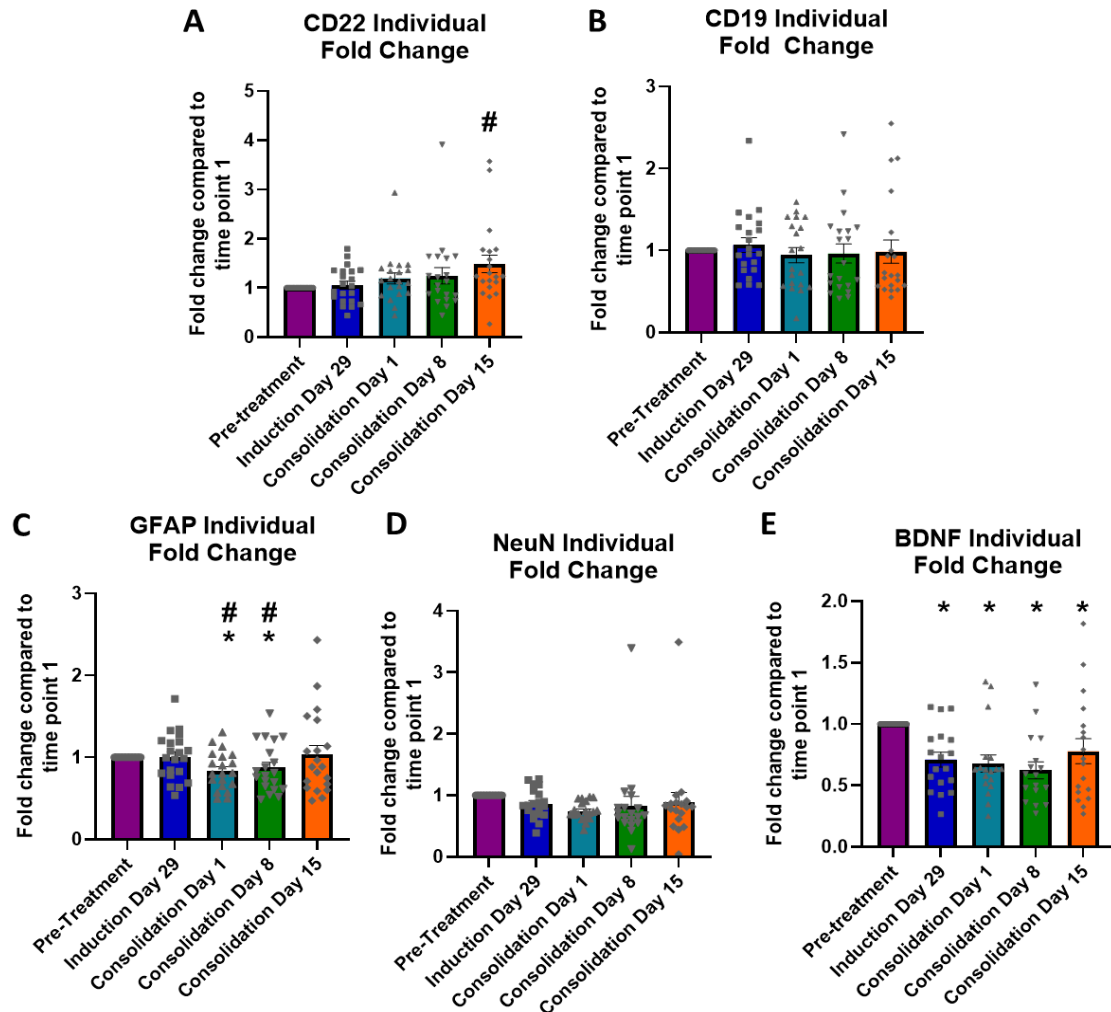


Figure 3.6 Immunoblotting of protein markers in EV lysates.

For all graphs in this figure, individual fold change was measured, followed by averaging the overall fold change across the different collection time points. Quantification of CD22 (**A**) and CD19 (**B**) as cell surface markers of leukemia. A significant increase of CD22 was detected in the EVs at consolidation day 15 compared to induction day 29 ($p < 0.05$). (**C**) A significant decrease in GFAP expression was observed in the EV lysates at consolidation days 1 and 8 compared to induction day 29 ($p < 0.05$). (**D**) An insignificant decline in the neuronal marker, NeuN, in the EVs was observed

during consolidation phase compared to pre-treatment or induction day 29.

(E) A statistically significant decrease in BDNF was observed in the EV lysates during both induction and consolidation phase collection points compared to pre-treatment ($p < 0.05$). *denotes $p < 0.05$ when compared to pre-treatment and # denotes $p < 0.05$ when compared to induction day 29.

GFAP (A) and NeuN (B) were measured in the CSF of patients using

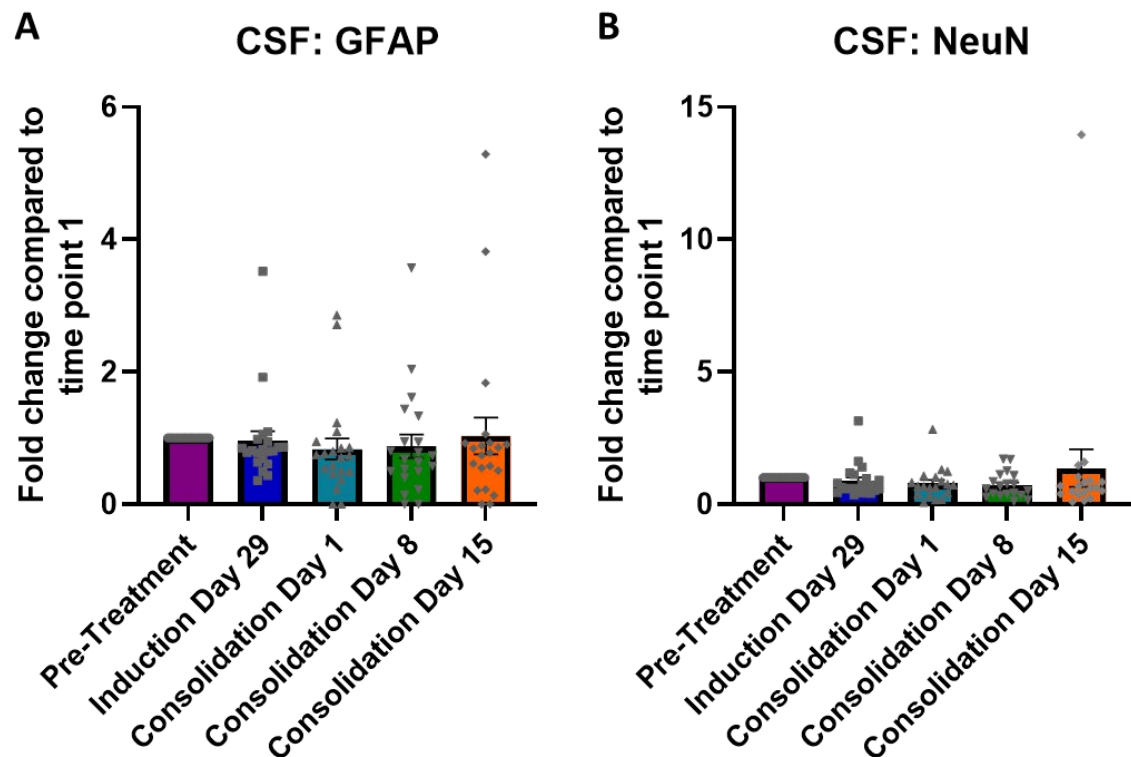


Figure 3.7 Protein immunoblotting in patient CSF.

capillary electrophoresis with Jess by Protein Simple. Each patient's individual fold change for each protein was quantified, followed by averaging the fold changes of all patients to analyze the overall fold change for these markers. Each protein was normalized by the protein normalization of that capillary to account for variation in protein loading.

Decrease in pro-inflammatory cytokines in serum after therapy

TNF- α has previously been shown to promote HNE-mediated neuronal damage in the brain, contributing to cognitive decline [26]. Inflammation has long been established as being elevated in numerous cancers [157]; furthermore, peripheral inflammation has been shown to cause blood-brain barrier breakdown, resulting in increased susceptibility to dysregulation in the brain microenvironment [158]. Therefore, we compared the levels of selected pro-inflammatory cytokines (TNF- α , IL-1 β , IL-6 and IL-8) in the serum of ALL patients to determine if the presence of the cancer or the exposure to chemotherapy agents these patients received contributes to the serum cytokine levels. TNF- α and IL-1 β have been demonstrated to stimulate astrocyte activation, which in turn may ultimately contribute to ROS production, leading to further damage in the brain microenvironment [23, 146, 159]. IL-6 can modulate blood-brain barrier function, and IL-8 has been observed to be an indicator of decreased gray matter *in vivo* [160, 161].

TNF- α (**Figure 3.8a**), IL-1 β (**Figure 3.8b**), IL-8 (**Figure 3.8c**), and IL-6 (**Figure 3.8d**) were measured by Meso Scale Diagnostics, which utilizes a sandwich ELISA to quantify numerous cytokines from a small sample volume in a 96-well format, allowing for high-throughput quantification. The highest levels of all cytokines evaluated were observed at the pre-treatment time point, suggesting the presence of the leukemia cells as a major contributing factor. A significant decrease of all four measured cytokines was observed at the four later time points compared to pre-treatment ($p < 0.05$) (**Figure 3.8**). TNF- α measured at

consolidation days 1 and 8 was significantly increased compared to induction day 29 ($p < 0.05$) (**Figure 3.8a**), and a significant decrease of IL-8 was observed during the consolidation phase compared to induction day 29 ($p < 0.05$) (**Figure 3.8c**).

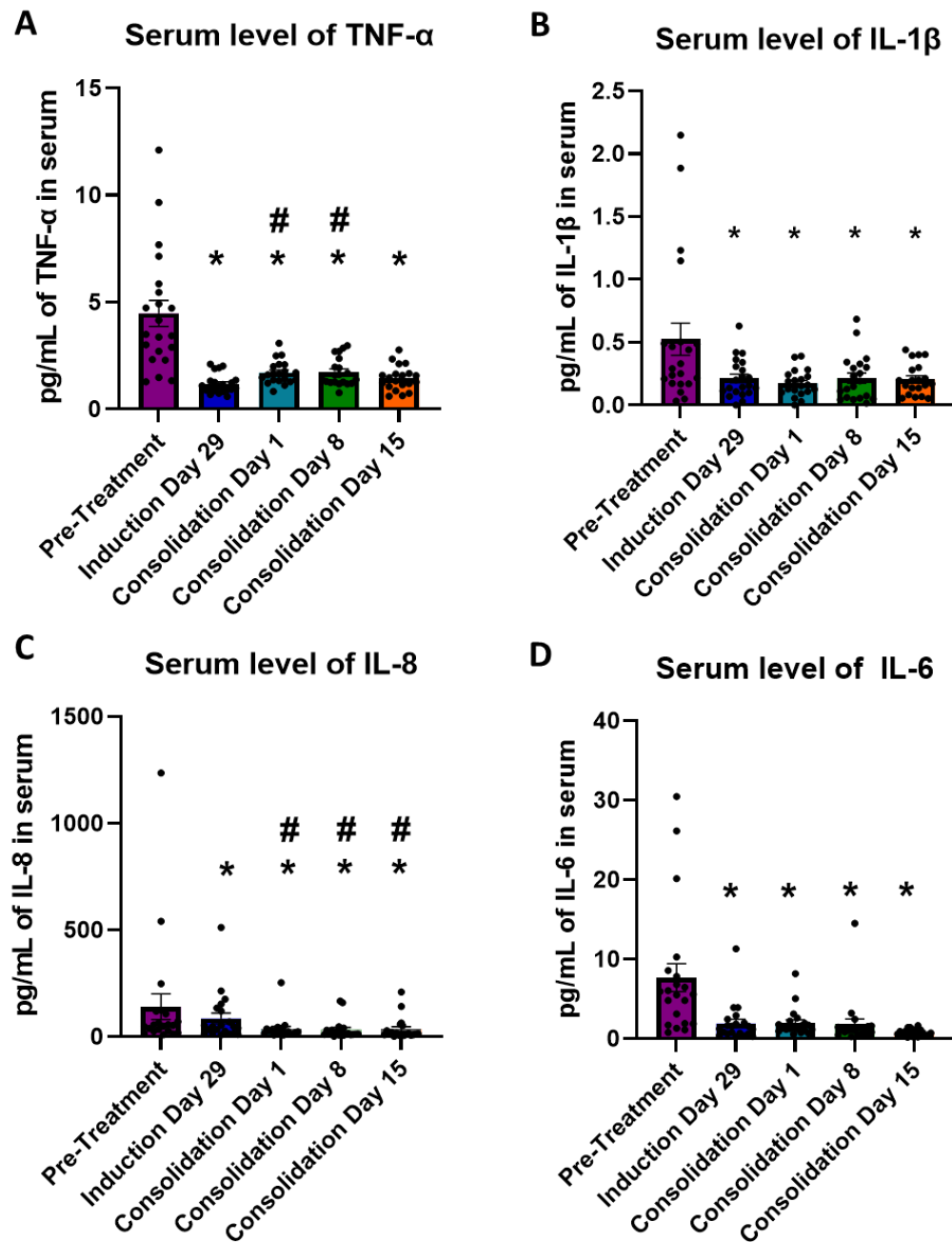


Figure 3.8 Quantification of pro-inflammatory cytokines in patient sera.

The amount of TNF- α (A), IL-1 β (B), IL-8 (C), and IL-6 (D) in patients. All values are given as picogram of cytokine per mL of serum. *denotes $p < 0.05$ when compared to pre-treatment and # denotes $p < 0.05$ when compared to induction day 29.

ALL derived EVs contribute to pro-inflammatory cytokine production and their production is increased by MTX treatment

The highest level of pro-inflammatory cytokines was observed in the patient samples at the pre-treatment time point, correlating with the highest level of leukemia cells present (**Table 3.2**). As previously mentioned, TNF- α and IL-1 β have been implicated in astrocyte activation [146, 159]. To determine the role of leukemia-derived EVs in the production of pro-inflammatory cytokines, EVs isolated from pre-B cell leukemia cells were used to treat macrophages *in vitro*. EVs were isolated from two pre-B ALL cell lines (Reh and SEM). U937 cells differentiated with PMA were treated with isolated EVs. Media was collected following EV treatment to quantify cytokine production. Following treatment with EVs from both cell lines, statistically significant increases in the production of TNF- α and IL-1 β were observed ($p < 0.05$) (**Figure 3.9a-d**), highlighting the contribution of leukemia-derived EVs to pro-inflammatory cytokine levels that was observed in the patients (**Figure 3.8**).

To further determine the impact of chemotherapy on EV generation, we measured the number of EVs generated from the *in vitro* cell lines following MTX treatment, due to the high frequency with which our patients received MTX (**Table**

3.4). Following treatment with 1 μ M MTX, the size of EVs from the Reh cells increased ($p<0.05$) (**Figure 3.9e**), but no change in size was observed in the SEM-derived EVs. Interestingly, an increase in the number of EVs generated following MTX treatment was observed in both Reh and SEM cells ($p<0.001$) (**Figure 3.9f**), suggesting MTX treatment generates more EVs, leading to increased cytokine generation.

Table 3.4 Chemotherapy and steroids used at different collection time

PT No.	Pre-Treatment	Induction Day 29	Consolidation Day 1	Consolidation Day 8	Consolidation Day 15
1	ARAC, VCR, PEG-Asp, Dexamethasone	MTX, VCR	VCR, 6-MP, MTX	VCR, 6-MP, MTX	6-MP, MTX
2	ARAC, MTX, PEG-Asp, VCR, Dexamethasone	MTX, VCR	MTX, CPM, ARAC, 6-MP	MTX, 6-MP, VCR, PEG-Asp	ARAC, 6-MP, MTX
3	PEG-Asp, VCR, ARAC, MTX, Dexamethasone	MTX	VCR, MTX, 6-MP	MTX, 6-MP, MTX	MTX, 6-MP
5	ARAC, VCR, PEG-Asp, Dexamethasone	MTX, VCR	-	6-MP, MTX, VCR	6-MP, MTX
6	ARAC, VCR, PEG-Asp, MTX, Dexamethasone	MTX, VCR	6-MP, MTX, ARAC, CPM	6-MP, ARAC, MTX	MTX, VCR, PEG-Asp
7	ARAC, VCR, DAUN, PEG-Asp, Dexamethasone	MTX, VCR, DAUN	Nelarabine, ARAC, 6-MP	ARAC, CPM, 6-MP	ARAC, 6-MP
8	ARAC, VCR, PEG-Asp, Dexamethasone	MTX, VCR	6-MP, MTX, VCR	6-MP, MTX, ARAC, CPM	ARAC
9	ARAC, VCR, DAUN, PEG-Asp, Prednisone	MTX, VCR, DAUN	MTX, 6-MP, ARAC, CPM	MTX, ARAC, 6-MP	MTX, 6-MP, VCR
10	ARAC, VCR, PEG-Asp, Dexamethasone	MTX	VCR, 6-MP, MTX	6-MP, MTX	6-MP, MTX
11	ARAC, VCR, PEG-Asp, Dexamethasone	MTX, VCR	6-MP, MTX, ARAC, CPM	6-MP, MTX, ARAC	VCR, PEG-Asp, MTX
12	ARAC, DAUN, VCR, Dexamethasone	MTX, Nelarabine	ARAC, MTX	VCR, PEG-Asp	VCR
13	ARAC, VCR, MTX, Dexamethasone	MTX	VCR, 6-MP, MTX	6-MP, MTX	6-MP, MTX
14	ARAC, VCR, MTX, Dexamethasone	MTX	VCR, 6-MP, MTX	6-MP, MTX	6-MP
15	ARAC, VCR, Dexamethasone	MTX	VCR, 6-MP, MTX	6-MP, MTX	6-MP, MTX
17	ARAC, VCR, Dexamethasone	MTX	VCR, 6-MP, MTX	MTX, 6-MP	MTX, 6-MP
18	ARAC, VCR, Dexamethasone	MTX	CPMM, ARAC, 6-MP, MTX	ARAC, 6-MP, MTX	MTX, VCR
19	ARAC, VCR, DAUN, Dexamethasone, Prednisone	MTX	CPMM, ARAC, 6-MP, MTX	ARAC, 6-MP, MTX	MTX, VCR, PEG-ASP
20	ARAC, VCR, Dexamethasone	MTX	VCR, 6-MP, MTX	6-MP, MTX	6-MP, MTX
21	ARAC, VCR, MTX, Dexamethasone	MTX	MTX, 6-MP, VCR	MTX, 6-MP	MTX, 6-MP
22	ARAC, VCR, MTX, Dexamethasone, Prednisone	MTX	MTX, CPM, ARAC, 6-MP	MTX, ARAC, 6-MP	VCR, MTX, 6-MP
23	ARAC, VCR, Dexamethasone	MTX	MTX, VCR, 6-MP	MTX, 6-MP	MTX, 6-MP

points

*6-MP: mercaptopurine; ARAC: cytarabine; CPM: cyclophosphamide; DAUN: daunorubicin; MTX: methotrexate; PEG-Asp: pegasparagase; VCR: vincristine

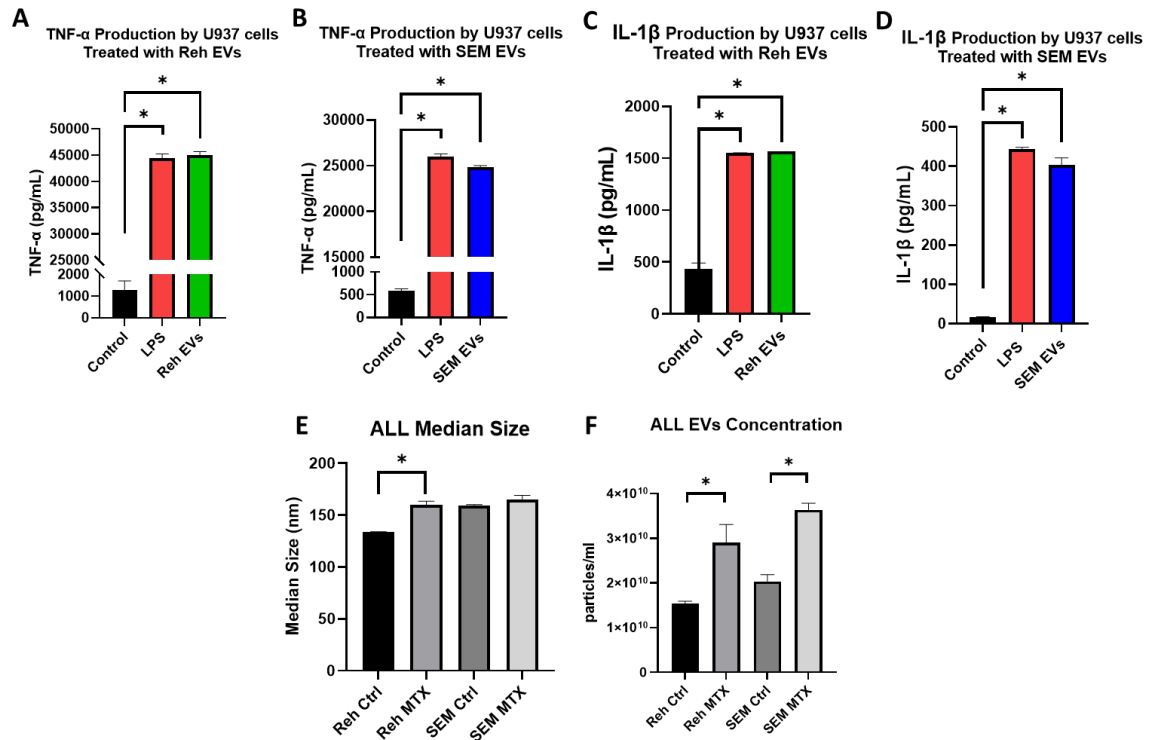


Figure 3.9 ALL cell-derived EVs contribute to pro-inflammatory cytokine production and their production is increased by MTX treatment.

Differentiated U937 cells treated with EVs isolated from Reh cells **(A)** and SEM cells **(B)** had a statistically significant increase in TNF- α production compared to non-treated controls. U937 cells also had a statistically significant increase in IL-1 β when treated with Reh EVs **(C)** and SEM EVs **(D)**. LPS was used as a positive control. The size of EVs from MTX-treated Reh cells increased, but no change in size was observed in the SEM cells **(E)**. Treatment with MTX resulted in a statistically significant increase in the number of EVs produced in both Reh and SEM cell lines **(F)** ($p < 0.001$).

Discussion

Off-target tissue injury, especially in the brain, is a serious consequence of cancer therapy experienced by cancer survivors, and pediatric ALL patients are particularly susceptible to these complications due to their still-developing brains. Detection of redox dysregulation and markers associated with off-target tissue damage, particularly in the brain, may provide opportunities to mitigate these negative outcomes. In this unique clinical study, we demonstrate that EVs have the potential to be sensitive indicators of oxidative stress, indicated by the presence of HNE-adducted proteins, throughout the treatment course of pediatric ALL patients. While an initial decrease in the level of HNE-adducted proteins was observed in the EVs from pre-treatment to induction day 29, an increase was observed during the consolidation phase that surpassed the basal level observed during pre-treatment and was not observed in the whole serum or CSF, illustrating the ability of EVs to be sensitive indicators of redox dysregulation. Additionally, the decline in the tissue specific protein marker, BDNF, suggests a potential decrease in neurogenesis in the brain after chemotherapy. Thus, quantifying HNE-adducted protein levels in isolated EVs, complemented with measuring tissue-specific damage, could provide insight into off-target effects occurring in cancer patients, overcoming the limitations of detecting negative outcomes later, when intervention may provide little benefit.

Oxidative stress has been implicated in a number of different human diseases (extensively reviewed by Pizzino *et al.* [162]); moreover, its contribution in neurodegenerative disease etiology has been well established [17, 93]. LPO is

generated as a result of the $\bullet\text{OH}$ attacking omega-6 polyunsaturated fatty acids, where the most toxic by-product of LPO is HNE [14]. After its formation, HNE can diffuse into the cytosol of cells, where it can modulate protein activity by adducting to cysteine, histidine, and lysine residues. Therefore, measuring levels of HNE-adducted proteins is a sensitive indicator of oxidative stress, especially when combined with the isolation of EVs, and can serve as a non-invasive indicator of collateral damage to normal tissues. For example, previous work has demonstrated the role HNE plays in disrupting neuronal and glial cell glutamate transporters, particularly, glial glutamate transporter 1 (GLT-1) [163]. Using inferior parietal lobule tissue samples from Alzheimer and control subjects, Lauderback *et al.* discovered GLT-1 as an HNE adducted protein. The dysregulation of proper GLT-1 function can ultimately lead to increased neuronal sensitivity to glutamate, inducing neuronal damage and death [163]. Therefore, the increase in HNE-adducted proteins observed in our patient-derived EVs warrants further validation for use in monitoring collateral damage in the CNS.

The decrease in the HNE-adducted protein levels detected in both the serum (**Figure 3.4c**) and the EVs (**Figure 3.5d**) from pre-treatment to induction day 29 corresponds with the eradication of the leukemia cells documented by the clinical team (**Table 3.2**), suggesting that presence of leukemia may have a role in oxidative damage which in turn may have caused neuronal toxicity. Importantly, while the level of HNE-adducted proteins in the serum during consolidation therapy increased from induction day 29 to consolidation therapy, the level of HNE-adducted proteins in EVs during the consolidation phase surpassed the initial level

measured at pre-treatment, despite the absence of leukemia in the patients (**Table 3.2**). We hypothesize that this increase in HNE-adducted proteins in the EVs during the consolidation phase is a result of prolonged exposure to the different chemotherapies these patients received. While the treatment regimen for each patient may have differed based on characteristics of their disease, a number of the chemotherapy agents more commonly used in our patient population have been shown to utilize ROS to exert their anticancer effects, such as mercaptopurine [164], cytarabine [130], daunorubicin [165, 166], and MTX [167]. We reason that exposure to these ROS-inducing drugs may be a source of oxidative stress contributing to the elevated levels of HNE-adducted proteins observed in the EVs during the consolidation phase.

The role of pro-inflammatory cytokines in contributing to neuronal damage has been of interest to our group and our collaborators [26, 148, 168]. We propose a mechanism of cancer therapy- induced cognitive impairment via the systemic generation of TNF- α , which can then cross the blood-brain barrier and lead to several downstream consequences in the brain. Evidence of this has been published previously by our group, where we have demonstrated that: 1) microglia activation can lead to further TNF- α release in the brain [169]; 2) mitochondrial respiration is a mediator of CNS injury induced by TNF- α [147]; and 3) inhibition of TNF- α with an anti-TNF- α antibody prevented CNS injury in an animal model, utilizing a well-established doxorubicin- treated model known to induce CNS injury [25]. Therefore, it is important to note the trend observed in the amount of TNF- α detected in the serum in the current study (**Figure 3.8a**): while it significantly

decreased from pre-treatment to induction day 29, interestingly, the trend observed overall from pre-treatment to consolidation day 15 strongly correlates with the amount of HNE-adducted proteins detected in the serum (**Figure 3.3c**) and the trend of GFAP decreasing at consolidation days 1 and 8, but increasing again at consolidation day 15 (**Figure 3.6c**). The relationship between HNE and TNF- α has previously been shown: in a TNF knockout (KO) mouse model, treatment with doxorubicin resulted in elevated levels of plasma HNE-adducted proteins compared to the saline treated control due to doxorubicin in the presence of oxygen, undergoing redox cycling from its quinone to semiquinone moiety, forming the superoxide anion radical [26]. Interestingly, despite the inability of dox to cross the blood brain barrier, when measuring the amount of HNE-adducted proteins in both the WT and TNF KO mice following doxorubicin treatment, elevated levels of HNE-adducted proteins was observed in the WT mice treated with dox compared to the saline treated; however, the TNF KO mice had no statistically significant difference between the saline and dox treated control, demonstrating the significant role of TNF- α in oxidative damage in the brain [26]. Furthermore, the trend for both HNE-adducted proteins (**Figure 3.4c**) and TNF- α (**Figure 3.8a**) in the sera is similar to the GFAP in the EVs (**Figure 3.6c**), suggesting elevation in HNE-adducted proteins and TNF- α may modulate astrocyte activation. Together, these data suggest that TNF- α plays a role in contributing to elevated oxidative stress (as quantified by HNE-adducted proteins) in the brain, highlighting the ability of TNF- α to mediate neuronal dysregulation. While the levels of TNF- α or HNE-adducted proteins in the serum are not significantly increased statistically,

compared to the pre-treatment level, the trend observed in both markers during consolidation supports the relationship between TNF- α and HNE.

Neurogenesis and neuronal stability is critical during development [170]. Our cohort of patients varied from ages 1 to 18 years, with a mean age of around 5 (**Table 3.1**). BDNF has been well-established to be a critical player in neuronal plasticity, neurogenesis, neuronal stability, and memory [171]. In the EVs of our patients, a decrease in BDNF protein levels was observed throughout the treatment course (**Figure 3.6e**); moreover, a decreasing trend in the neuronal marker, NeuN, was also observed throughout the collection time points, though not reaching statistical significance (**Figure 3.6d**). BDNF was not detectable in the CSF of these patients, suggesting that EVs are sensitive indicators of this observed decrease in the neuronal stability marker. This observation, combined with EVs demonstrating an increase in HNE-adducted proteins during the consolidation phase that surpasses the pre-treatment level (and which was not detectable in the serum or the CSF), supports the utility of EVs to provide insight into off-target tissue effects and redox dysregulation.

Interestingly, when quantifying the amount of CD22 (**Figure 3.6a**) and CD19 (**Figure 3.6b**) in the EVs isolated from the pediatric ALL patients, no decrease is observed in either marker despite the absence of leukemia in the serum (**Table 3.2**). While CD19 is a marker of pre-B cell ALL, CD19 is still located on normal B cells [154], which may explain why no decrease in CD19 is observed in the EVs isolated from the patients. CD22 has been suggested to be a marker of recurrence and chemotherapy refractory ALL [155, 172]. The observed increase in CD22

found in the isolated EVs from the patients could potentially be a marker for individuals more susceptible to have ALL recurrence; however, long-term studies would be required to understand the significance of this increased CD22 expression in the EVs.

We have demonstrated that EVs isolated from leukemia cells *in vitro* lead to increased production of pro-inflammatory cytokines TNF- α and IL-1 β . While this brings to light the potential contribution of leukemia-derived EVs in contributing to neuronal dysregulation, further experiments need to be conducted to identify the exact mechanism by which these EVs interact with immune cells to induce pro-inflammatory cytokine production. We hypothesize that the presence of HNE-adducted proteins may be a source of immune stimulation, but it is unclear whether it is due to the presence of HNE-adducted proteins within the EVs themselves (**Figure 3.4d**) or to HNE adductions associated with the membrane of the EVs (**Figure 3.4e-f**). The elevation in GFAP in the EVs that correlates with the increased amount of TNF- α and HNE-adducted proteins at consolidation day 15, where an initial decrease was observed at consolidation days 1 and 8, suggests that inflammation and redox dysregulation may be contributing to astrocyte activation. However, we have shown that the addition of chemotherapy agents (in this case, MTX) known to contribute to ROS production leads to greater EV production compared to leukemia cells not treated with any drug (**Figure 3.8f**). This brings into question the impact of the numerous chemotherapy and steroid drugs patients receive during their treatment protocol and the effects they may have on EV production, which could be addressed with further research.

In summary, our present study explored the potential of EVs to be used as early indicators of oxidative stress and off-target tissue injury, focusing on the brain, due to the median age of diagnosis of pediatric ALL patients being between 2 to 5 years of age, a critical developmental period. However, we do acknowledge some limitations of our study. First, we provide no direct proof of a mechanism by which EVs mediate neuronal injury in humans; however, the insights provided here are built upon numerous previous studies [25, 26, 102, 147, 168, 169]. Second, while we interpret the changes in protein markers in EVs as indicative off-target tissue damage, successfully characterizing the neurological effects induced by chemotherapy would require long-term psychological and neurological follow-up with our patient cohort. Nevertheless, we have demonstrated the ability of EVs to be sensitive indicators of oxidative stress in pediatric ALL patients, as shown by the elevated levels of HNE-adducted proteins present in EVs isolated from their serum, and to be a sensitive indicator of a decrease in the neuronal growth factor, BDNF (**Figure 3.10**). Overall, this unique clinical study provides insight into the potential clinical and translational utilization of EVs.

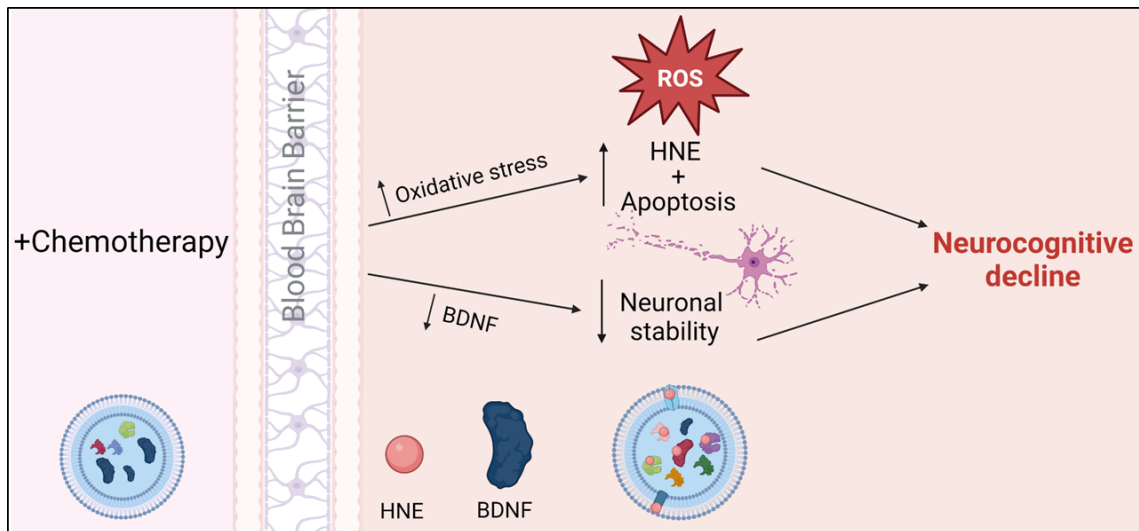


Figure 3.10 Proposed effect of systemic chemotherapy on neurocognitive decline and the ability of EVs to be a sensitive indicator of oxidative stress and decreased neuronal stability.

Following treatment with systemic chemotherapy agents, an increase in oxidative stress in the brain may occur, causing an increase in ROS production and leading to apoptosis occurring in the brain. Additionally, a decrease in the neuronal growth factor, BDNF, occurs following the introduction of chemotherapy agents. These two downstream effects together lead to this observed neurocognitive decline observed in survivors of pediatric ALL. Our present study demonstrates the ability of EVs to be sensitive indicators of this increased oxidative stress (through the quantification of HNE-adducted proteins) and this decrease in neuronal stability (through the quantification of BDNF in the EVs), highlighting its utilization as a sensitive indicator of cancer-therapy induced neuronal injury.

CHAPTER 4. CONCLUSION AND FUTURE DIRECTIONS

Conclusion

The results presented in this dissertation demonstrate that extracellular vesicles (EVs) can be used as sensitive indicators of oxidative stress and off-target tissue damage induced by cancer treatment. EVs were more sensitive indicators of oxidative stress that followed cranial radiation treatment (as demonstrated by the quantification of HNE-adducted proteins in the EVs lysates) compared to both the serum and brain tissue collected from mice. Additionally, compared to both serum and CSF isolated from pediatric ALL patients, EVs were more sensitive indicators of oxidative damage occurring during consolidation therapy, despite the absence of leukemia cells. Additionally, EVs released from leukemia cells induced pro-inflammatory cytokine production. Overall, the results reveal the utility of EVs as sensitive indicators of oxidative stress and mediators of inflammation.

Cancer therapeutics are known to utilize the generation of ROS to effectively kill cancer cells: radiation generates ROS through the hydrolysis of water, and approximately 50% of chemotherapy agents currently in use are associated with generating ROS and/or RNS. A by-product of this increase in reactive species is off-target damage to normal tissues, affecting the quality of life of cancer survivors. Pediatric ALL patients have a high survival rate, which makes it critical to identify potential targets of intervention to mitigate the impact of off-target tissue injury. Specifically, neuronal injury has been documented in survivors of pediatric ALL, and current limitations in detecting injury remain a barrier to

mitigate the damage seen in survivors. The role of oxidative stress on a number of disease etiologies is well -documented. The increase in oxidative stress can lead to LPO, causing an increase in the formation of HNE, which has been shown to be a contributor to neurocognitive diseases, highlighting the importance of detecting changes in HNE-adducted proteins. Here, our data support that EVs are sensitive markers of oxidative stress occurring as a result of radiation and chemotherapy agents. Interestingly, the elevation in HNE-adducted protein was not also found in the serum or brain tissue of our *in vivo* cranial radiation model, or in the CSF of our ALL- derived samples. EVs were also early detectors of astrocyte activation occurring due to cranial radiation, and our current data suggest BDNF detected in EVs is an indicator of decreased neuronal repair. Together, these findings suggest that EVs are useful clinical tools to detect oxidative stress and are tissue-specific markers of off-target tissue damage following cancer therapy.

GFAP has been well-established as a marker of astrocyte activation [173, 174], where astrocyte activation can lead to increased ROS production and neuroinflammation [23, 175]. An elevation in ROS production and inflammation can ultimately contribute to protein aggregation, inhibition of lysosome function, and neuronal injury, key events in neurodegenerative disorders. Additionally, neurogenesis occurs during childhood but rarely in adulthood [170]. BDNF is a neurotrophin that regulates neuronal plasticity by acting on tyrosine kinase receptors and facilitating long-term synaptic potentiation [171]. The decrease in BDNF observed in EVs from our patients suggests a decrease in neuronal

plasticity throughout the treatment course. The role of these two markers in the brain microenvironment is well-established and it points to how EVs can be used as markers to indicate alterations in the brain.

Furthermore, our findings reported in chapter three demonstrate that the utilization of MTX contributes to more EVs production. This increase in EVs generation can ultimately lead to increased stimulation of pro-inflammatory cytokines that previously have been documented to be modulators in neuronal damage following cancer treatment [25, 26, 147, 169, 176]. This observation suggests that while EVs may be useful as sensitive indicators of oxidative stress and altered expression of neuronal proteins, suggesting astrocyte activation and decreased neurogenesis, the downstream consequences of EVs warrant further exploration.

Overall, the findings from both studies contribute to and further the current understanding of EVs and their potential utilization in the clinic. This dissertation has demonstrated that: 1) EVs are sensitive indicators of oxidative stress; 2) proteins specific to alterations in the brain are detected in EVs following cancer treatment; and 3) EVs contribute to the production of pro-inflammatory cytokines, which may contribute to the mechanism of cancer therapy-induced cognitive impairment proposed by our research group [25, 26, 147, 169].

Future Directions

The results of this dissertation warrant future investigations, including the following:

1. What other markers in EVs could be used to monitor off-target tissue damage?

A number of different biomolecules within EVs could be used as potential indicators of off-target tissue damage following cancer treatment. Different methods to assess the proteins (i.e., proteomics) and the lipid content (lipidomics) in EVs could lead to the identification of other biomolecule markers.

2. What is the mechanism of immune activation by EVs?

Our findings demonstrate the ability of EVs to stimulate pro-inflammatory cytokine production. However, it is unclear whether the activation of immune cells occurs by cell surface receptors on the immune cell interacting with ligands on the surface of EVs, or whether uptake of EVs by immune cells is required. Furthermore, it remains to be elucidated how the presence of HNE-adducted proteins within the EVs (chapters two and three), and the localization of HNE adducted proteins on the EVs membranes (chapter three), modulate immune activation.

3. What are the effects of other chemotherapy agents given to the pediatric ALL patients that could contribute to EVs stimulation?

Our *in vitro* study reported in chapter three focused solely on MTX and its contribution to increasing EVs production in leukemia cell lines. Additionally, chapter two focuses solely on radiation, which is well-established as a means to generate ROS. However, the pediatric ALL patients receive a number of different chemotherapy agents and steroids throughout their treatment. To reproduce more

accurately the results of pediatric ALL treatment, all the numerous treatment drugs ALL patients receive would need to be introduced. Furthermore, the current gap in knowledge in understanding the effects of steroid drugs on EVs production could be addressed by utilizing more of the steroid drugs used to treat ALL patients.

4. What are the consequences to the brain microenvironment resulting from the chemotherapies the pediatric ALL patients receive?

While chapter three looks at markers within the EVs associated with neuronal alterations, HNE-adducted protein levels, systemic cytokine levels, and the effects of leukemia-derived EVs, the effects of EVs on glial cells remain to be elucidated. Both microglia and astrocytes have been documented to increase ROS and pro-inflammatory cytokine production that initiates damage in the brain [177, 178]; therefore, similar to our study here, it would be interesting to identify what the effects of cancer-derived EVs on the glial cells. Additionally, treating neuronal cells directly with EVs would provide insight into the role of EVs in neuronal injury.

5. Would inhibition of EVs formation mitigate off-target tissue damage occurring as a result of cancer therapy?

The results from this dissertation demonstrate the contribution of EVs to pro-inflammatory cytokine production, which may cross the blood brain barrier and lead to glial cell activation, contributing to cancer-therapy induced neuronal injury. It would be interesting to inhibit EVs formation to identify exactly how much EVs contribute to neuronal injury and inflammation. If inhibition of EVs released resulted in a significantly decreased immune stimulation, it would warrant investigating

potential methods to inhibit EVs production to mitigate immune activation and neuronal injury.

6. How long do EVs with HNE adductions remain in circulation?

A major obstacle to overcome in elucidating the role and downstream consequences of EVs is understanding the kinetics of EVs. Some studies have provided insights into the half-life of EVs [179]; while the study provided understanding of the movement and detection of EVs *in vivo*, it did not address EVs derived from multiple different cell types. Improved understanding of how long EVs are in circulation (particularly, those derived from cancer cells or with increased oxidative damage) would allow for greater appreciation of the consequences of EVs derived from different pathophysiological states.

7. Are other cytokines or chemokines upregulated or downregulated in the pediatric ALL patients throughout their treatment?

In chapter three, we document the amount of pro-inflammatory cytokines present in the patient sera throughout the first 2 months of cancer treatment. While overall we saw a decrease in TNF- α , IL-1 β , IL-8, and IL-6 from pre-treatment through consolidation day 15, quantifying other pro-inflammatory cytokines and anti-inflammatory cytokines would provide further insight into the contribution the immune system makes to neuronal injury.

APPENDICES

APPENDIX A: ACRONYMS

6-MP	6-mercaptopurine
AD	Alzheimer's disease
AFM	Atomic force microscopy
ALL	Acute lymphoblastic leukemia
ARAC	Cytarabine
BCA	Bicinchoninic acid
BDNF	Brain derived neurotrophic factor
CNS	Central nervous system
CPM	Cyclophosphamide
CSF	Cerebrospinal fluid
DAUN	Daunorubicin
DOX	Doxorubicin
ESCRT	Endosomal complexes required for transport machinery
EV	Extracellular vesicles
GFAP	Glial fibrillary acidic protein
GPx	Glutathione peroxidase
Gy	Gray
HNE	4-hydroxy-2-nonenal
IHC	Immunohistochemistry
IL-1 β	Interleukin-1 beta

IL-8	Interleukin-8
IL-10	Interleukin-10
ILV	Intraluminal vesicle
IR	Ionizing radiation
IT	Intrathecal
LPO	Lipid peroxidation
MISEV2018	Minimal information for studies of extracellular vesicles published in 2018 by Thery, et al.
MnSOD	Manganese superoxide dismutase
MTX	Methotrexate
MVB	Multivesicular endosomal body
NeuN	Neuronal nuclear protein
NTA	Nanoparticle tracking analysis
NSE	Neuronal specific enolase
PBS	Phosphate-buffered saline
PEG-Asp	Pegaspargase
PUFAs	Polyunsaturated fatty acids
PYGB	Glycogen phosphorylase
RNS	Reactive nitrogen species
ROS	Reactive oxygen species
SNARE	Soluble NSF attachment protein receptor
SOD	Superoxide dismutase
TEM	Transmission electron microscopy

TNF- α	Tumor necrosis factor alpha
VCR	Vincristine

REFERENCES

1. van Niel, G., G. D'Angelo, and G. Raposo, *Shedding light on the cell biology of extracellular vesicles*. Nat Rev Mol Cell Biol, 2018. **19**(4): p. 213-228. DOI: 10.1038/nrm.2017.125
2. Shah, R., T. Patel, and J.E. Freedman, *Circulating Extracellular Vesicles in Human Disease*. N Engl J Med, 2018. **379**(22): p. 2180-2181. DOI: 10.1056/NEJMc1813170
3. Shao, H., et al., *Protein typing of circulating microvesicles allows real-time monitoring of glioblastoma therapy*. Nat Med, 2012. **18**(12): p. 1835-40. DOI: 10.1038/nm.2994
4. Vader, P., et al., *Extracellular vesicles for drug delivery*. Adv Drug Deliv Rev, 2016. **106**(Pt A): p. 148-156. DOI: 10.1016/j.addr.2016.02.006
5. Skog, J., et al., *Glioblastoma microvesicles transport RNA and proteins that promote tumour growth and provide diagnostic biomarkers*. Nat Cell Biol, 2008. **10**(12): p. 1470-6. DOI: 10.1038/ncb1800
6. Peinado, H., et al., *Corrigendum: Melanoma exosomes educate bone marrow progenitor cells toward a pro-metastatic phenotype through MET*. Nat Med, 2016. **22**(12): p. 1502. DOI: 10.1038/nm1216-1502b
7. Al-Nedawi, K., et al., *Intercellular transfer of the oncogenic receptor EGFRvIII by microvesicles derived from tumour cells*. Nat Cell Biol, 2008. **10**(5): p. 619-24. DOI: 10.1038/ncb1725

8. Lachenal, G., et al., *Release of exosomes from differentiated neurons and its regulation by synaptic glutamatergic activity*. Mol Cell Neurosci, 2011. **46**(2): p. 409-18. DOI: 10.1016/j.mcn.2010.11.004
9. Thery, C., M. Ostrowski, and E. Segura, *Membrane vesicles as conveyors of immune responses*. Nat Rev Immunol, 2009. **9**(8): p. 581-93. DOI: 10.1038/nri2567
10. Harmati, M., et al., *Small extracellular vesicles convey the stress-induced adaptive responses of melanoma cells*. Scientific Reports, 2019. **9**(1): p. 15329. DOI: 10.1038/s41598-019-51778-6
11. Siegel, R.L., et al., *Cancer statistics, 2022*. CA Cancer J Clin, 2022. **72**(1): p. 7-33. DOI: 10.3322/caac.21708
12. Vitali, M., et al., *Cognitive impairment and chemotherapy: a brief overview*. Crit Rev Oncol Hematol, 2017. **118**: p. 7-14. DOI: 10.1016/j.critrevonc.2017.08.001
13. Halliwell, B.G.J.M.C., *Free radicals in biology and medicine*. 2015.
14. Dalleau, S., et al., *Cell death and diseases related to oxidative stress: 4-hydroxynonenal (HNE) in the balance*. Cell Death Differ, 2013. **20**(12): p. 1615-30. DOI: 10.1038/cdd.2013.138
15. Lovell, M.A. and W.R. Markesbery, *Oxidative DNA damage in mild cognitive impairment and late-stage Alzheimer's disease*. Nucleic Acids Res, 2007. **35**(22): p. 7497-504. DOI: 10.1093/nar/gkm821

16. Sultana, R. and D.A. Butterfield, *Role of oxidative stress in the progression of Alzheimer's disease*. J Alzheimers Dis, 2010. **19**(1): p. 341-53. DOI: 10.3233/jad-2010-1222
17. Di Domenico, F., A. Tramutola, and D.A. Butterfield, *Role of 4-hydroxy-2-nonenal (HNE) in the pathogenesis of alzheimer disease and other selected age-related neurodegenerative disorders*. Free Radic Biol Med, 2017. **111**: p. 253-261. DOI: 10.1016/j.freeradbiomed.2016.10.490
18. Perluigi, M., R. Coccia, and D.A. Butterfield, *4-Hydroxy-2-nonenal, a reactive product of lipid peroxidation, and neurodegenerative diseases: a toxic combination illuminated by redox proteomics studies*. Antioxid Redox Signal, 2012. **17**(11): p. 1590-609. DOI: 10.1089/ars.2011.4406
19. Green, J.L., et al., *Motor functioning during and following treatment with chemotherapy for pediatric acute lymphoblastic leukemia*. Pediatr Blood Cancer, 2013. **60**(8): p. 1261-6. DOI: 10.1002/pbc.24537
20. Anderson, F.S. and A.S. Kunin-Batson, *Neurocognitive late effects of chemotherapy in children: the past 10 years of research on brain structure and function*. Pediatr Blood Cancer, 2009. **52**(2): p. 159-64. DOI: 10.1002/pbc.21700
21. Chen, Y., et al., *Collateral damage in cancer chemotherapy: oxidative stress in nontargeted tissues*. Mol Interv, 2007. **7**(3): p. 147-56. DOI: 10.1124/mi.7.3.6
22. Hall, E.J., *Radiobiology for the radiologist*. 1973: Hagerstown, Md. : Medical Dept., Harper & Row, [1973] ©1973.

23. Andersen, J.K., *Oxidative stress in neurodegeneration: cause or consequence?* Nat Med, 2004. **10 Suppl**: p. S18-25. DOI: 10.1038/nrn1434
24. Salim, S., *Oxidative Stress and the Central Nervous System.* J Pharmacol Exp Ther, 2017. **360**(1): p. 201-205. DOI: 10.1124/jpet.116.237503
25. Tangpong, J., et al., *Adriamycin-induced, TNF-alpha-mediated central nervous system toxicity.* Neurobiol Dis, 2006. **23**(1): p. 127-39. DOI: 10.1016/j.nbd.2006.02.013
26. Ren, X., et al., *The triangle of death of neurons: Oxidative damage, mitochondrial dysfunction, and loss of choline-containing biomolecules in brains of mice treated with doxorubicin. Advanced insights into mechanisms of chemotherapy induced cognitive impairment ("chemobrain") involving TNF-alpha.* Free Radic Biol Med, 2019. **134**: p. 1-8. DOI: 10.1016/j.freeradbiomed.2018.12.029
27. Suematsu, N., et al., *Oxidative stress mediates tumor necrosis factor-alpha-induced mitochondrial DNA damage and dysfunction in cardiac myocytes.* Circulation, 2003. **107**(10): p. 1418-23. DOI: 10.1161/01.cir.0000055318.09997.1f
28. Cheung, Y.T., et al., *Leukoencephalopathy and long-term neurobehavioural, neurocognitive, and brain imaging outcomes in survivors of childhood acute lymphoblastic leukaemia treated with chemotherapy: a longitudinal analysis.* Lancet Haematol, 2016. **3**(10): p. e456-e466. DOI: 10.1016/S2352-3026(16)30110-7

29. Teng, F. and M. Fussenegger, *Shedding Light on Extracellular Vesicle Biogenesis and Bioengineering*. Adv Sci (Weinh), 2020. **8**(1): p. 2003505. DOI: 10.1002/advs.202003505
30. Valadi, H., et al., *Exosome-mediated transfer of mRNAs and microRNAs is a novel mechanism of genetic exchange between cells*. Nat Cell Biol, 2007. **9**(6): p. 654-9. DOI: 10.1038/ncb1596
31. Thery, C., et al., *Minimal information for studies of extracellular vesicles 2018 (MISEV2018): a position statement of the International Society for Extracellular Vesicles and update of the MISEV2014 guidelines*. J Extracell Vesicles, 2018. **7**(1): p. 1535750. DOI: 10.1080/20013078.2018.1535750
32. Jahn, R. and R.H. Scheller, *SNAREs--engines for membrane fusion*. Nat Rev Mol Cell Biol, 2006. **7**(9): p. 631-43. DOI: 10.1038/nrm2002
33. Bonifacino, J.S. and B.S. Glick, *The Mechanisms of Vesicle Budding and Fusion*. Cell, 2004. **116**(2): p. 153-166. DOI: [https://doi.org/10.1016/S0092-8674\(03\)01079-1](https://doi.org/10.1016/S0092-8674(03)01079-1)
34. Pap, E., et al., *Highlights of a new type of intercellular communication: microvesicle-based information transfer*. Inflamm Res, 2009. **58**(1): p. 1-8. DOI: 10.1007/s00011-008-8210-7
35. Christ, L., et al., *Cellular Functions and Molecular Mechanisms of the ESCRT Membrane-Scission Machinery*. Trends Biochem Sci, 2017. **42**(1): p. 42-56. DOI: 10.1016/j.tibs.2016.08.016
36. Kowal, J., M. Tkach, and C. Thery, *Biogenesis and secretion of exosomes*. Curr Opin Cell Biol, 2014. **29**: p. 116-25. DOI: 10.1016/j.ceb.2014.05.004

37. Stuffers, S., et al., *Multivesicular endosome biogenesis in the absence of ESCRTs*. Traffic, 2009. **10**(7): p. 925-37. DOI: 10.1111/j.1600-0854.2009.00920.x
38. Strauss, K., et al., *Exosome secretion ameliorates lysosomal storage of cholesterol in Niemann-Pick type C disease*. J Biol Chem, 2010. **285**(34): p. 26279-88. DOI: 10.1074/jbc.M110.134775
39. Hoshino, D., et al., *Exosome Secretion Is Enhanced by Invadopodia and Drives Invasive Behavior*. Cell Reports, 2013. **5**(5): p. 1159-1168. DOI: <https://doi.org/10.1016/j.celrep.2013.10.050>
40. Stenmark, H., *Rab GTPases as coordinators of vesicle traffic*. Nature Reviews Molecular Cell Biology, 2009. **10**(8): p. 513-525. DOI: 10.1038/nrm2728
41. Hankins, H.M., et al., *Role of flippases, scramblases and transfer proteins in phosphatidylserine subcellular distribution*. Traffic, 2015. **16**(1): p. 35-47. DOI: 10.1111/tra.12233
42. Laulagnier, K., et al., *PLD2 is enriched on exosomes and its activity is correlated to the release of exosomes*. FEBS Lett, 2004. **572**(1-3): p. 11-4. DOI: 10.1016/j.febslet.2004.06.082
43. Bicalho, B., J.L. Holovati, and J.P. Acker, *Phospholipidomics reveals differences in glycerophosphoserine profiles of hypothermically stored red blood cells and microvesicles*. Biochim Biophys Acta, 2013. **1828**(2): p. 317-26. DOI: 10.1016/j.bbame.2012.10.026

44. Abels, E.R. and X.O. Breakefield, *Introduction to Extracellular Vesicles: Biogenesis, RNA Cargo Selection, Content, Release, and Uptake*. Cell Mol Neurobiol, 2016. **36**(3): p. 301-12. DOI: 10.1007/s10571-016-0366-z
45. Huber, V., et al., *Human Colorectal Cancer Cells Induce T-Cell Death Through Release of Proapoptotic Microvesicles: Role in Immune Escape*. Gastroenterology, 2005. **128**(7): p. 1796-1804. DOI: <https://doi.org/10.1053/j.gastro.2005.03.045>
46. Clancy, J.W. and C. D'Souza-Schorey, *Tumor-Derived Extracellular Vesicles: Multifunctional Entities in the Tumor Microenvironment*. Annual Review of Pathology: Mechanisms of Disease, 2023. **18**(1): p. null. DOI: 10.1146/annurev-pathmechdis-031521-022116
47. Pigati, L., et al., *Selective release of microRNA species from normal and malignant mammary epithelial cells*. PLoS One, 2010. **5**(10): p. e13515. DOI: 10.1371/journal.pone.0013515
48. Sukati, S., et al., *Extracellular vesicles released after cranial radiation: An insight into an early mechanism of brain injury*. Brain Research, 2022. **1782**: p. 147840. DOI: <https://doi.org/10.1016/j.brainres.2022.147840>
49. Vinik, Y., et al., *Proteomic analysis of circulating extracellular vesicles identifies potential markers of breast cancer progression, recurrence, and response*. Sci Adv, 2020. **6**(40). DOI: 10.1126/sciadv.aba5714
50. Bandu, R., J.W. Oh, and K.P. Kim, *Mass spectrometry-based proteome profiling of extracellular vesicles and their roles in cancer biology*.

- Experimental & Molecular Medicine, 2019. **51**(3): p. 1-10. DOI: 10.1038/s12276-019-0218-2
51. Skliar, M. and V.S. Chernyshev, *Imaging of Extracellular Vesicles by Atomic Force Microscopy*. J Vis Exp, 2019(151). DOI: 10.3791/59254
52. Nguyen, U., et al., *The Simple Western™: a gel-free, blot-free, hands-free Western blotting reinvention*. Nature Methods, 2011. **8**(11): p. v-vi. DOI: 10.1038/nmeth.f.353
53. Cvjetkovic, A., et al., *Detailed Analysis of Protein Topology of Extracellular Vesicles-Evidence of Unconventional Membrane Protein Orientation*. Scientific reports, 2016. **6**: p. 36338-36338. DOI: 10.1038/srep36338
54. Gardiner, C., et al., *Techniques used for the isolation and characterization of extracellular vesicles: results of a worldwide survey*. Journal of Extracellular Vesicles, 2016. **5**(1): p. 32945. DOI: 10.3402/jev.v5.32945
55. Carnino, J.M., H. Lee, and Y. Jin, *Isolation and characterization of extracellular vesicles from Broncho-alveolar lavage fluid: a review and comparison of different methods*. Respiratory Research, 2019. **20**(1): p. 240. DOI: 10.1186/s12931-019-1210-z
56. Brennan, K., et al., *A comparison of methods for the isolation and separation of extracellular vesicles from protein and lipid particles in human serum*. Scientific Reports, 2020. **10**(1): p. 1039. DOI: 10.1038/s41598-020-57497-7
57. Cvjetkovic, A., J. Lötvall, and C. Lässer, *The influence of rotor type and centrifugation time on the yield and purity of extracellular vesicles*. Journal

- of extracellular vesicles, 2014. **3**: p. 10.3402/jev.v3.23111. DOI: 10.3402/jev.v3.23111
58. Reuter, S., et al., *Oxidative stress, inflammation, and cancer: how are they linked?* Free Radic Biol Med, 2010. **49**(11): p. 1603-16. DOI: 10.1016/j.freeradbiomed.2010.09.006
 59. Xia, C., et al., *Reactive oxygen species regulate angiogenesis and tumor growth through vascular endothelial growth factor.* Cancer Res, 2007. **67**(22): p. 10823-30. DOI: 10.1158/0008-5472.CAN-07-0783
 60. Kang, S.W., S. Lee, and E.K. Lee, *ROS and energy metabolism in cancer cells: alliance for fast growth.* Arch Pharm Res, 2015. **38**(3): p. 338-45. DOI: 10.1007/s12272-015-0550-6
 61. Brand, M.D., *The sites and topology of mitochondrial superoxide production.* Exp Gerontol, 2010. **45**(7-8): p. 466-72. DOI: 10.1016/j.exger.2010.01.003
 62. Chaiswing, L., et al., *Extracellular redox state regulates features associated with prostate cancer cell invasion.* Cancer Res, 2008. **68**(14): p. 5820-6. DOI: 10.1158/0008-5472.CAN-08-0162
 63. Harris, C. and J.M. Hansen, *Oxidative stress, thiols, and redox profiles.* Methods Mol Biol, 2012. **889**: p. 325-46. DOI: 10.1007/978-1-61779-867-2_21
 64. Jones, D.P., et al., *Cysteine/cystine couple is a newly recognized node in the circuitry for biologic redox signaling and control.* FASEB J, 2004. **18**(11): p. 1246-8. DOI: 10.1096/fj.03-0971fje

65. Fukai, T. and M. Ushio-Fukai, *Superoxide dismutases: role in redox signaling, vascular function, and diseases*. Antioxidants & redox signaling, 2011. **15**(6): p. 1583-1606. DOI: 10.1089/ars.2011.3999
66. Yarana, C. and D.K. St Clair, *Chemotherapy-Induced Tissue Injury: An Insight into the Role of Extracellular Vesicles-Mediated Oxidative Stress Responses*. Antioxidants (Basel), 2017. **6**(4). DOI: 10.3390/antiox6040075
67. Wardman, P. and L.P. Candeias, *Fenton Chemistry: An Introduction*. Radiation Research, 1996. **145**(5): p. 523-531. DOI: 10.2307/3579270
68. Dhar, S.K. and D.K. St Clair, *Manganese superoxide dismutase regulation and cancer*. Free Radic Biol Med, 2012. **52**(11-12): p. 2209-22. DOI: 10.1016/j.freeradbiomed.2012.03.009
69. Miriyala, S., et al., *Manganese superoxide dismutase, MnSOD and its mimics*. Biochimica et biophysica acta, 2012. **1822**(5): p. 794-814. DOI: 10.1016/j.bbadis.2011.12.002
70. Nandi, A., et al., *Role of Catalase in Oxidative Stress- and Age-Associated Degenerative Diseases*. Oxidative medicine and cellular longevity, 2019. **2019**: p. 9613090-9613090. DOI: 10.1155/2019/9613090
71. Lubos, E., J. Loscalzo, and D.E. Handy, *Glutathione peroxidase-1 in health and disease: from molecular mechanisms to therapeutic opportunities*. Antioxidants & redox signaling, 2011. **15**(7): p. 1957-1997. DOI: 10.1089/ars.2010.3586

72. Valko, M., et al., *Free radicals and antioxidants in normal physiological functions and human disease*. Int J Biochem Cell Biol, 2007. **39**(1): p. 44-84. DOI: 10.1016/j.biocel.2006.07.001
73. Shadel, G.S. and T.L. Horvath, *Mitochondrial ROS signaling in organismal homeostasis*. Cell, 2015. **163**(3): p. 560-9. DOI: 10.1016/j.cell.2015.10.001
74. Wilson, C. and C. Gonzalez-Billault, *Regulation of cytoskeletal dynamics by redox signaling and oxidative stress: implications for neuronal development and trafficking*. Front Cell Neurosci, 2015. **9**: p. 381. DOI: 10.3389/fncel.2015.00381
75. Li, J., et al., *The NADPH oxidase NOX4 drives cardiac differentiation: Role in regulating cardiac transcription factors and MAP kinase activation*. Mol Biol Cell, 2006. **17**(9): p. 3978-88. DOI: 10.1091/mbc.e05-06-0532
76. Veal, E.A., A.M. Day, and B.A. Morgan, *Hydrogen peroxide sensing and signaling*. Mol Cell, 2007. **26**(1): p. 1-14. DOI: 10.1016/j.molcel.2007.03.016
77. Florence, T.M., *The production of hydroxyl radical from hydrogen peroxide*. Journal of Inorganic Biochemistry, 1984. **22**(4): p. 221-230. DOI: [https://doi.org/10.1016/0162-0134\(84\)85007-2](https://doi.org/10.1016/0162-0134(84)85007-2)
78. Sonntag, C.v., *The chemical basis of radiation biology*. 1989, London; Philadelphia, PA: Taylor & Francis.
79. Liou, G.Y. and P. Storz, *Reactive oxygen species in cancer*. Free Radic Res, 2010. **44**(5): p. 479-96. DOI: 10.3109/10715761003667554

80. Chan, D.W., et al., *Loss of MKP3 mediated by oxidative stress enhances tumorigenicity and chemoresistance of ovarian cancer cells*. Carcinogenesis, 2008. **29**(9): p. 1742-50. DOI: 10.1093/carcin/bgn167
81. Chaiswing, L., et al., *Characterization of redox state of two human prostate carcinoma cell lines with different degrees of aggressiveness*. Free Radic Biol Med, 2007. **43**(2): p. 202-15. DOI: 10.1016/j.freeradbiomed.2007.03.031
82. Zhou, D., L. Shao, and D.R. Spitz, *Reactive oxygen species in normal and tumor stem cells*. Adv Cancer Res, 2014. **122**: p. 1-67. DOI: 10.1016/B978-0-12-420117-0.00001-3
83. Ralph, S.J., et al., *The causes of cancer revisited: "mitochondrial malignancy" and ROS-induced oncogenic transformation - why mitochondria are targets for cancer therapy*. Mol Aspects Med, 2010. **31**(2): p. 145-70. DOI: 10.1016/j.mam.2010.02.008
84. Conklin, K.A., *Chemotherapy-Associated Oxidative Stress: Impact on Chemotherapeutic Effectiveness*. Integrative Cancer Therapies, 2004. **3**(4): p. 294-300. DOI: 10.1177/1534735404270335
85. Li, Y., et al., *Mitochondrial dysfunction and oxidative stress in bone marrow stromal cells induced by daunorubicin leads to DNA damage in hematopoietic cells*. Free Radic Biol Med, 2020. **146**: p. 211-221. DOI: 10.1016/j.freeradbiomed.2019.11.007

86. Doroshow, J.H. and K.J. Davies, *Redox cycling of anthracyclines by cardiac mitochondria. II. Formation of superoxide anion, hydrogen peroxide, and hydroxyl radical*. J Biol Chem, 1986. **261**(7): p. 3068-74. DOI:
87. Ayala, A., M.F. Muñoz, and S. Argüelles, *Lipid Peroxidation: Production, Metabolism, and Signaling Mechanisms of Malondialdehyde and 4-Hydroxy-2-Nonenal*. Oxidative Medicine and Cellular Longevity, 2014. **2014**: p. 360438. DOI: 10.1155/2014/360438
88. Yen, H.C., et al., *The protective role of manganese superoxide dismutase against adriamycin-induced acute cardiac toxicity in transgenic mice*. J Clin Invest, 1996. **98**(5): p. 1253-60. DOI: 10.1172/JCI118909
89. Chaiswing, L., et al., *Oxidative damage precedes nitrate damage in adriamycin-induced cardiac mitochondrial injury*. Toxicol Pathol, 2004. **32**(5): p. 536-47. DOI: 10.1080/01926230490502601
90. Nithipongvanitch, R., et al., *Evidence for p53 as guardian of the cardiomyocyte mitochondrial genome following acute adriamycin treatment*. J Histochem Cytochem, 2007. **55**(6): p. 629-39. DOI: 10.1369/jhc.6A7146.2007
91. Chen, Y., et al., *Redox proteomic identification of oxidized cardiac proteins in adriamycin-treated mice*. Free Radic Biol Med, 2006. **41**(9): p. 1470-7. DOI: 10.1016/j.freeradbiomed.2006.08.006
92. Petersen, D.R. and J.A. Doorn, *Reactions of 4-hydroxynonenal with proteins and cellular targets*. Free Radic Biol Med, 2004. **37**(7): p. 937-45. DOI: 10.1016/j.freeradbiomed.2004.06.012

93. Butterfield, D.A. and B. Halliwell, *Oxidative stress, dysfunctional glucose metabolism and Alzheimer disease*. Nat Rev Neurosci, 2019. **20**(3): p. 148-160. DOI: 10.1038/s41583-019-0132-6
94. Grune, T. and K.J.A. Davies, *The proteasomal system and HNE-modified proteins*. Molecular Aspects of Medicine, 2003. **24**(4): p. 195-204. DOI: [https://doi.org/10.1016/S0098-2997\(03\)00014-1](https://doi.org/10.1016/S0098-2997(03)00014-1)
95. Markesbery, W.R. and M.A. Lovell, *Four-hydroxynonenal, a product of lipid peroxidation, is increased in the brain in Alzheimer's disease*. Neurobiol Aging, 1998. **19**(1): p. 33-6. DOI: 10.1016/s0197-4580(98)00009-8
96. Bruce-Keller, A.J., et al., *4-Hydroxynonenal, a product of lipid peroxidation, damages cholinergic neurons and impairs visuospatial memory in rats*. J Neuropathol Exp Neurol, 1998. **57**(3): p. 257-67. DOI: 10.1097/00005072-199803000-00007
97. Perry, E.A., et al., *Neurofilaments are the major neuronal target of hydroxynonenal-mediated protein cross-links*. Free Radic Res, 2013. **47**(6-7): p. 507-10. DOI: 10.3109/10715762.2013.794265
98. Shringarpure, R., et al., *4-Hydroxynonenal-modified amyloid-beta peptide inhibits the proteasome: possible importance in Alzheimer's disease*. Cell Mol Life Sci, 2000. **57**(12): p. 1802-9. DOI: 10.1007/pl00000660
99. VanWinkle, W.B., et al., *Cytoskeletal alterations in cultured cardiomyocytes following exposure to the lipid peroxidation product, 4-hydroxynonenal*. Cell Motil Cytoskeleton, 1994. **28**(2): p. 119-34. DOI: 10.1002/cm.970280204

100. Leonarduzzi, G., et al., *4-Hydroxynonenal and cholesterol oxidation products in atherosclerosis*. Mol Nutr Food Res, 2005. **49**(11): p. 1044-9. DOI: 10.1002/mnfr.200500090
101. Zhao, Y., et al., *Redox proteomic identification of HNE-bound mitochondrial proteins in cardiac tissues reveals a systemic effect on energy metabolism after doxorubicin treatment*. Free radical biology & medicine, 2014. **72**: p. 55-65. DOI: 10.1016/j.freeradbiomed.2014.03.001
102. Yarana, C., et al., *Extracellular Vesicles Released by Cardiomyocytes in a Doxorubicin-Induced Cardiac Injury Mouse Model Contain Protein Biomarkers of Early Cardiac Injury*. Clin Cancer Res, 2018. **24**(7): p. 1644-1653. DOI: 10.1158/1078-0432.CCR-17-2046
103. Chaiswing, L., W.H. St Clair, and D.K. St Clair, *Redox Paradox: A Novel Approach to Therapeutics-Resistant Cancer*. Antioxid Redox Signal, 2018. **29**(13): p. 1237-1272. DOI: 10.1089/ars.2017.7485
104. S, E.L.A., et al., *Extracellular vesicles: biology and emerging therapeutic opportunities*. Nat Rev Drug Discov, 2013. **12**(5): p. 347-57. DOI: 10.1038/nrd3978
105. Alexander, M., et al., *Exosome-delivered microRNAs modulate the inflammatory response to endotoxin*. Nature Communications, 2015. **6**(1): p. 7321. DOI: 10.1038/ncomms8321
106. Ratajczak, M.Z., et al., *Pivotal role of paracrine effects in stem cell therapies in regenerative medicine: can we translate stem cell-secreted paracrine*

- factors and microvesicles into better therapeutic strategies?* Leukemia, 2012. **26**(6): p. 1166-73. DOI: 10.1038/leu.2011.389
107. Xu, R., et al., *Extracellular vesicles in cancer - implications for future improvements in cancer care.* Nat Rev Clin Oncol, 2018. **15**(10): p. 617-638. DOI: 10.1038/s41571-018-0036-9
 108. Sung, B.H., et al., *Directional cell movement through tissues is controlled by exosome secretion.* Nature Communications, 2015. **6**(1): p. 7164. DOI: 10.1038/ncomms8164
 109. Yang, M., et al., *Microvesicles secreted by macrophages shuttle invasion-potentiating microRNAs into breast cancer cells.* Mol Cancer, 2011. **10**: p. 117. DOI: 10.1186/1476-4598-10-117
 110. Buzas, E.I., et al., *Emerging role of extracellular vesicles in inflammatory diseases.* Nat Rev Rheumatol, 2014. **10**(6): p. 356-64. DOI: 10.1038/nrrheum.2014.19
 111. Thompson, A.G., et al., *Extracellular vesicles in neurodegenerative disease - pathogenesis to biomarkers.* Nat Rev Neurol, 2016. **12**(6): p. 346-57. DOI: 10.1038/nrneurol.2016.68
 112. Aykin-Burns, N., et al., *Increased levels of superoxide and H₂O₂ mediate the differential susceptibility of cancer cells versus normal cells to glucose deprivation.* Biochem J, 2009. **418**(1): p. 29-37. DOI: 10.1042/BJ20081258
 113. Ohno, S., et al., *Systemically injected exosomes targeted to EGFR deliver antitumor microRNA to breast cancer cells.* Mol Ther, 2013. **21**(1): p. 185-91. DOI: 10.1038/mt.2012.180

114. Yao, J., et al., *M2 macrophage-derived exosomal microRNAs inhibit cell migration and invasion in gliomas through PI3K/AKT/mTOR signaling pathway*. Journal of Translational Medicine, 2021. **19**(1): p. 99. DOI: 10.1186/s12967-021-02766-w
115. Walker, S., et al., *Extracellular vesicle-based drug delivery systems for cancer treatment*. Theranostics, 2019. **9**(26): p. 8001-8017. DOI: 10.7150/thno.37097
116. Bunggulawa, E.J., et al., *Recent advancements in the use of exosomes as drug delivery systems*. Journal of Nanobiotechnology, 2018. **16**(1): p. 81. DOI: 10.1186/s12951-018-0403-9
117. Goetzl, E.J., et al., *Declining levels of functionally specialized synaptic proteins in plasma neuronal exosomes with progression of Alzheimer's disease*. FASEB J, 2018. **32**(2): p. 888-893. DOI: 10.1096/fj.201700731R
118. Balaj, L., et al., *Tumour microvesicles contain retrotransposon elements and amplified oncogene sequences*. Nature communications, 2011. **2**: p. 180-180. DOI: 10.1038/ncomms1180
119. Kahlert, C., et al., *Identification of double-stranded genomic DNA spanning all chromosomes with mutated KRAS and p53 DNA in the serum exosomes of patients with pancreatic cancer*. J Biol Chem, 2014. **289**(7): p. 3869-75. DOI: 10.1074/jbc.C113.532267
120. Liu, C., et al., *Low-cost thermophoretic profiling of extracellular-vesicle surface proteins for the early detection and classification of cancers*. Nature

- Biomedical Engineering, 2019. **3**(3): p. 183-193. DOI: 10.1038/s41551-018-0343-6
121. Baulch, J.E., et al., *Cranial grafting of stem cell-derived microvesicles improves cognition and reduces neuropathology in the irradiated brain*. Proc Natl Acad Sci U S A, 2016. **113**(17): p. 4836-41. DOI: 10.1073/pnas.1521668113
 122. Tome, W.A., et al., *A mouse model replicating hippocampal sparing cranial irradiation in humans: A tool for identifying new strategies to limit neurocognitive decline*. Sci Rep, 2015. **5**: p. 14384. DOI: 10.1038/srep14384
 123. Pui, C.H., et al., *Treating childhood acute lymphoblastic leukemia without cranial irradiation*. N Engl J Med, 2009. **360**(26): p. 2730-41. DOI: 10.1056/NEJMoa0900386
 124. Hardy, S.J., et al., *Cognitive Changes in Cancer Survivors*. American Society of Clinical Oncology Educational Book, 2018(38): p. 795-806. DOI: 10.1200/edbk_201179
 125. Howlader N, N.A., Krapcho M, Miller D, Brest A, Yu M, Ruhl J, Tatalovich Z, Mariotto A, Lewis DR, Chen HS, Feuer EJ, Cronin KA (eds). *SEER Cancer Statistics Review, 1975-2017*, National Cancer Institute. 2020; Available from: https://seer.cancer.gov/csr/1975_2017/.
 126. Brinkman, T.M., et al., *Attainment of Functional and Social Independence in Adult Survivors of Pediatric CNS Tumors: A Report From the St Jude*

- Lifetime Cohort Study*. J Clin Oncol, 2018. **36**(27): p. 2762-2769. DOI: 10.1200/JCO.2018.77.9454
127. Cooper, S.L. and P.A. Brown, *Treatment of pediatric acute lymphoblastic leukemia*. Pediatric clinics of North America, 2015. **62**(1): p. 61-73. DOI: 10.1016/j.pcl.2014.09.006
 128. Terwilliger, T. and M. Abdul-Hay, *Acute lymphoblastic leukemia: a comprehensive review and 2017 update*. Blood Cancer Journal, 2017. **7**(6): p. e577-e577. DOI: 10.1038/bcj.2017.53
 129. Angiolillo, A.L., et al., *Excellent Outcomes With Reduced Frequency of Vincristine and Dexamethasone Pulses in Standard-Risk B-Lymphoblastic Leukemia: Results From Children's Oncology Group AALL0932*. Journal of Clinical Oncology, 2021. **39**(13): p. 1437-1447. DOI: 10.1200/jco.20.00494
 130. Iacobini, M., et al., *Involvement of oxygen radicals in cytarabine-induced apoptosis in human polymorphonuclear cells*. Biochem Pharmacol, 2001. **61**(8): p. 1033-40. DOI: 10.1016/s0006-2952(01)00548-2
 131. Gibson, E.M., et al., *Methotrexate Chemotherapy Induces Persistent Tri-glial Dysregulation that Underlies Chemotherapy-Related Cognitive Impairment*. Cell, 2019. **176**(1-2): p. 43-55 e13. DOI: 10.1016/j.cell.2018.10.049
 132. Baker, W.J., G.L. Royer, Jr., and R.B. Weiss, *Cytarabine and neurologic toxicity*. J Clin Oncol, 1991. **9**(4): p. 679-93. DOI: 10.1200/jco.1991.9.4.679
 133. Zheng, D.J., et al., *Longitudinal analysis of quality-of-life outcomes in children during treatment for acute lymphoblastic leukemia: A report from*

- the Children's Oncology Group AALL0932 trial*. Cancer, 2018. **124**(3): p. 571-579. DOI: 10.1002/cncr.31085
134. Johansson, A.C., et al., *Regulation of apoptosis-associated lysosomal membrane permeabilization*. Apoptosis, 2010. **15**(5): p. 527-40. DOI: 10.1007/s10495-009-0452-5
 135. Hara, T., et al., *Suppression of basal autophagy in neural cells causes neurodegenerative disease in mice*. Nature, 2006. **441**(7095): p. 885-9. DOI: 10.1038/nature04724
 136. Prolo, L.M., H. Vogel, and R.J. Reimer, *The lysosomal sialic acid transporter sialin is required for normal CNS myelination*. J Neurosci, 2009. **29**(49): p. 15355-65. DOI: 10.1523/jneurosci.3005-09.2009
 137. Melo, S.A., et al., *Cancer exosomes perform cell-independent microRNA biogenesis and promote tumorigenesis*. Cancer Cell, 2014. **26**(5): p. 707-21. DOI: 10.1016/j.ccell.2014.09.005
 138. Subramaniam, R., et al., *The lipid peroxidation product, 4-hydroxy-2-trans-nonenal, alters the conformation of cortical synaptosomal membrane proteins*. J Neurochem, 1997. **69**(3): p. 1161-9. DOI: 10.1046/j.1471-4159.1997.69031161.x
 139. Ma, C.M., et al., *AAPM protocol for 40-300 kV x-ray beam dosimetry in radiotherapy and radiobiology*. Med Phys, 2001. **28**(6): p. 868-93. DOI: 10.1118/1.1374247

140. Chen, Q., et al., *Technical Note: Vendor miscalibration of preclinical orthovoltage irradiator identified through independent output check*. Med Phys, 2021. **48**(2): p. 881-889. DOI: 10.1002/mp.14642
141. Aluise, C.D., et al., *In vivo amelioration of adriamycin induced oxidative stress in plasma by gamma-glutamylcysteine ethyl ester (GCEE)*. Cancer Lett, 2009. **282**(1): p. 25-9. DOI: 10.1016/j.canlet.2009.02.047
142. Zhang, S., et al., *Intercellular transfer of pathogenic alpha-synuclein by extracellular vesicles is induced by the lipid peroxidation product 4-hydroxynonenal*. Neurobiol Aging, 2018. **61**: p. 52-65. DOI: 10.1016/j.neurobiolaging.2017.09.016
143. Chatterjee, P., et al., *Plasma glial fibrillary acidic protein is elevated in cognitively normal older adults at risk of Alzheimer's disease*. Translational Psychiatry, 2021. **11**(1): p. 27. DOI: 10.1038/s41398-020-01137-1
144. Middeldorp, J. and E.M. Hol, *GFAP in health and disease*. Prog Neurobiol, 2011. **93**(3): p. 421-43. DOI: 10.1016/j.pneurobio.2011.01.005
145. Keeney, J.T.R., et al., *Doxorubicin-induced elevated oxidative stress and neurochemical alterations in brain and cognitive decline: protection by MESNA and insights into mechanisms of chemotherapy-induced cognitive impairment ("chemobrain")*. Oncotarget, 2018. **9**(54): p. 30324-30339. DOI: 10.18632/oncotarget.25718
146. Hyvarinen, T., et al., *Co-stimulation with IL-1beta and TNF-alpha induces an inflammatory reactive astrocyte phenotype with neurosupportive*

- characteristics in a human pluripotent stem cell model system*. Sci Rep, 2019. **9**(1): p. 16944. DOI: 10.1038/s41598-019-53414-9
147. Tangpong, J., et al., *Adriamycin-mediated nitration of manganese superoxide dismutase in the central nervous system: insight into the mechanism of chemobrain*. J Neurochem, 2007. **100**(1): p. 191-201. DOI: 10.1111/j.1471-4159.2006.04179.x
 148. Aluise, C.D., et al., *2-Mercaptoethane sulfonate prevents doxorubicin-induced plasma protein oxidation and TNF-alpha release: implications for the reactive oxygen species-mediated mechanisms of chemobrain*. Free Radic Biol Med, 2011. **50**(11): p. 1630-8. DOI: 10.1016/j.freeradbiomed.2011.03.009
 149. Sompol, P., et al., *A neuronal model of Alzheimer's disease: an insight into the mechanisms of oxidative stress-mediated mitochondrial injury*. Neuroscience, 2008. **153**(1): p. 120-30. DOI: 10.1016/j.neuroscience.2008.01.044
 150. Siegel, D.A., et al., *Rates and Trends of Pediatric Acute Lymphoblastic Leukemia - United States, 2001-2014*. MMWR Morb Mortal Wkly Rep, 2017. **66**(36): p. 950-954. DOI: 10.15585/mmwr.mm6636a3
 151. Campbell, L.K., et al., *A meta-analysis of the neurocognitive sequelae of treatment for childhood acute lymphocytic leukemia*. Pediatric Blood & Cancer, 2007. **49**(1): p. 65-73. DOI: <https://doi.org/10.1002/pbc.20860>

152. Vora, A., et al., *Influence of Cranial Radiotherapy on Outcome in Children With Acute Lymphoblastic Leukemia Treated With Contemporary Therapy*. J Clin Oncol, 2016. **34**(9): p. 919-26. DOI: 10.1200/JCO.2015.64.2850
153. Niemann, A., et al., *Therapeutic drug monitoring of methotrexate in cerebrospinal fluid after systemic high-dose infusion in children: can the burden of intrathecal methotrexate be reduced?* Ther Drug Monit, 2010. **32**(4): p. 467-75. DOI: 10.1097/FTD.0b013e3181e5c6b3
154. Wang, K., G. Wei, and D. Liu, *CD19: a biomarker for B cell development, lymphoma diagnosis and therapy*. Experimental Hematology & Oncology, 2012. **1**(1): p. 36. DOI: 10.1186/2162-3619-1-36
155. Shah, N.N., et al., *Characterization of CD22 expression in acute lymphoblastic leukemia*. Pediatr Blood Cancer, 2015. **62**(6): p. 964-9. DOI: 10.1002/pbc.25410
156. Gusel'nikova, V.V. and D.E. Korzhevskiy, *NeuN As a Neuronal Nuclear Antigen and Neuron Differentiation Marker*. Acta Naturae, 2015. **7**(2): p. 42-7. DOI:
157. Coussens, L.M. and Z. Werb, *Inflammation and cancer*. Nature, 2002. **420**(6917): p. 860-7. DOI: 10.1038/nature01322
158. Galea, I., *The blood–brain barrier in systemic infection and inflammation*. Cellular & Molecular Immunology, 2021. **18**(11): p. 2489-2501. DOI: 10.1038/s41423-021-00757-x

159. Ye, L., et al., *IL-1 β and TNF- α induce neurotoxicity through glutamate production: a potential role for neuronal glutaminase*. J Neurochem, 2013. **125**(6): p. 897-908. DOI: 10.1111/jnc.12263
160. Zhang, J., et al., *Anti-IL-6 neutralizing antibody modulates blood-brain barrier function in the ovine fetus*. Faseb j, 2015. **29**(5): p. 1739-53. DOI: 10.1096/fj.14-258822
161. Willette, A.A., et al., *Interleukin-8 and interleukin-10, brain volume and microstructure, and the influence of calorie restriction in old rhesus macaques*. Age (Dordr), 2013. **35**(6): p. 2215-27. DOI: 10.1007/s11357-013-9518-y
162. Pizzino, G., et al., *Oxidative Stress: Harms and Benefits for Human Health*. Oxid Med Cell Longev, 2017. **2017**: p. 8416763. DOI: 10.1155/2017/8416763
163. Lauderback, C.M., et al., *The glial glutamate transporter, GLT-1, is oxidatively modified by 4-hydroxy-2-nonenal in the Alzheimer's disease brain: the role of Abeta1-42*. J Neurochem, 2001. **78**(2): p. 413-6. DOI: 10.1046/j.1471-4159.2001.00451.x
164. Rehman, S.U., et al., *Redox cycling of Cu(II) by 6-mercaptopurine leads to ROS generation and DNA breakage: possible mechanism of anticancer activity*. Tumor Biology, 2015. **36**(2): p. 1237-1244. DOI: 10.1007/s13277-014-2743-x
165. Boland, M.P., S.J. Foster, and L.A. O'Neill, *Daunorubicin activates NFkappaB and induces kappaB-dependent gene expression in HL-60*

- promyelocytic and Jurkat T lymphoma cells*. J Biol Chem, 1997. **272**(20): p. 12952-60. DOI: 10.1074/jbc.272.20.12952
166. Al-Aamri, H.M., et al., *Time dependent response of daunorubicin on cytotoxicity, cell cycle and DNA repair in acute lymphoblastic leukaemia*. BMC Cancer, 2019. **19**(1): p. 179. DOI: 10.1186/s12885-019-5377-y
 167. Phillips, D.C., K.J. Woollard, and H.R. Griffiths, *The anti-inflammatory actions of methotrexate are critically dependent upon the production of reactive oxygen species*. Br J Pharmacol, 2003. **138**(3): p. 501-11. DOI: 10.1038/sj.bjp.0705054
 168. Hayslip, J., et al., *Plasma TNF-alpha and Soluble TNF Receptor Levels after Doxorubicin with or without Co-Administration of Mesna-A Randomized, Cross-Over Clinical Study*. PLoS One, 2015. **10**(4): p. e0124988. DOI: 10.1371/journal.pone.0124988
 169. Tangpong, J., et al., *Tumor necrosis factor alpha-mediated nitric oxide production enhances manganese superoxide dismutase nitration and mitochondrial dysfunction in primary neurons: an insight into the role of glial cells*. Neuroscience, 2008. **151**(2): p. 622-9. DOI: 10.1016/j.neuroscience.2007.10.046
 170. Sorrells, S.F., et al., *Human hippocampal neurogenesis drops sharply in children to undetectable levels in adults*. Nature, 2018. **555**(7696): p. 377-381. DOI: 10.1038/nature25975

171. Miranda, M., et al., *Brain-Derived Neurotrophic Factor: A Key Molecule for Memory in the Healthy and the Pathological Brain*. Front Cell Neurosci, 2019. **13**: p. 363. DOI: 10.3389/fncel.2019.00363
172. Lanza, F., et al., *CD22 Expression in B-Cell Acute Lymphoblastic Leukemia: Biological Significance and Implications for Inotuzumab Therapy in Adults*. Cancers (Basel), 2020. **12**(2). DOI: 10.3390/cancers12020303
173. Yang, Z. and K.K. Wang, *Glial fibrillary acidic protein: from intermediate filament assembly and gliosis to neurobiomarker*. Trends Neurosci, 2015. **38**(6): p. 364-74. DOI: 10.1016/j.tins.2015.04.003
174. Tzeng, S.F., H.Y. Hsiao, and O.T. Mak, *Prostaglandins and cyclooxygenases in glial cells during brain inflammation*. Curr Drug Targets Inflamm Allergy, 2005. **4**(3): p. 335-40. DOI: 10.2174/1568010054022051
175. Kwon, H.S. and S.-H. Koh, *Neuroinflammation in neurodegenerative disorders: the roles of microglia and astrocytes*. Translational Neurodegeneration, 2020. **9**(1): p. 42. DOI: 10.1186/s40035-020-00221-2
176. Ren, X., et al., *Plausible biochemical mechanisms of chemotherapy-induced cognitive impairment ("chemobrain"), a condition that significantly impairs the quality of life of many cancer survivors*. Biochim Biophys Acta Mol Basis Dis, 2019. **1865**(6): p. 1088-1097. DOI: 10.1016/j.bbadis.2019.02.007
177. Town, T., V. Nikolic, and J. Tan, *The microglial "activation" continuum: from innate to adaptive responses*. Journal of Neuroinflammation, 2005. **2**(1): p. 24. DOI: 10.1186/1742-2094-2-24

178. Nahirnyj, A., et al., *ROS detoxification and proinflammatory cytokines are linked by p38 MAPK signaling in a model of mature astrocyte activation*. PLoS One, 2013. **8**(12): p. e83049. DOI: 10.1371/journal.pone.0083049
179. Lai, C.P., et al., *Dynamic Biodistribution of Extracellular Vesicles in Vivo Using a Multimodal Imaging Reporter*. ACS Nano, 2014. **8**(1): p. 483-494. DOI: 10.1021/nn404945r

VITA

Education

- | | |
|--------------|--|
| 2018-present | Ph.D. student, Toxicology and Cancer Biology,
University of Kentucky, Lexington, KY |
| 2017 | B.S., Biology and Minor in Chinese, University of
Kentucky, Lexington, KY |

Professional Positions

- | | |
|--------------|--|
| 2018-present | Graduate Research Assistant, University of
Kentucky, Lexington, KY |
| 2016-2017 | Undergraduate Research Assistant, Department of
Biology at the University of Kentucky, College of
Arts and Sciences. Lexington, KY |

Scholastic and Professional Honors

- | | |
|-------------|---|
| August 2022 | Yulan Sun Outstanding Graduate
Student Award
Department of Toxicology and Cancer
Biology, University of Kentucky, College
of Medicine |
|-------------|---|

November 2022-October 2021

T32ES07266

National Institute of Environmental
Health Sciences T32 Training Grant –
Department of Toxicology and Cancer
Biology at the University of Kentucky,
College of Medicine

May 2021

Markey Cancer Center Research Day

2nd Place – Trainee Presentations

April 2021

University of Kentucky, College of

Medicine Annual Trainee Poster

Session

2nd Place – Graduate Student Category

August 2013-May 2017

Presidential Scholarship Recipient

University of Kentucky

Publications

1. **Ho, J.**, Smith, S., Oakley, E., and Vanderford, N. L. A Joint Trainee-Faculty-Staff Book Club to Promote Trainee Professional Development. *Heliyon*. 2022. 8(1): p. 08675. DOI: <https://doi.org/10.1016/j.heliyon.2021.e08675>

2. Sukati, S.*, **Ho, J.***, Chaiswing, L., Sompol, P., Pandit, H., Wei, W., Izumi, T., Chen, Q., Weiss, H., Noel, T., Bondada, S., Butterfield, D.A., and St. Clair, D.K. Extracellular vesicles released after cranial radiation: An insight into an early mechanism of brain injury. *Brain Research*. 2022 1782: p. 147840. DOI: <https://doi.org/10.1016/j.brainres.2022.147840>

3. Hanley, C. D., **Ho, J.**, Prichard, C., and Vanderford, N. L. The Use of Virtual Research Experiences for Appalachian Career Training in Oncology (ACTION) Program High School Participants During the COVID-19 Pandemic. <https://doi.org/10.15695/jstem/v5i2.03>

4. **Ho, J.**, Chaiswing, L., and St. Clair, D. K. Extracellular vesicles and cancer therapy: insight into the role of oxidative stress. *Antioxidants*. 2022, 11(6) 1194. <https://doi.org/10.3390/antiox11061194>

5. **Ho, J.**, Sukati, S., Taylor, T., Carter, S., Fuller, B., Marmo, A., Sorge, C., D’Orazio, J., Butterfield, D. A., Weiss, H., Chaiswing, L., Bondada, S., and St. Clair, D. K. Extracellular vesicles released by acute lymphoblastic leukemia patients contain HNE-adducted proteins: implications of collateral damage. ***In preparation***

6. **Ho, J.**, Zhao, Y., Napier, D., Wei, Q., Butterfield, D. A., Villano, J., Bauer, B., Kolesar, J., St. Clair, W. H., Bondada, S., Bocklage, T., Weiss, H., St. Clair, D. K., and Chaiswing, L. Isolation and characterization of extracellular vesicles from glioma patients: Pros and Cons of commercially available isolation kits. ***In preparation***